Kentucky Geological Survey
James C. Cobb, State Geologist and Director
University of Kentucky, Lexington

Middle and Late Devonian New Albany Shale in the Kentucky Geological Survey Marvin Blan No. 1 Well, Hancock County, Kentucky

Brandon C. Nuttall

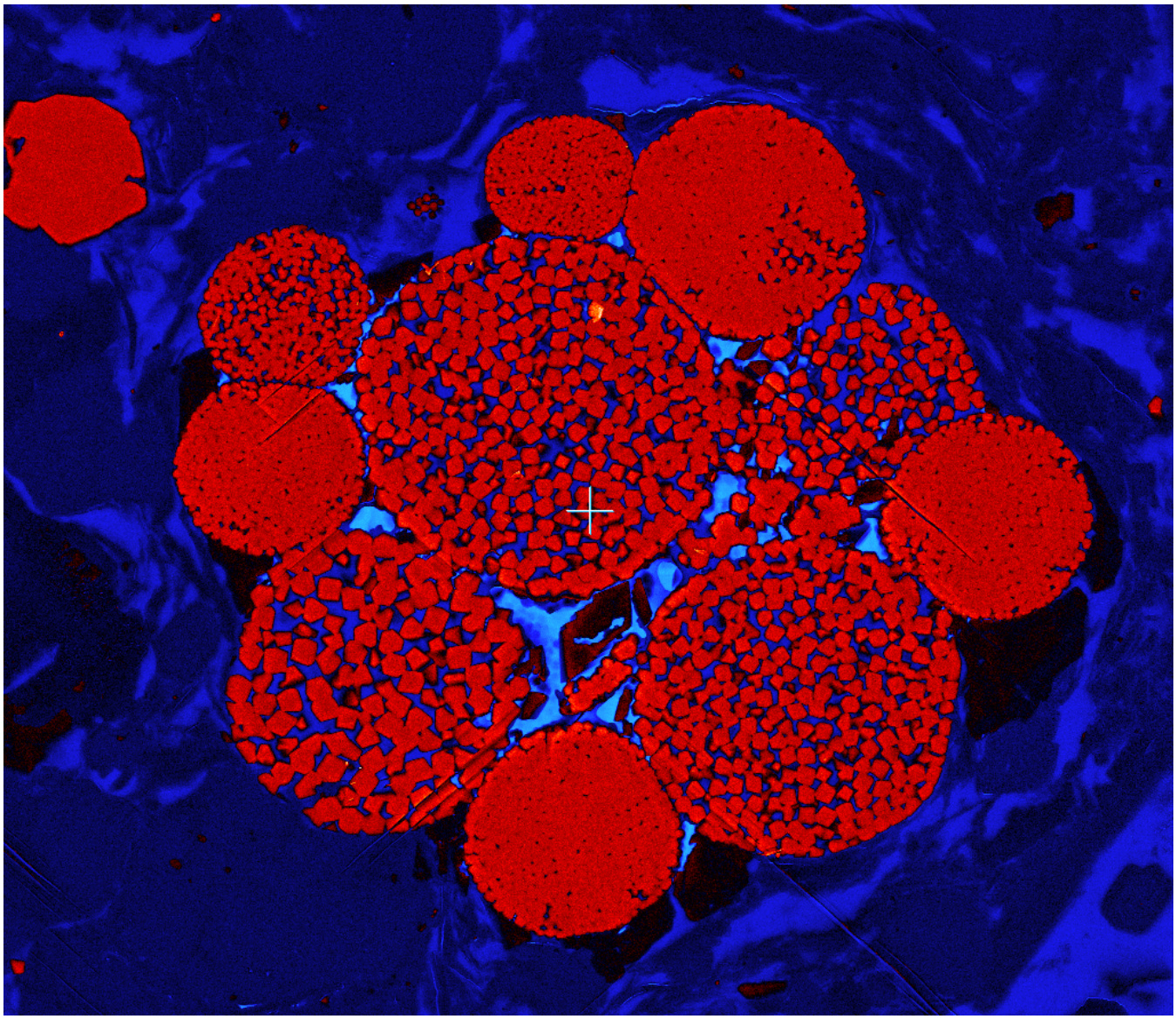

Report of Investigations 17 Series XII, 2013

Cover:
Pyrite framboid showing significant intraparticulate micro- and nanoscale pores from the Kentucky Geological Survey Marvin Blan No. 1 well at a depth of 1,879 ft in the Devonian New Albany Shale (magnification 8,000X, backscatter scanning electron microscopy image of sample prepared using argon-ion beam milling). Photo by Robert Reed, Texas Bureau of Economic Geology. False-color post-processing by Brandon C. Nuttall.

Kentucky Geological Survey
James C. Cobb, State Geologist and Director
University of Kentucky, Lexington

Middle and Late Devonian New Albany Shale in the Kentucky Geological Survey Marvin Blan No. 1 Well, Hancock County, Kentucky

Brandon C. Nuttall

Report of Investigations 17 Series XII, 2013

Our Mission

Our mission is to increase knowledge and understanding of the mineral, energy, and water resources, geologic hazards, and geology of Kentucky for the benefit of the Commonwealth and Nation.

Earth Resources—Our Common Wealth

www.uky.edu/kgs

Technical Level

General Intermediate Technical

ISSN 0075-5591

Contents

Figures

Figures
(Continued)

Figures
(Continued)

Tables

Middle and Late Devonian New Albany Shale in the Kentucky Geological Survey Marvin Blan No. 1 Well, Hancock County, Kentucky

Brandon C. Nuttall

Abstract

A 30-ft section of core was recovered in the Grassy Creek Member of the New Albany Shale in the Kentucky Geological Survey Marvin Blan No. 1 well, Hancock County, Ky. (permit 104925, API No. 16091013960000). Analysis characterized the New Albany Shale as a regional seal for preventing vertical migration of carbon dioxide stored in deeper zones, as a natural gas reservoir, and for its potential for enhanced gas recovery and sequestration of carbon dioxide. A show of natural gas at the top of the New Albany Shale was encountered during drilling. Core was recovered in an aluminum sleeve cut into 3-ft sections. The sleeved sections were capped, sealed, and shipped to Weatherford Laboratories for analysis. An X-ray computed tomography scan of the core, a standard open-hole nuclear log suite, and spectral gamma-ray data formed the basis for establishing a sampling and analysis protocol. Three 1-ft intervals were selected for archiving and were sealed in wax. The remaining core was slabbed. The quarter-section slabs were reserved for examination and archiving. The three-quarter-section slabs were photographed and sampled.

The New Albany Shale in the Blan well averages 9.5×10^{-5} md permeability with a compressive strength of 13,487 psi, a static Young's modulus of 1.58×10^{6} psi, and a static Poisson's ratio of 0.20. These properties demonstrate that the shale is an adequate seal for deeper reservoirs. Although thermal maturity is low, the shale is oil-prone, with excellent marine kerogen and bitumen contents. The methane gas content is 55.9 standard cubic feet of gas per ton of shale. This low gas content, when considered in light of low permeability, indicates the New Albany has low potential for thermogenic gas production in the area of the Blan well. Economic gas recovery would likely require horizontal drilling and advanced well-completion technologies. Adsorption isotherms indicate an estimated carbon dioxide gas content of 137.7 scf/ton at an estimated reservoir pressure of 812 psi, indicating preferential adsorption. In addition, as much as 181 tons of carbon dioxide could be sequestered per acre in the New Albany Shale (over its total thickness), suggesting a possible mechanism for enhanced natural gas recovery.

Introduction

The emergence of continuous, organic-rich shale plays as significant domestic natural gas resources has led to modern drilling and completion technologies being applied to develop shale gas in sedimentary basins across the United States, including the Illinois Basin portions of southern Illinois, southwestern Indiana, and western Kentucky (Hasenmueller and others, 2000). In addition to being a natural gas resource, relatively impermeable

shales are being investigated as regional seals for deep carbon sequestration reservoirs. The Middle and Late Devonian New Albany Shale is a regional, black, fissile, organic-rich, low-permeability, fractured gas shale that underlies much of the area of the Illinois Basin (Hasenmueller and others, 2000). Devonian shale gas was first used in 1825 for streetlights (Orton, 1891; U.S. Department of Energy, Office of Fossil Energy, 2001; Natural Gas, 2003; Lash and Lash, 2011). In Kentucky, Devonian black shale was first exploited circa 1856 when an oil distillation plant for processing shale to kerosene was constructed near Vanceburg, Lewis County, eastern Kentucky (Miller, 1919). The Rock Haven Gas Field in Meade County, Ky., on the eastern margin of the Illinois Basin, was discovered in 1858 (Eyl, 1922; Jillson, 1922). During the Civil War, 1863–65, drilling for brine in the vicinity of Doe Run, also near Rock Haven, encountered shale gas that was used as fuel to evaporate the brines for manufacturing salt (Orton, 1891; Hamilton-Smith, 1993). Early geologic maps of Meade County (Sutton and Wagner, 1930) show gas wells associated with salt works.

Considering the regional distribution of the Devonian shale and its low permeability, Busch and others (2008) and Nuttall and others (2009) have examined the CO_2 adsorption in black shale as a mechanism to enhance its sealing capacity and the potential for enhanced gas production. The Incentives for Energy Independence Act of 2007 (Second Special Session, House Bill 1, Section 57, www.lrc.ky.gov/record/07s2/HB1.htm) directed the Kentucky Geological Survey to conduct research to better understand shale as a potential reservoir seal for deep sequestration targets and as a target for sequestering CO_2 and enhanced natural gas production. The act also established a requirement to drill a deep sequestration test well in the Western Kentucky Coal Field. A site in eastern Hancock County was selected to meet these requirements, with the goal to test the maximum number of potential reservoirs and sealing zones while remaining within budget limitations. In addition to funding from House Bill 1 and the Midwest Geological Sequestration Consortium, funding was secured from industry and government partners. The Kentucky Geological Survey Marvin Blan No. 1 research well presented an opportunity to advance our understanding of the New Albany Shale. The Blan well was spudded April 24, 2009, and completed June 15, 2009, at a total depth of 8,126 ft in the Precambrian Middle Run Formation (Bowersox and Williams, in press). Thirty feet of full core was recovered from the New Albany Shale during drilling, and laboratory analysis provided a range of data critical to assessing gas content and carbon dioxide sequestration potential.

Geologic Setting

The Blan well is located in eastern Hancock County on the eastern flank of the Illinois Basin, western Kentucky (Fig. 1). The Devonian New Albany Shale thickens (Fig. 2) and deepens (Fig. 3) westward away from the location of the Blan well. Previous work (Hamilton-Smith, 1993; Roen and Kepferle, 1993; Hasenmueller and others, 2000) indicates the New Albany Shale in Hancock County consists of the Blocher, Selmier, and Grassy Creek Members (Fig. 4). Hasenmueller (1993) provided petrographic descriptions of the members of the New Albany Shale. In practice, subsurface stratigraphy of these shale units is based on gamma-ray differences. The Blocher Member is the lowest member of the New Albany Shale in Kentucky. Hasenmueller (1993) described the unit as "distinct [as] the only brownish-black shale unit that contains much calcite." A characteristic gamma-ray and density log signature that meets that criteria was established using advanced downhole lithologic logs that indicate carbonate content, available for the North Coast No. 1 Mudd-Whobrey well in Grayson County (kgs.uky.edu/kgsweb/DataSearching/OILGAS/OGresults.asp?recno=130135&areatype=recno). The overlying Selmier Member of the New Albany Shale is a greenish-gray shale with a lower gamma-ray signature than the Blocher Member, usually between 150 and 200 API units. The organic-matter- and pyrite-rich Grassy Creek Member is the uppermost unit of the New Albany Shale and has a high gamma-ray response often greater than 300 API units.

Methods

Thirty feet of 4-in.-diameter core from the Grassy Creek Member of the New Albany Shale was recovered in the Blan well over a depth of 1,875 to 1,904 ft. The cored interval started 10 ft be-

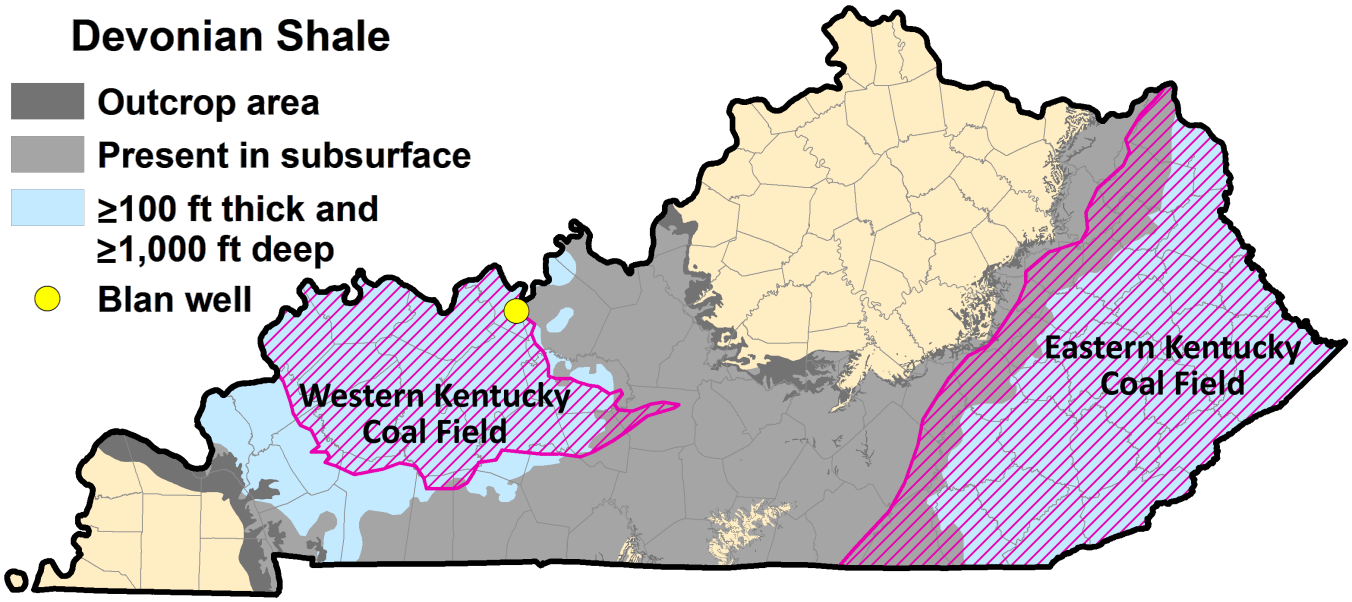

Figure 1. Location of the Blan well (yellow dot), Hancock County, in the Western Kentucky Coal Field (purple shading).

low the top of the New Albany Shale (Fig. 5). The core was retrieved in an aluminum sleeve, which was cut into 3-ft sections. The original coring plan called for adding mineral oil to the annulus between the cored material and the aluminum sleeve to help cushion the material during transport, but the small size of the annulus precluded this procedure. Plastic caps were placed on each end of the cut sections, sealed with band clamps for preservation, and shipped to Weatherford Laboratories in Houston, Texas. At Weatherford, a suite of rock properties, discussed below, were measured in the cored sections.

X-ray computed tomography (CT) scans of the core, along with open-hole gamma-ray, density, and spectral gamma-ray logs, were used to establish a sampling and analysis protocol for shale characterization. Three 1-ft intervals were selected to be typical of a 10-ft interval of core at depths of 1,877–1,878, 1,885.5–1,886.5, and 1,897–1,898 ft and were archived by wrapping them in plastic film and aluminum foil and then sealed with wax. After the preserved samples were removed, the remaining core was cut and the smaller quarter-slab portion was reserved for archiving. Density, porosity, oil and gas saturations, and permeability (pressure decay from shale rock properties and mercury injection capillary pressure measurements) were measured to assess reservoir properties. As appropriate for a selected analysis, samples were processed on an as-received basis and sometimes oven-dried to expel volatiles (water, natural gas liquids, etc.). Thin sections, X-ray diffraction of bulk and clay fractions, and CT and scanning electron microscopy (SEM) imaging were used to examine lithology and petrography, including type and distribution of porosity. Gas content was investigated using CO_2 and methane adsorption isotherms. Maturity was investigated using Rock-Eval pyrolysis and Leco total organic carbon in zones with higher and lower gamma-ray responses related to variations in organic content. Engineering and injection zone data were acquired to help characterize the response to fracture stimulation. The initial sampling plan and final data acquisition are summarized in Figure 6.

A sample was submitted to Princeton University for geomechanical assessment using the beam-bending method for determining permeability in low-permeability media (Scherer, 2004; Scherer and others, 2007). The core was also submitted to the Texas Bureau of Economic Geology for an examination of the micro- and nanoporosity system in the shale using focused-argon-ion beam milling (Loucks and others, 2009).

After coring the New Albany, drilling continued to a depth of 3,660 ft, at which point a standard suite of open-hole nuclear logs, including spectral gamma-ray, were acquired. Digital files (LAS) of these log data were recorded at 0.5-ft intervals for

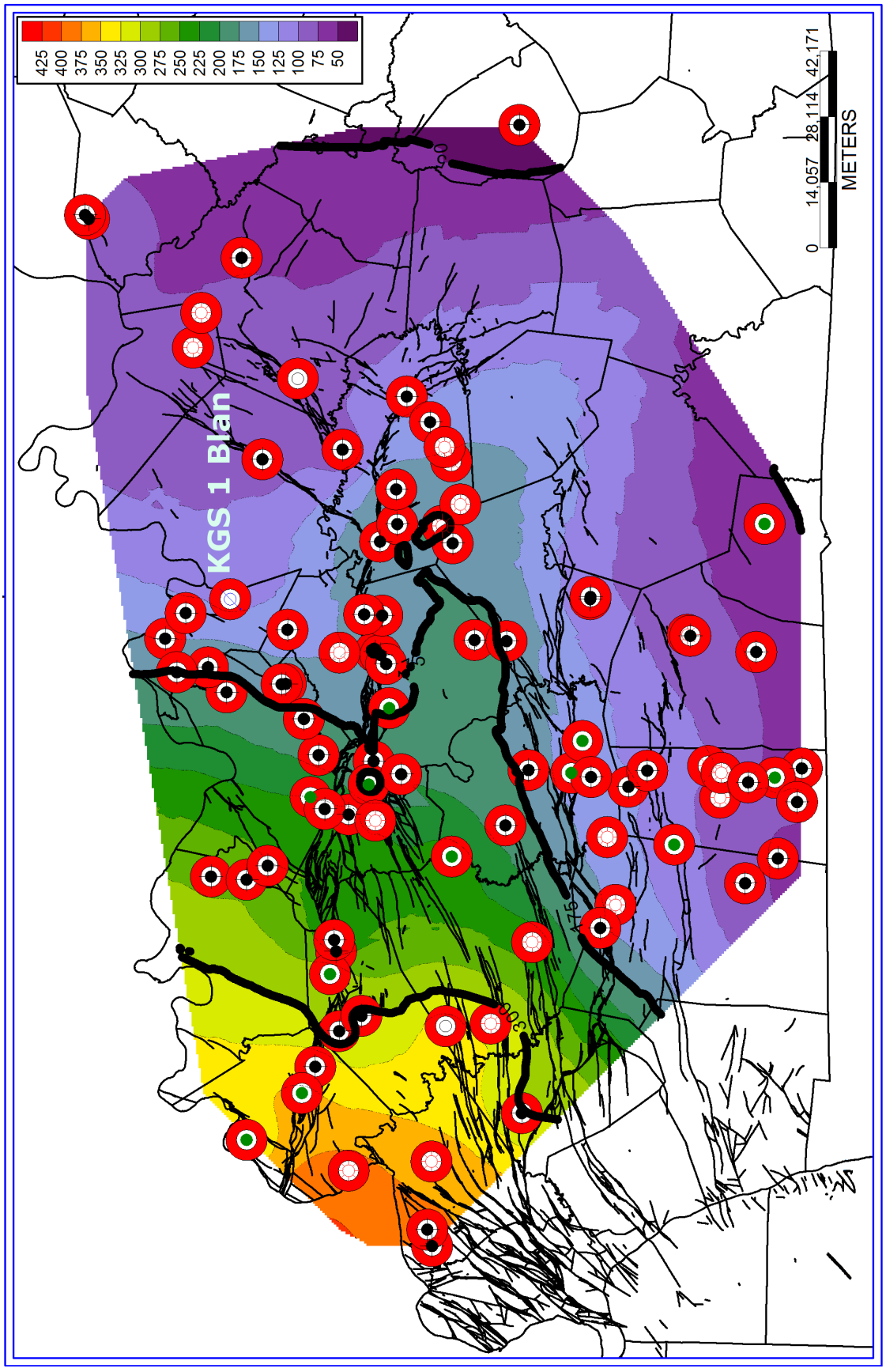

Figure 2. Thickness (in feet) of the New Albany Shale, based on correlated digital well logs in western Kentucky.

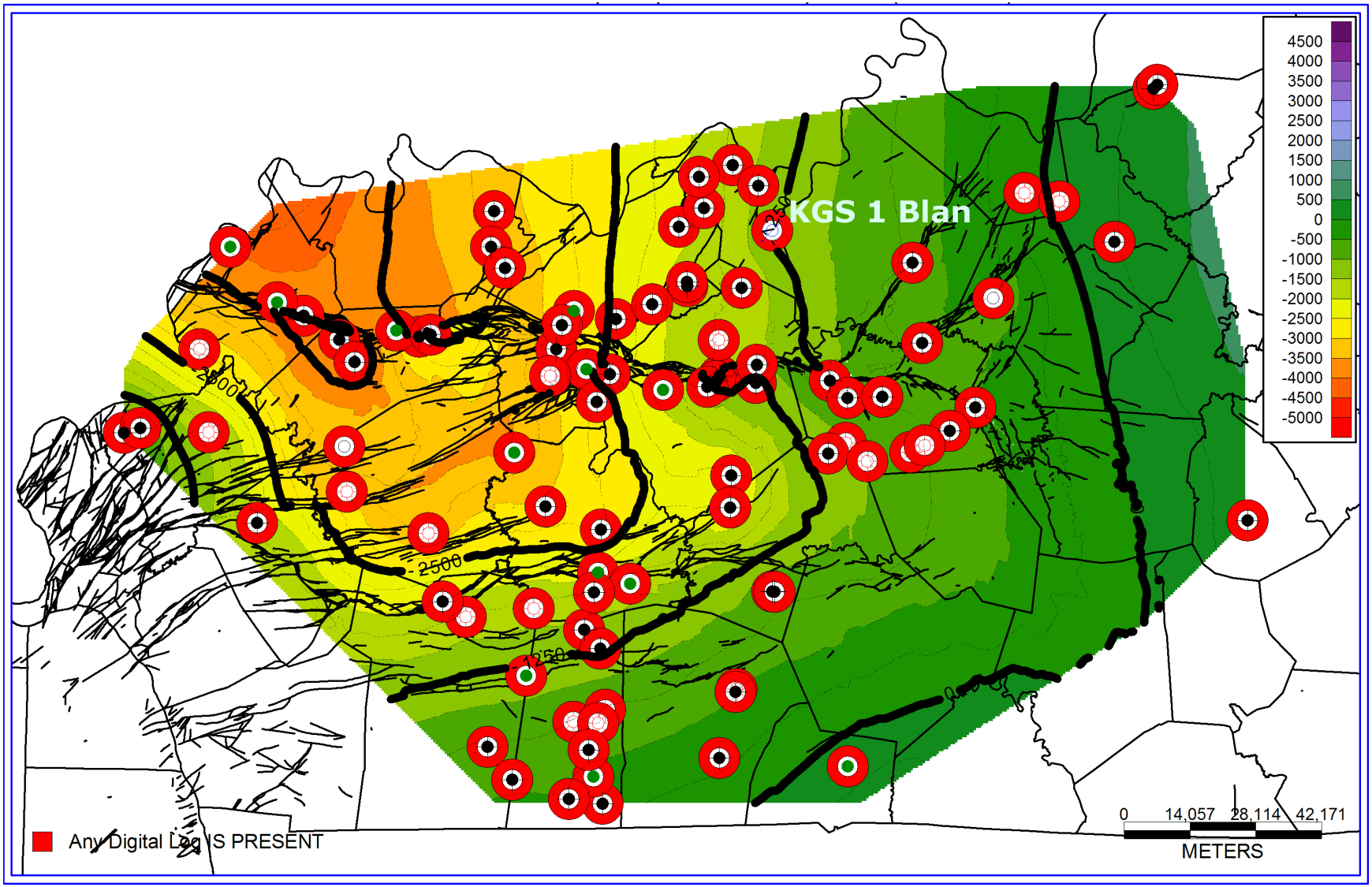

Figure 3. Structure (feet) on the top of the Devonian New Albany Shale in western Kentucky based on correlated digital well logs.

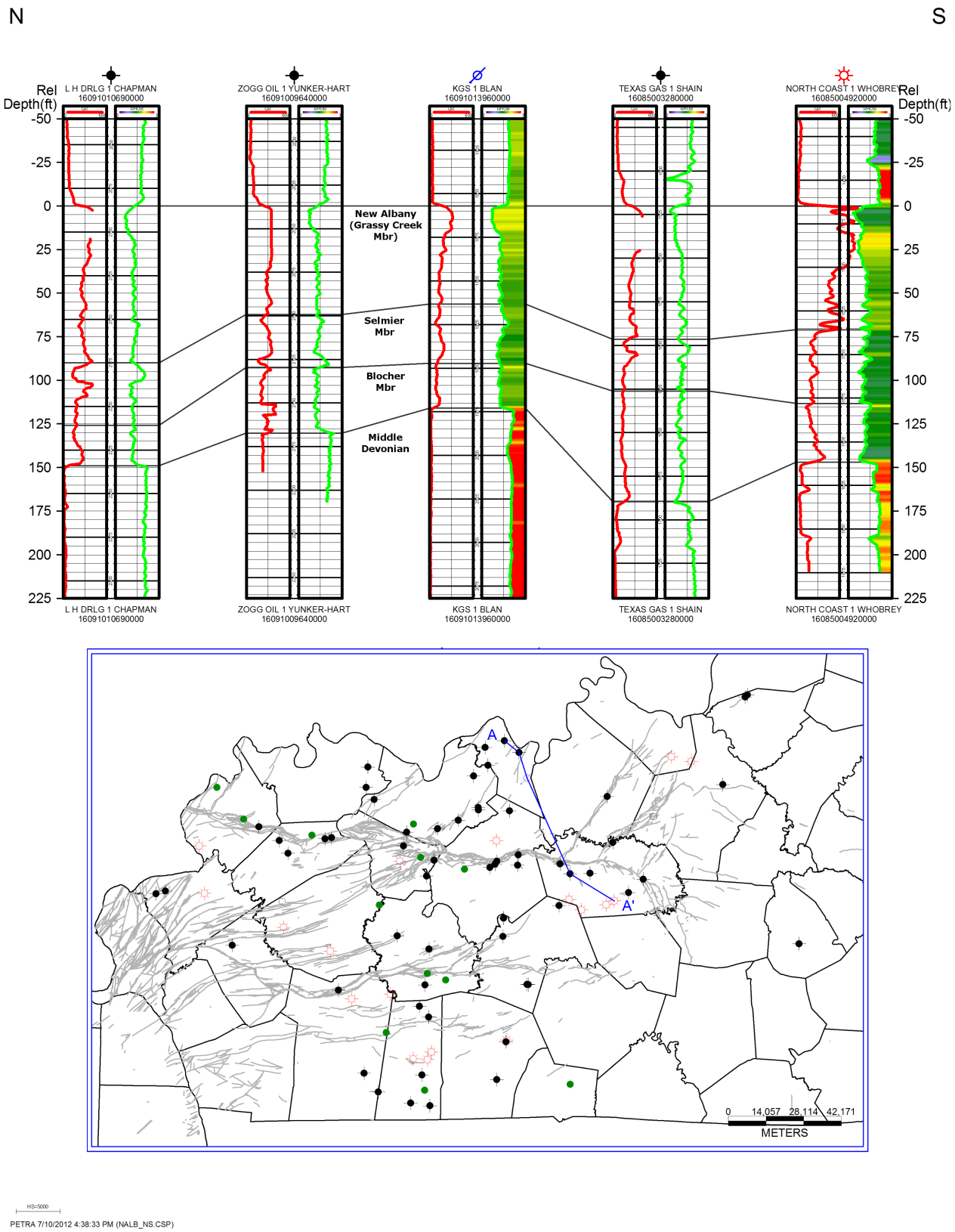

Figure 4. North-south stratigraphic cross section of the New Albany Shale (horizontal distance between wells not to scale). Gaps in gamma-ray trace (red, 0–600 API) for some wells indicate no data (off-scale on analog recording equipment). The range of the bulk-density trace (green) is 2.0 to 3.0 g/cm^3.

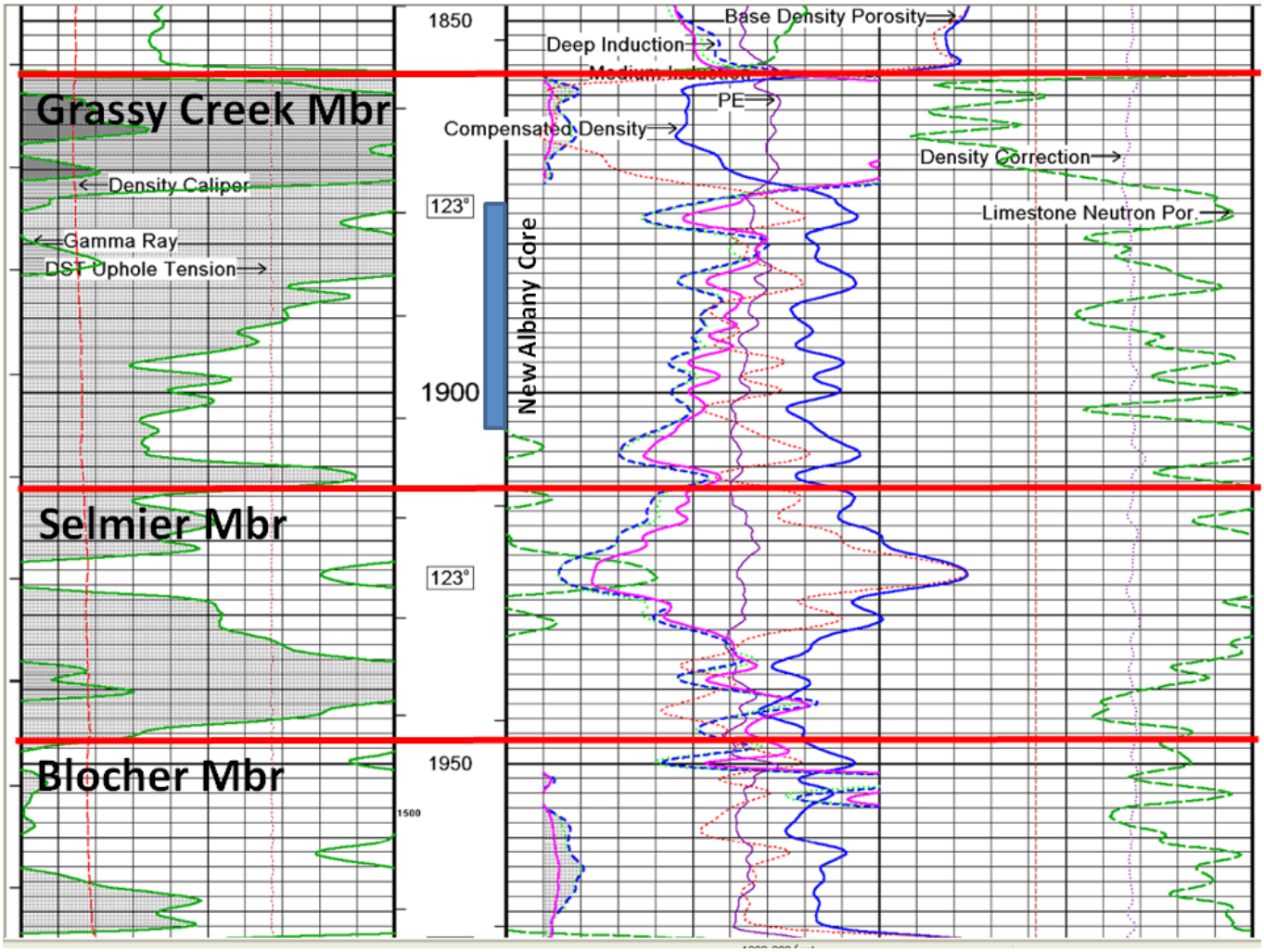

Figure 5. Gamma-ray and porosity log through the New Albany Shale section in the Blan well. Base of shale is at the bottom of the illustrated interval.

further analysis. At 3,660 ft, 8.625-in. casing was set and cemented to surface. Drilling then continued to a total depth of 8,126 ft in the Precambrian Middle Run Formation. Additional cores were recovered to assess potential deeper carbon storage reservoirs and seals. The log and core analyses for these deeper zones are discussed in Bowersox and Williams (in press).

Mineralogy

Analysis of the spectral gamma-ray log (Fig. 7) indicates that in the Grassy Creek Shale interval, the clay fraction is dominantly mixed-layer clays, illite, and mica. X-ray diffraction analysis of the bulk and clay fractions in the high- and low-gamma-ray zones (Fig. 8) confirmed the spectral gamma-ray data and shows that illite and mixed-layer clays average about 50 weight-percent, and quartz averages 34 weight-percent. The principal difference is the abundance of pyrite, which equals 13 weight-percent in the high-gamma-ray zone versus 2 weight-percent in the low-gamma-ray zone. This difference in pyrite content is an indicator of increasingly dysoxic conditions and the degree of preservation of organic matter. Higher organic content is associated with higher uranium content, as indicated on the spectral gamma-ray (Fig. 6) and open-hole natural gamma-ray logs (Fig. 5).

Shale Rock Properties, Total Organic Carbon, and Maturity

Shale rock properties are a suite of routine laboratory analyses of crushed shale core, includ-

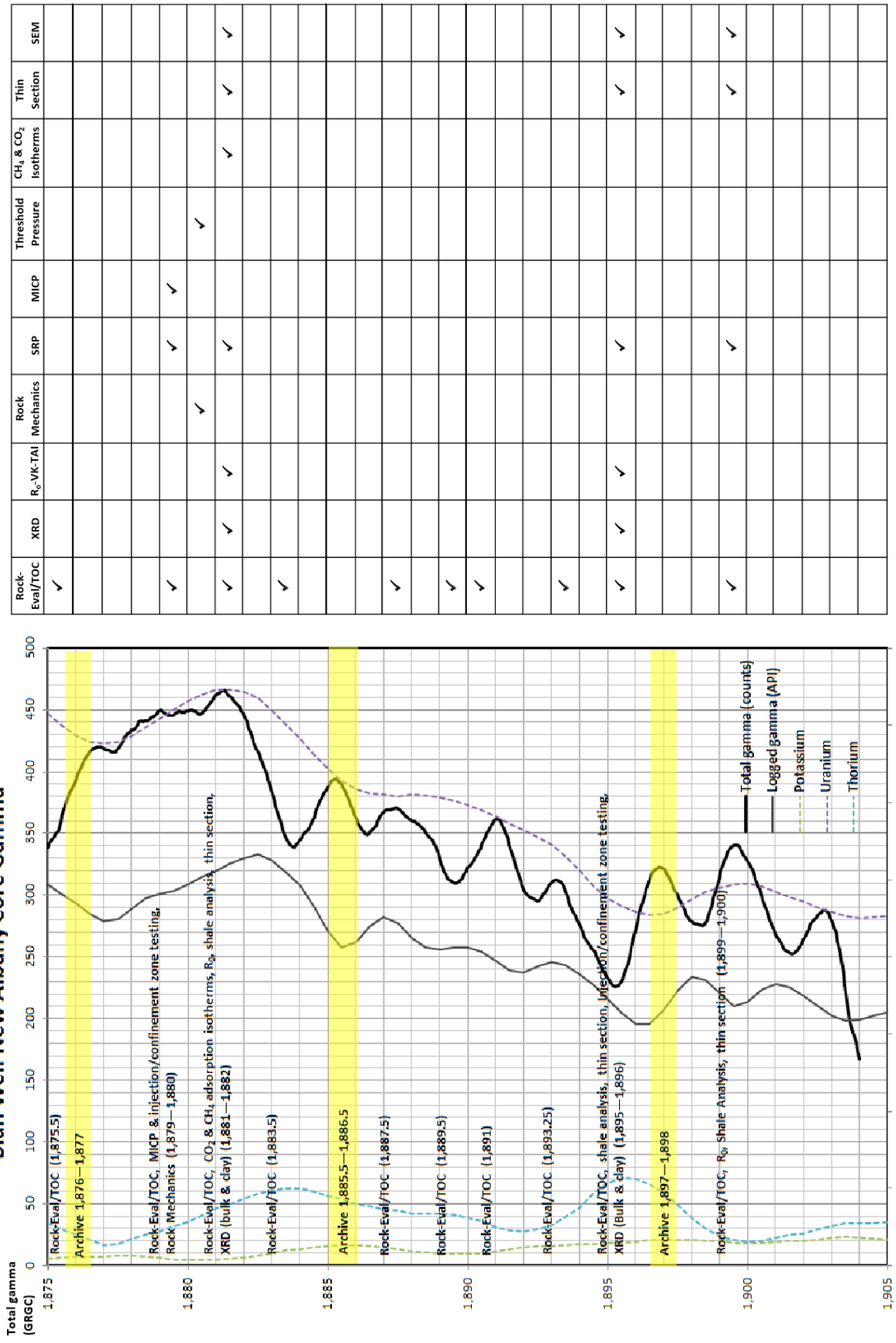

Rock-Eval/TOC	XRD	R_o-VK-TAI	Rock Mechanics	SRP	MICP	Threshold Pressure	CH_4 & CO_2 Isotherms	Thin Section	SEM
✓									
✓				✓	✓				
			✓			✓			
✓	✓	✓		✓			✓	✓	✓
✓									
✓									
✓									
✓									
✓									
✓									
✓	✓	✓		✓				✓	✓
✓				✓				✓	✓

Figure 6. Initial analysis plan for the Blan well and laboratory analysis actually performed.

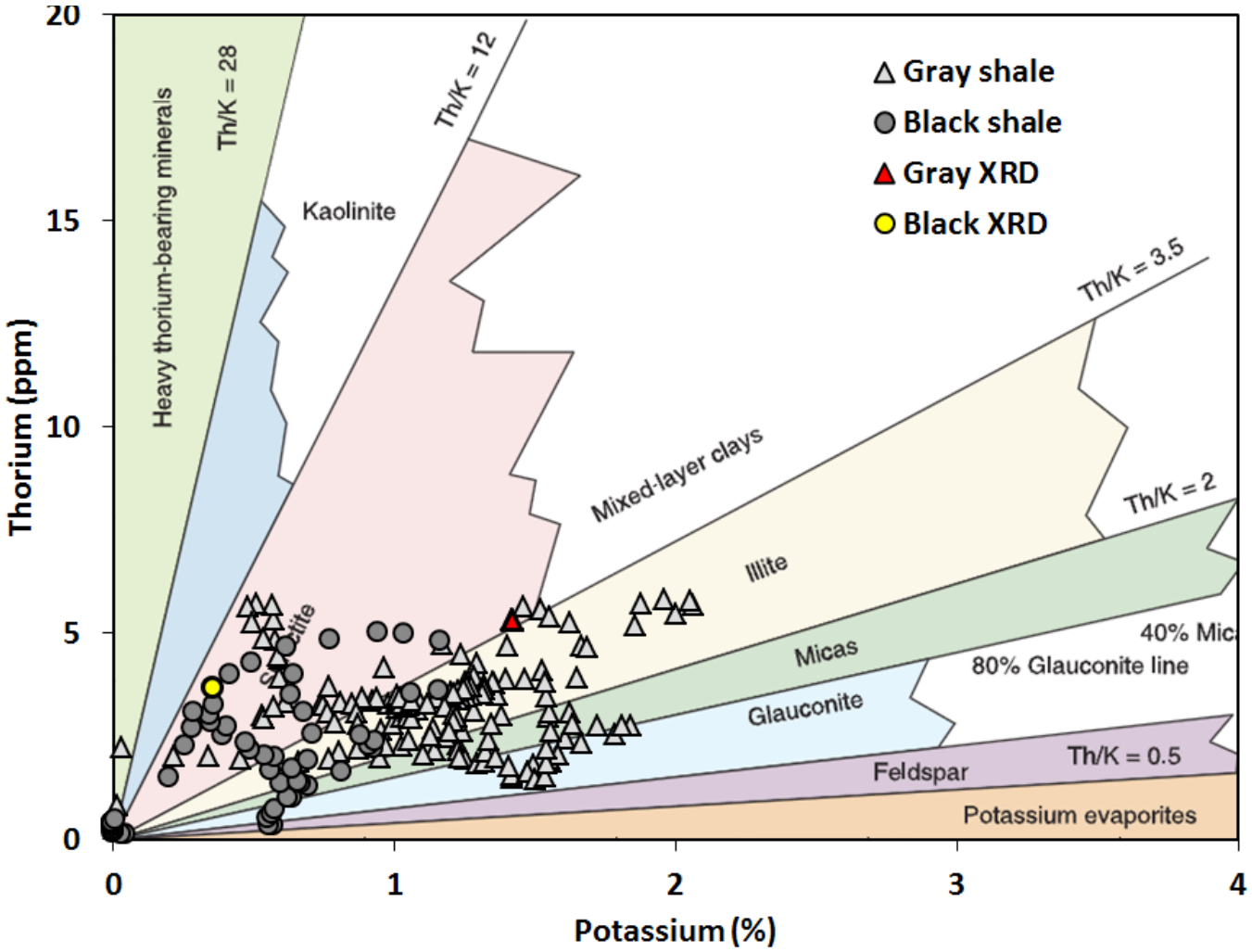

Figure 7. Thorium-potassium cross plot from the spectral gamma-ray log for determining clay mineralogy. "XRD" refers to spectral gamma-ray data at depths from which X-ray diffraction samples were collected. Chart GN-8-11, Weatherford Laboratories (2009). Used with permission.

ing bulk density, oil, gas, and water saturation as a percentage of pore volume; gas-filled porosity as a percentage of the bulk volume; and permeability on an as-received and dry basis. Permeability of the New Albany Shale determined from shale rock properties ranges from 0.77×10^{-5} to 18×10^{-5} md (average 9.48×10^{-5} md) (Table 1). A sample taken from 1,880.4 ft was tested to investigate the threshold injection pressure with respect to CO_2. The sample was prepared by saturating it with a potassium chloride brine. The test was unsuccessful, and no CO_2 entered the sample over the range of pressures tested (850 to 1,500 psi). In the area of the Blan well, the New Albany Shale is not water-saturated, indicating the brine may have interacted with swelling clays, resulting in damage to the sample. A fresh sample was collected from 1,879 ft, and a mercury injection capillary pressure test was conducted. From this test, the permeability to air was calculated to be 11×10^{-5} md, within the range of permeability determined from shale rock properties testing. Average pore volume from shale rock properties analysis is 6.2 percent of the bulk volume; water saturation averages 46.4 percent; oil averages 37.3 percent; and gas averages 37.3 percent of the pore volume. Figure 9 illustrates the relation between permeability and gas saturation as a percentage of the total porosity.

Table 2 and Figure 10 present the data and geochemical log from Rock-Eval pyrolysis analysis. Parameters measured by Rock-Eval are explained in Jarvie (1991), Merrill (1991, Table 4,

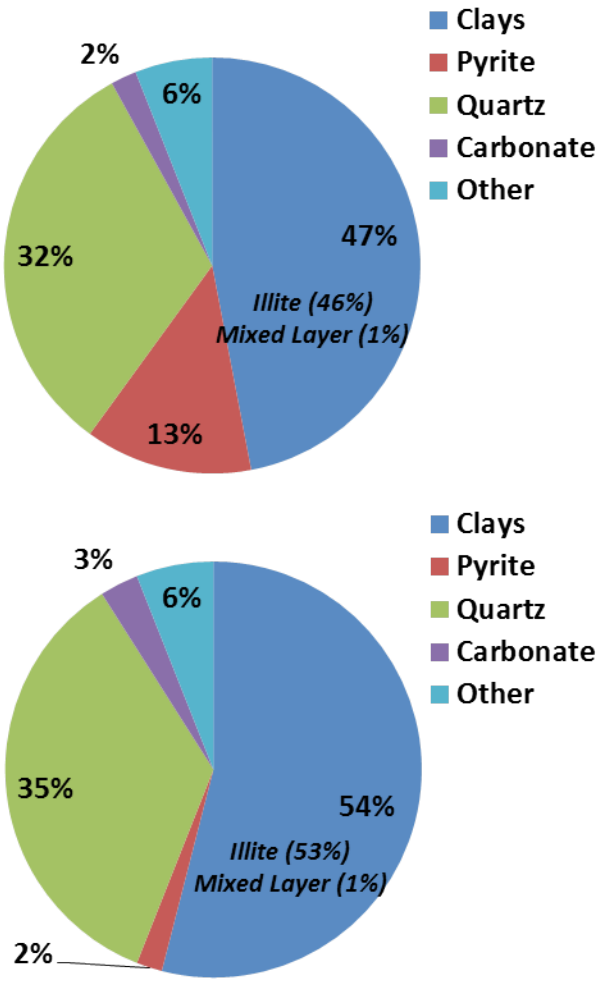

Figure 8. Comparison of X-ray diffraction mineralogy (weight-percent) in a high-gamma-ray zone at a depth of 1,881 ft (sample 1-7P, top) and a lower-gamma-ray zone at a depth of 1,895 ft (sample 1-21P, bottom).

p. xvii), and Philip and Galvez-Sinibaldi (1991). Rock-Eval measurement of 10 samples shows total organic carbon in the New Albany to range from 4.75 to 9.74 weight-percent (Fig. 10, log 1), and hydrocarbon potential from S2 measurement (Fig. 10, log 2) ranges from 27.27 to 56.38 mg/g. These data indicate the New Albany Shale in the Blan well has good to excellent potential but that it is an immature source rock with abundant marine Type II oil-prone kerogen. Much of the organic matter is finely dispersed or sometimes concentrated in thin laminae of amorphous kerogen (bitumite) and vitrinite consisting mainly of *Tasmanites* and palynomorphs (see in particular petrology for sample 1-25P in Appendix B). For samples 1-7P (1,881 ft) and 1-25P (1,899.9 ft), the thermal alteration index

Table 1. Shale rock properties summary.

Sample ID	Top Depth (ft)	Bottom Depth (ft)	As-Received Bulk Density (g/cm³)	As-Received Grain Density (g/cm³)	As-Received Water Saturation (% of Pore Volume)	As-Received Oil Saturation (% of Pore Volume)	As-Received Gas Saturation (% of Pore Volume)	As-Received Gas-Filled Porosity (% of Bulk Volume)	As-Received Pressure Decay Permeability (md)	Dry Bulk Density (g/cm³)	Dry Grain Density (g/cm³)	Dry Helium Porosity (% of Bulk Volume)
1-5SRP	1,879.5	1,879.6	2.37	2.41	38.69	32.49	28.82	2.07	0.00018	2.32	2.50	7.17
1-7SRP	1,881.0	1,881.2	2.40	2.43	47.62	34.25	18.13	1.08	0.000122	2.36	2.51	5.96
1-21SRP	1,895.0	1,895.1	2.47	2.48	56.66	38.26	5.09	0.31	0.00000777	2.42	2.57	6.13
1-25SRP	1,899.9	1,900.0	2.36	2.37	42.49	44.17	13.34	0.76	0.0000696	2.31	2.45	5.72
Average values:			2.40	2.42	46.40	37.30	16.30	1.10	0.00009484	2.35	2.51	6.20

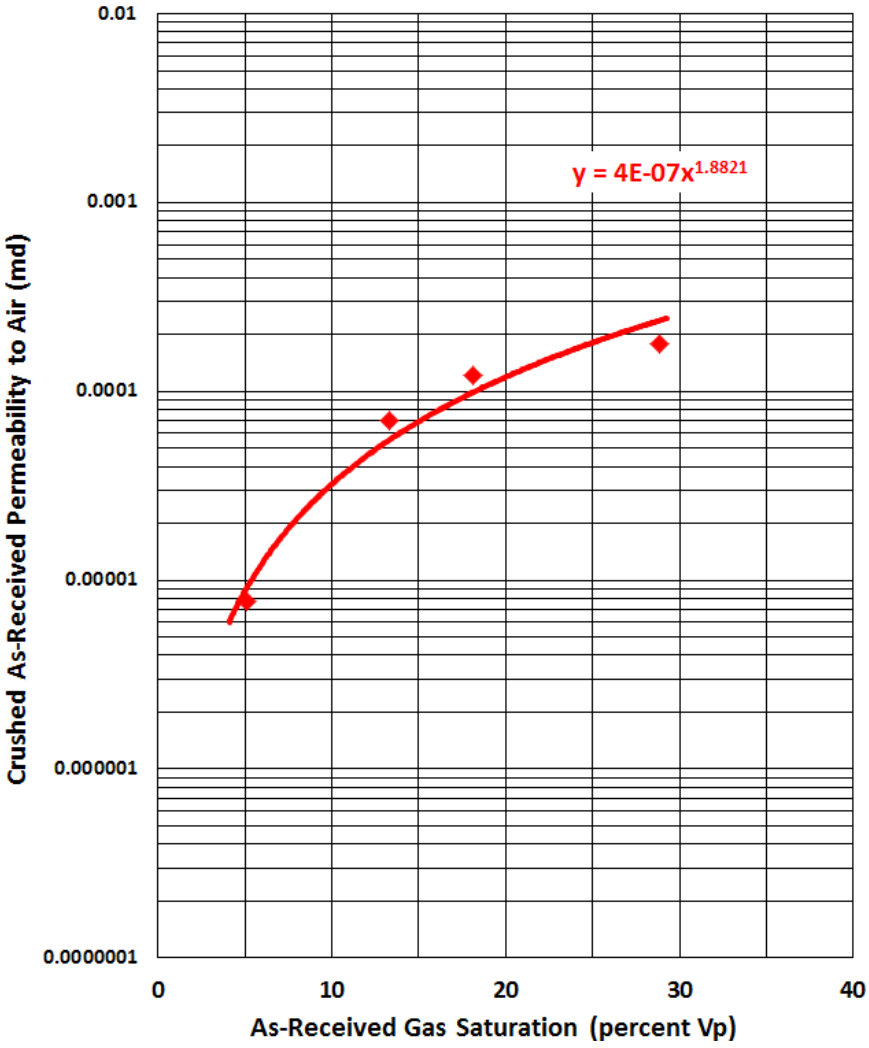

Figure 9. Rock-Eval geochemical logs for samples 1-7P (1,881 ft) and 1-25P (1,899.9 ft).

ranged from 2 to 2.3 (for both samples), indicating slight alteration.

Observed vitrinite reflectance values range from an Ro maximum of 0.45 to 0.55 percent and are considered the lower limits for oil generation (Tissot and Welte, 1984; Cole and others, 1994; Gentzis and others, 1996). For the New Albany Shale in the Blan well, percent Ro was determined from thin-section analysis to be 0.51 (sample 1-7P, 1,881.0 ft) and 0.46 (sample 1-25P, 1,899.9 ft), indicating low thermal maturity in this area, as reported by Hamilton-Smith (1993). T_{max} is the temperature of maximum hydrocarbon yield measured by Rock-Eval pyrolysis (Fig. 10). T_{max} ranges from 431 to 440°C, indicating a normalized oil content in the mature to oil and gas production range. This discrepancy between percent Ro and T_{max} was documented for the Illinois Basin by Nuccio and Hatch (1996), who suggested percent Ro suppression in the Hancock County area is between 0.25 and 0.30. Assuming this magnitude of suppression, percent Ro data for the Blan well are consistent with T_{max} and indicate low maturity, but certainly within the oil window.

A mercury injection capillary pressure test was conducted to supplement the porosity and permeability determined by shale rock properties analysis. Mercury uptake began at a pressure of 4,059.19 psia, corresponding to a pore throat radius of 0.027 µ. The reported median pore throat radius is 0.0047 µ. Porosity by mercury injection capillary pressure is 5.6 percent, a lower value than determined using shale rock properties analysis (see Table 1).

Gas Content and Sequestration Capacity

During drilling, a good natural gas kick was noted on first penetration of the New Albany Shale. The gas content measured by mud log increased to 1,316 total gas units, up from background levels of 100 to 200 units in the overlying Borden Formation. Because the New Albany has low thermal maturity at this location, the gas might be interpreted as having a biogenic origin. The distance of the well from potential updip recharge zones and the lack of detected formation water—both characteristics associated with biogenic gas generation—suggest that the gas is thermogenic, a finding supported by Schlegel and others (2011). No gas sample was collected for isotopic analysis to establish a thermogenic source.

Organic-rich shale wells are commonly completed in zones exhibiting 200 Ω or more of resistance on a deep induction log. Such zones typically correspond to higher gamma-ray, lower-density, more organic-rich intervals in shales. The deep in-

Table 2. Total organic carbon and Rock-Eval pyrolysis data.

Sample	Top Depth (ft)	Leco TOC	S1[1]	S2[1]	S3	T_{max}[1] (°C)	HI[1]	OI[1]	S2/S3[1]	S1/TOC × 100[1]	PI[1]
1-1GC	1,875.5	8.61	8.80	45.29	1.19	434	525.89	13.82	38.06	102.13	0.16
1-5GC	1,879.5	7.69	6.80	39.16	0.41	433	509.30	5.33	95.51	88.38	0.15
1-7SRP	1,881.0	8.05	4.95	44.27	1.83	431	549.66	22.72	24.19	61.51	0.10
1-9GC	1,883.5	8.80	7.23	48.07	1.26	434	546.31	14.32	38.15	82.15	0.13
1-13GC	1,887.5	9.48	10.07	55.29	0.82	435	583.04	8.65	67.43	106.20	0.15
1-15GC	1,889.5	9.74	7.85	56.38	0.50	432	578.73	5.13	112.76	80.61	0.12
1-17GC	1,891.0	6.67	10.69	44.46	0.63	438	666.27	9.44	70.57	160.22	0.19
1-19GC	1,893.25	6.92	10.67	41.89	0.43	438	605.61	6.22	97.42	154.19	0.20
1-21SRP	1,895.0	4.75	3.02	27.27	0.60	436	574.23	12.63	45.45	63.67	0.10
1-25SRP	1,899.9	8.32	5.81	51.75	0.48	440	622.22	5.77	107.81	69.81	0.10

[1]For a discussion of headings, see Merrill (1991, Table 4, p. xvii)
TOC = total organic carbon; organic richness
S1 = milligrams of hydrocarbon per gram of rock; free oil content
S2 = milligrams of hydrocarbon per gram of rock; remaining hydrocarbon potential
S3 = milligrams of organic CO_2 per gram of rock; kerogen indicator
T_{max} = degrees Celsius, temperature of maximum rate of evolution of S2 hydrocarbons; thermal maturity
HI = normalized hydrogen content (index); kerogen type indicator computed from S2
OI = normalized oxygen content (index); kerogen type indicator computed from S3
S1/TOC × 100 = ratio of free hydrocarbons to total organic carbon
PI = production index; indicates conversion of kerogen into free hydrocarbons

duction (RILD) well log, shown in Figures 11 and 12, indicates the average RILD is 65.5 Ω, well below the 200 Ω cutoff typically considered characteristic of shale-gas production zones. The induction log indicates only two thin zones that marginally exceed a 200 Ω cutoff: one near the top of the Grassy Creek Member and one near the base of the Blocher Member (base of the New Albany in this area).

Adsorption isotherms for both CO_2 and CH_4 were acquired to estimate the gas content of the New Albany Shale (Fig. 13). These isotherms indicate that at a given pressure, CO_2 is preferentially adsorbed with respect to CH_4. The Langmuir gas storage capacity model (Gs) used in this study is shown in equation 1, where V_L is the Langmuir volume and P_L is the Langmuir pressure as determined from adsorption isotherms. The laboratory data are summarized in Table 3. For this study, the calculated reservoir pressure, p, was estimated to be 812 psi using a standard hydrostatic gradient (0.433 psi/ft) at the reservoir midpoint, a depth of 1,875 ft.

$$Gs = \frac{(V_L \times p)}{(P_L + p)} \qquad \text{equation 1}$$

The CO_2 sequestration capacity of organic-rich shale can be estimated from its total organic carbon content (Nuttall and others, 2009). Total organic carbon content, in turn, can be estimated from the formation bulk-density log, using methods developed by Schmoker (1993).

$$TOC = 55.822 \times \left(\frac{RhoB_{max}}{RhoB} - 1 \right) \qquad \text{equation 2 (Schmoker, 1993)}$$

$$CO_2 = 7.9 \times TOC + 20.7 \qquad \text{equation 3 (Nuttall and others, 2009)}$$

In equation 2, $RhoB_{max}$ is maximum observed formation bulk density of the gray shales and RhoB is log-measured formation bulk density.

Schmoker (1993) derived a relation between bulk-density logs and total organic carbon (equation 2) that models the observed density of organic-rich black shales as a four-component system: matrix, pore system, pyrite, and organic matter. Schmoker's method relies on determination of an observed maximum bulk density of the gray shale intervals ($RhoB_{max}$), assuming then that observed lower densities in shale are due to increasing organic content. A histogram of formation bulk-density data acquired across the New Albany Shale

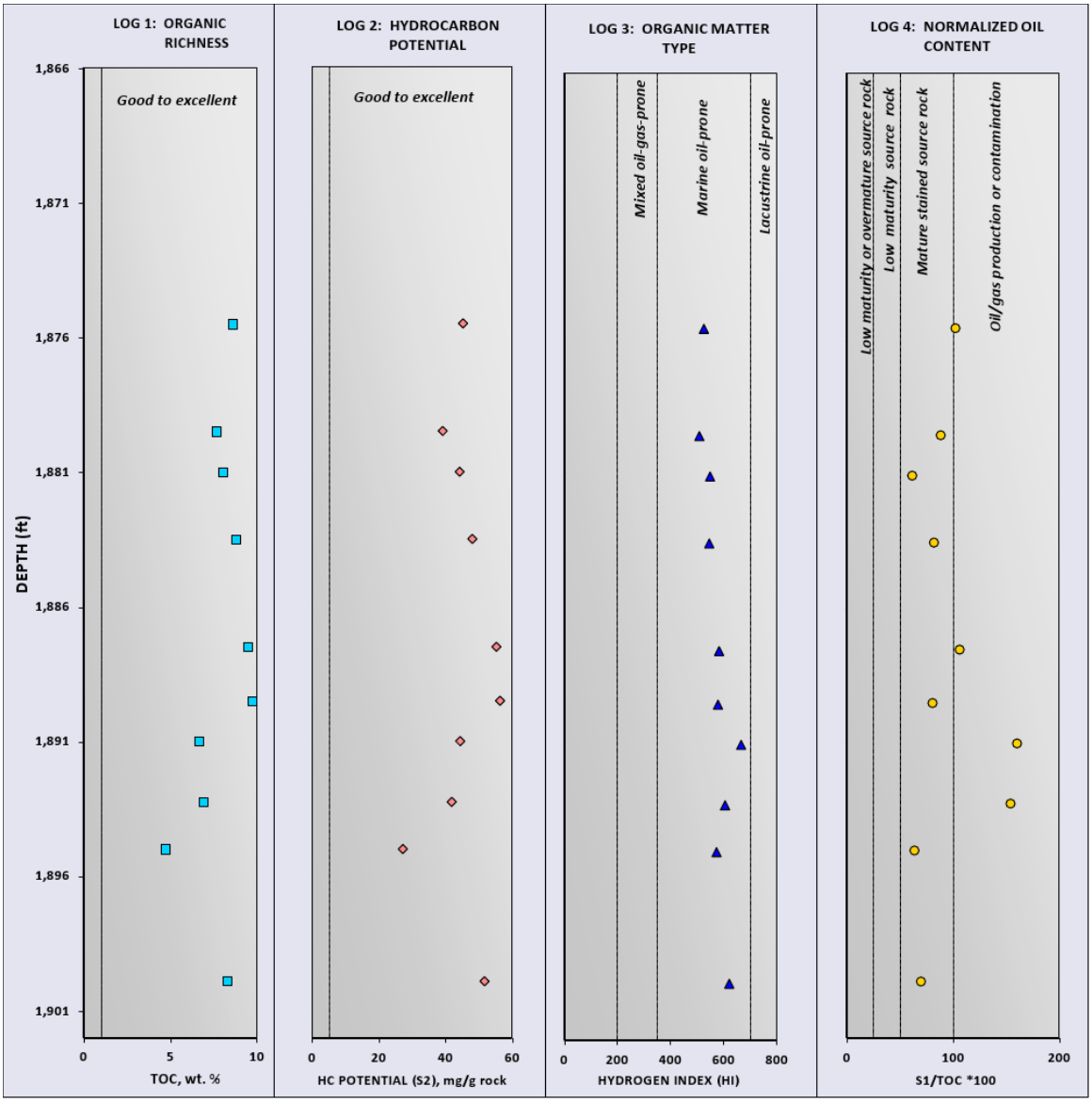

Figure 10. Permeability versus as-received gas saturation expressed as percentage of pore volume (V_p).

interval was used to select a representative gray shale density value of 2.62 g/cm^3 for $RhoB_{max}$ for calculating an initial total organic carbon log curve. Figure 14 (green dashed curve) shows the vertical distribution of calculated total organic carbon calculated from the density log in the Blan well over the New Albany Shale interval in the Blan well calculated by Schmoker's method. When compared to the laboratory-measured Leco total organic carbon values reported from core analysis, this initial calculation based on the bulk-density log seemed to result in lower-than-expected total organic carbon values. The presence of up to 13 percent pyrite (density of 4.99 g/cm^3) likely caused a lower calculated total organic carbon content. To compensate, the $RhoB_{max}$ value was adjusted using the Excel linear solver facility to minimize the root mean square difference between the log-derived and laboratory-measured total organic carbon values at depths corresponding to those of the laboratory samples. This computation yielded a $RhoB_{max}$ of 2.75 g/cm^3. The final total organic carbon estimates used for CO_2 capacity calculations were derived from this adjusted log trace (red curve in Figure 14).

CO_2 storage efficiency in organic-rich shales is unknown. Using available Langmuir isotherm data, reservoir simulation, and a Monte Carlo approach,

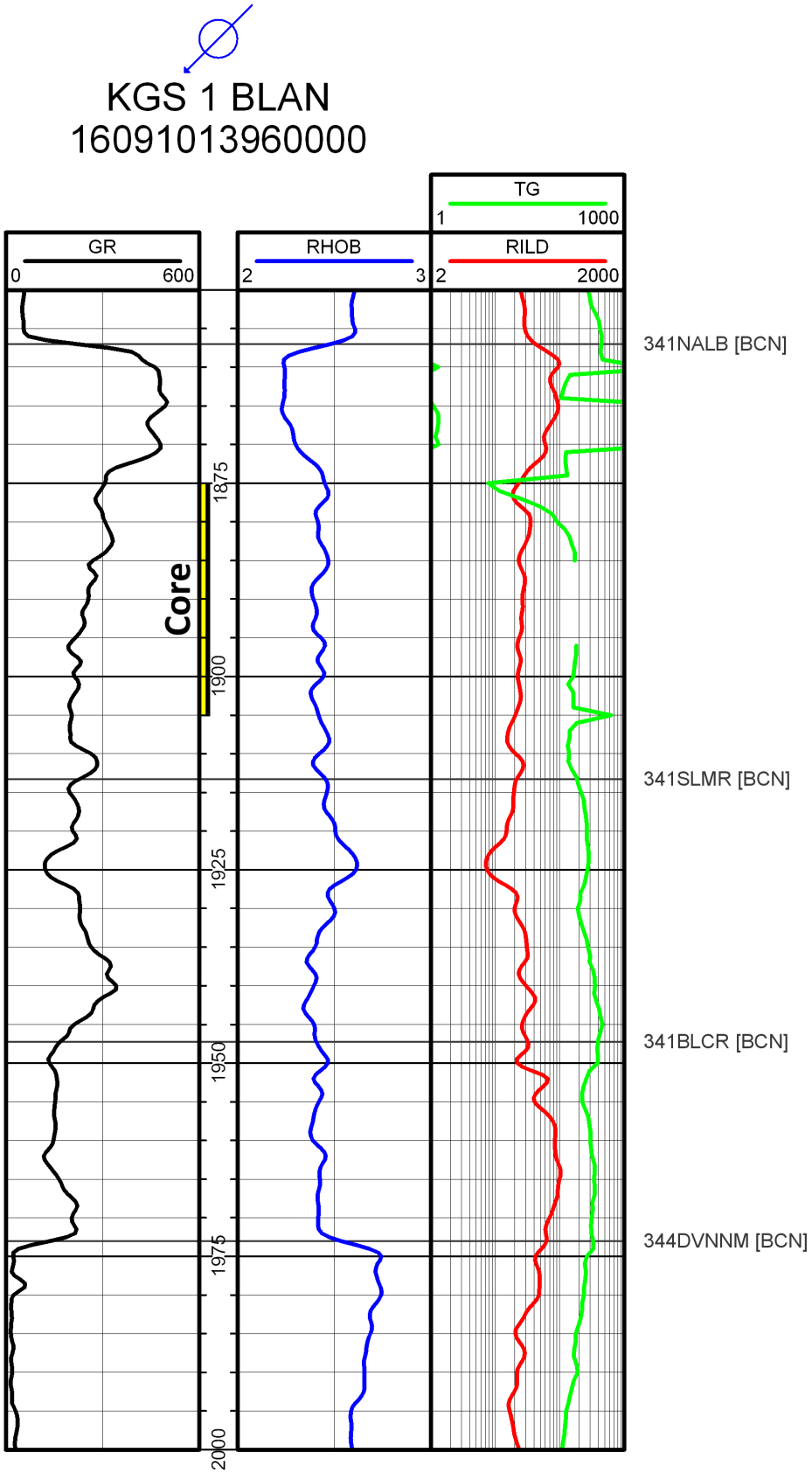

Figure 11. Gamma-ray density log of the New Albany Shale interval showing deep induction resistivity (RILD) measured in ohms (in red) and total gas (TG) in mud-log units (in green).

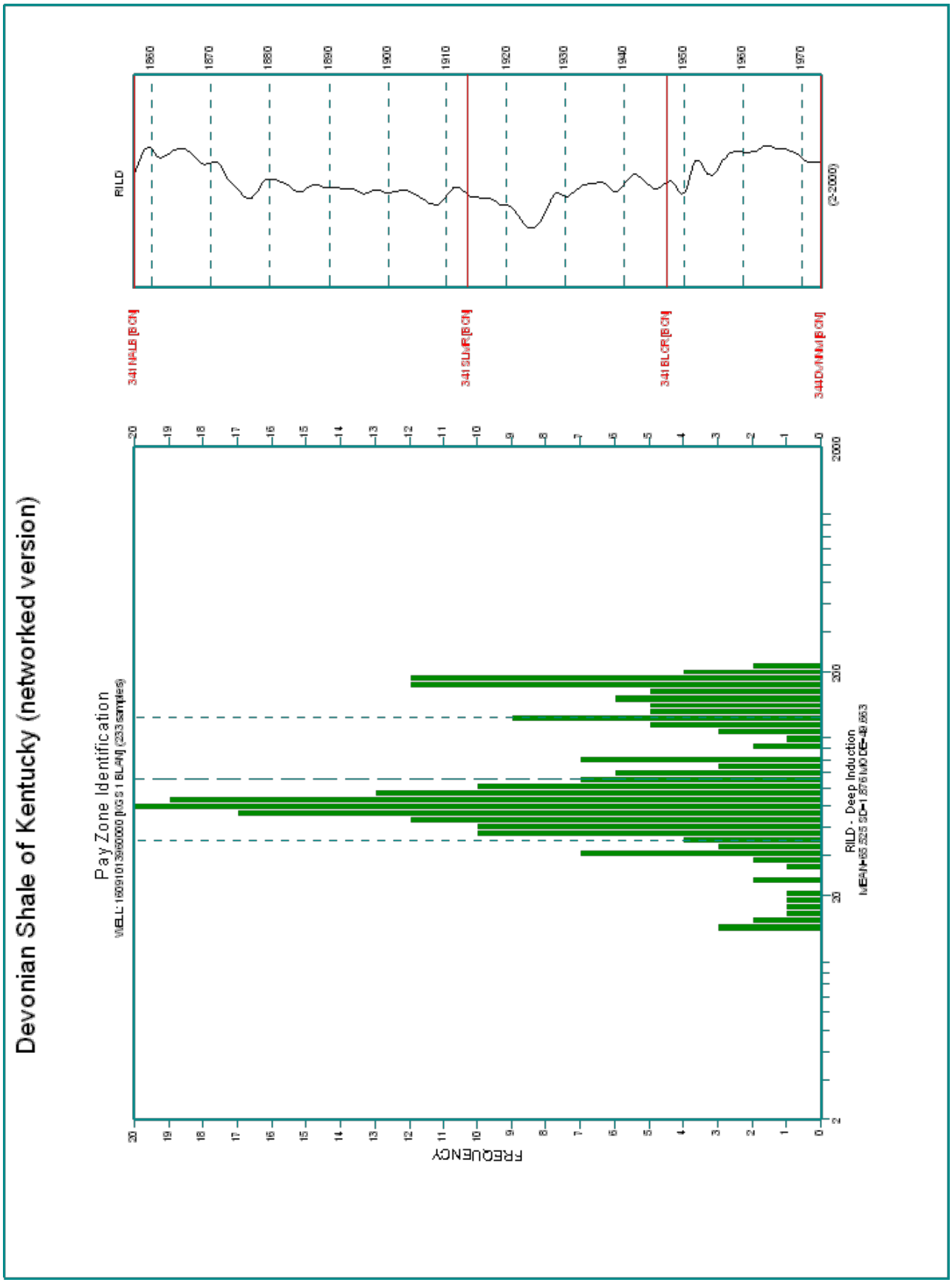

Figure 12. Observed deep induction resistivity (RILD) in ohms. Most of the New Albany in this study does not have sufficiently high resistivity (200 Ω) to identify potential gas completion intervals.

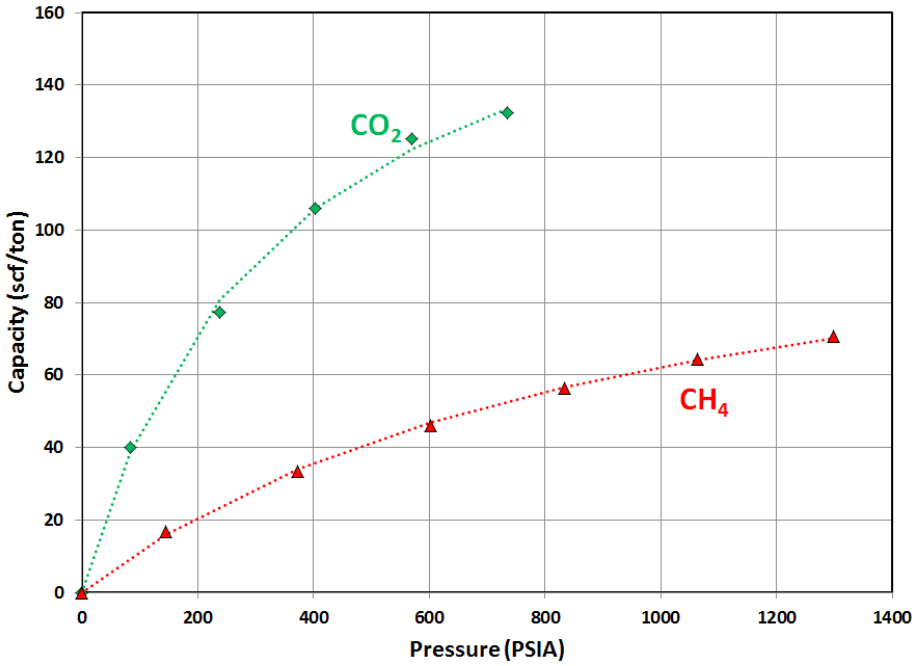

Figure 13. Carbon-dioxide and methane adsorption isotherms for the New Albany Shale in sample 43630-1, depth 1,881.0–1,881.2 ft, in the Blan well.

Carr and others (2008) developed a probabilistic estimate of storage efficiency factors for unmineable coal ranging from 28 percent (15th percentile probability) to 40 percent (85th percentile probability). As an analog for shale, this range is considered to be too high. Boswell (1996) reported a recovery factor of 17 percent for the Devonian Ohio Shale in the Big Sandy Gas Field of eastern Kentucky. This study selected a 10 percent storage efficiency factor as a conservative and reasonable estimate that is less than the recovery factor. CO_2 storage capacity was calculated on 0.5-ft increments (corresponding to the sample rate of the available digital logs). When summed by foot using the 10 percent storage efficiency factor, CO_2 storage per acre-foot of shale ranged from 0.9 ton to 2.2 tons (Fig. 15). These data yield a cumulative estimate of 181 tons of CO_2 per acre for the New Albany Shale where its thickness is 116 ft.

Table 3. New Albany Shale gas content and adsorption isotherm summary for sample 43630-1, depth 1,881.0–1,881.2 ft.

Parameter	*Methane*	*Carbon Dioxide*
Temperature, °F	75.02	75.02
Langmuir volume (V_L, scf/ton)	121.53	195.50
Langmuir pressure (P_L, psia)	953.55	340.60
Calculated reservoir pressure (p, psia)	812.00	812.00
Storage capacity (scf/ton)	55.90	137.70

Porosity Types

Porosity in organic-rich continuous shale plays strongly influences gas storage capacity (gas in place) and gas diffusion through the shale matrix (Bustin and others, 2008; Ross and Bustin, 2008; Loucks and others, 2009, 2011; Ambrose and others, 2010). In particular, Loucks and others (2009) found a direct relation between increasing maturity of the organic matter and an increase in nanopores within the organic grains. Characterizing porosity and the petrographic analysis of continuous resource plays has thus stepped beyond conventional sedimentology and into the literature of chemistry and physics (Choquette and Pray, 1970; Rouquerol and others, 1994; Zdravkov and others, 2007). The term "nanoporosity" is often used loosely—see Sondergeld and others (2010), for example. Loucks and others (2012) presented the pore type and size classification system used in this report. Pore types are interparticle and intraparticle pores between or within shale matrix material. Intraparticle pores occur within preserved organic matter. Shales also have fracture porosity at several scales. Pore size classes range from mesopores ($62.5\,\mu m \geq size < 4\,mm$) and micropores ($1\,\mu m \geq size < 62.5\,\mu m$) to nanopores ($<1\,\mu m$) and picopores ($<1\,nm$). Pores with diameters of 1 µm or less, the upper range of the nanopore size class, are resolvable on focused-ion beam-milled SEM images, whereas picopores are strictly molecular scale. According to Loucks and others (2011, 2012), it is this network of meso- to nanoscale pores and fractures that comprise the flow-path network—permeability system—for gas diffusion through the shale matrix into the fracture system induced by well stimulation.

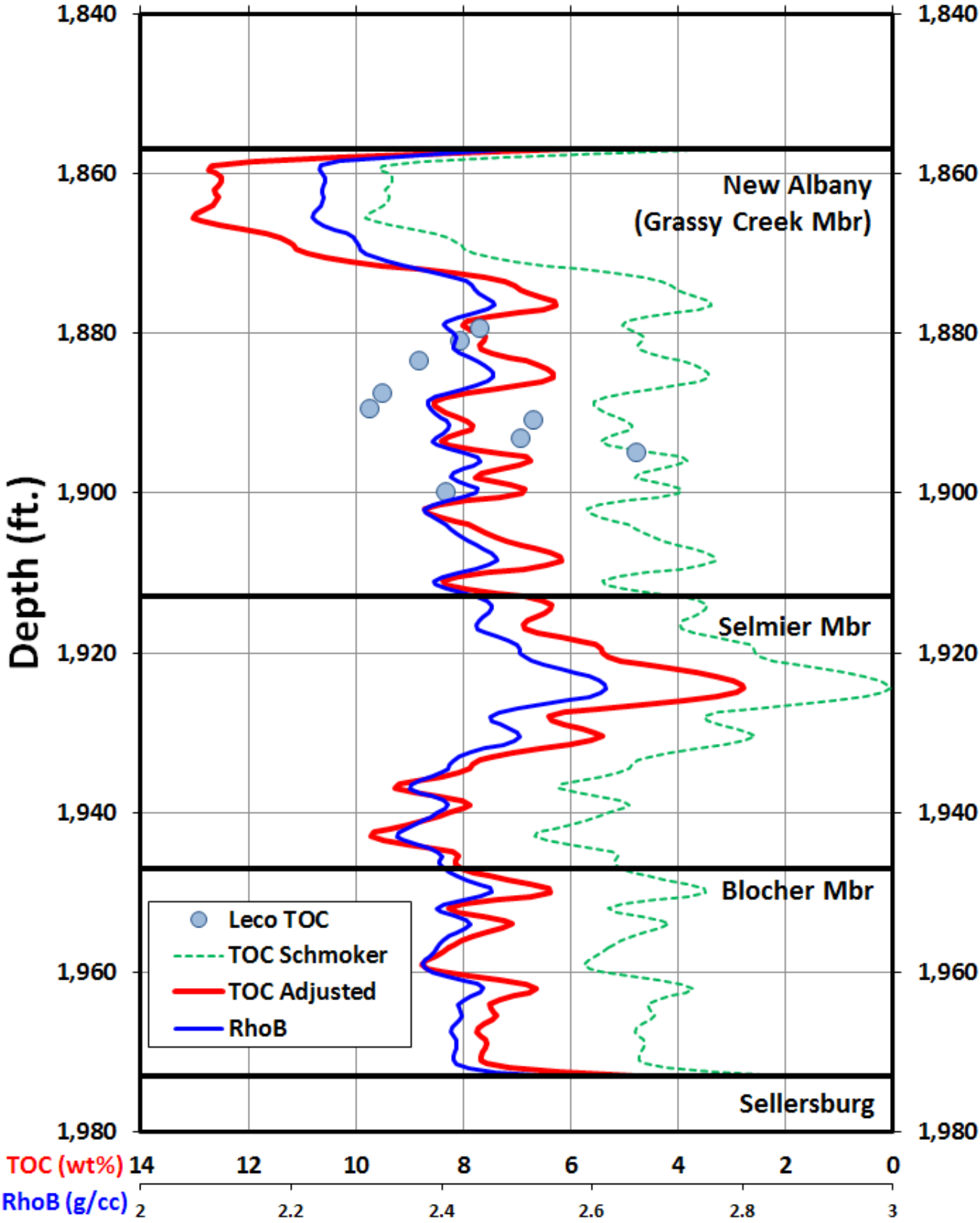

Figure 14. Total organic carbon (TOC, weight-percent) calculated from bulk-density log (RhoB).

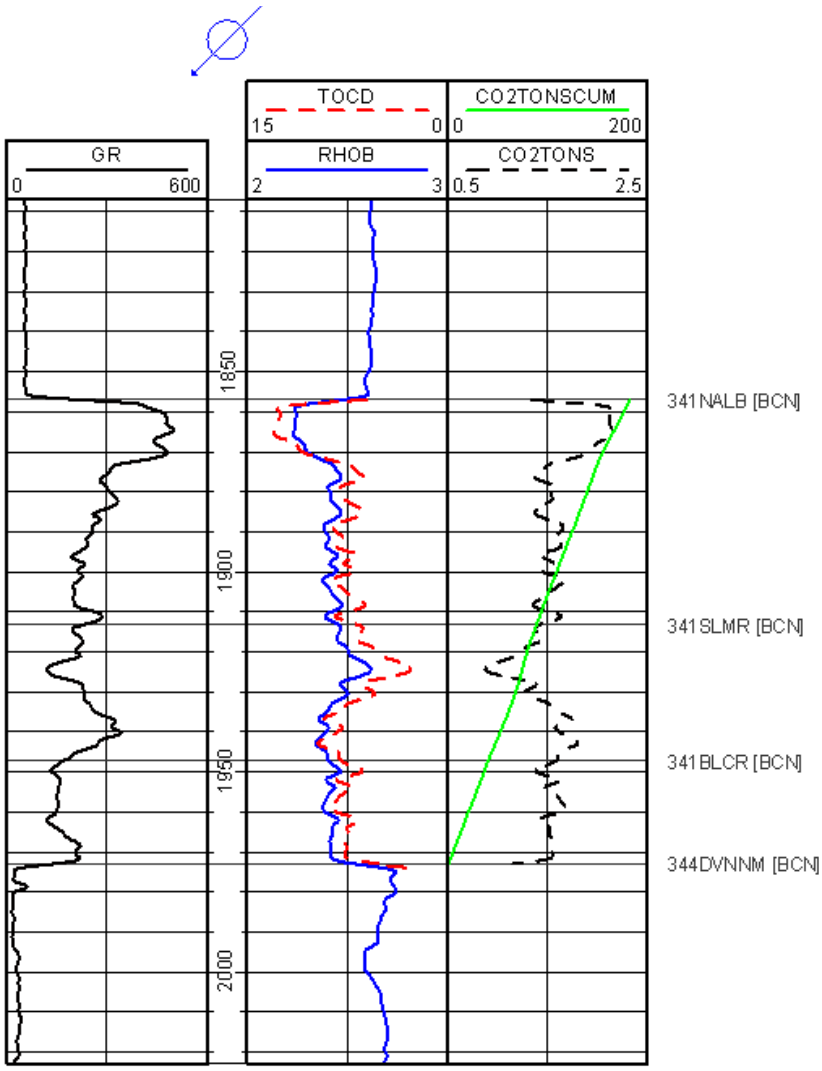

Figure 15. Cumulative CO_2 tons per acre calculation, using a 10 percent storage efficiency factor, for the New Albany Shale in the Blan well.

In the Blan well, three types of porosity were noted at both meso- and nanopore scales: (1) intraparticulate porosity (Fig. 16), (2) intraparticle porosity within syngenetic and diagenetic pyrite (Fig. 17) and dolomite (Fig. 18), and (3) intraparticle porosity in organic matter (Fig. 19). The prominent fractures exhibited around the grain and across the clay matrix in Figure 16 are likely caused by sample preparation. The ubiquitous distribution of microscale pyrite framboids (Fig. 20) suggests that intraparticle porosity within the framboids may be a significant part of the total porosity system in the New Albany Shale. Furthermore, Steven Ruppel and Robert Loucks (Texas Bureau of Economic Geology, personal communication, 2012) observed that the relatively low maturity of the organic matter and consequent minor development of meso- and nanoporosity in the kerogen indicates that the New Albany is likely a good potential source rock (as also indicated by Rock-Eval analysis), but those conditions may limit the shale as a prolific natural gas producer in the area of the Blan well.

Reservoir Seal Assessment

The mechanical properties of shale provide insight into wellbore stability, the conduct and effectiveness of fracture stimulations, and the conditions under which CO_2 might enter and pass through material. Matrix permeability measurements average 9.48×10^{-5} md (Table 1). Thus, permeability of the New Albany Shale in the Blan well is significantly less than the low-permeability case (0.01 md) to ensure CO_2 retention as modeled by White and others (2003), and indicates the shale would serve as an adequate secondary regional seal for deeper CO_2 storage reservoirs. Triaxial compression tests indicate a compressive strength of 13,487 psi, with a static Young's modulus (tensile strength) of 1.58×10^6 psi and a static Poisson's ratio (susceptibility to deformation under an applied stress) of 0.20. Threshold pressure injection was determined for a sample saturated with a potassium chloride brine to investigate imbibition of CO_2 and displacement of CH_4. No fluid entry or production was observed over a pressure range from 850 to 1,500 psi. In Hancock County, no formation water is present, with the exception of irreducible bound water that is often associated with clays in the shale. In the Illinois Basin, the low-permeability New Albany Shale is expected to act as a secondary regional seal for CO_2 sequestered in deeper zones that are overlain by more proximal primary seals.

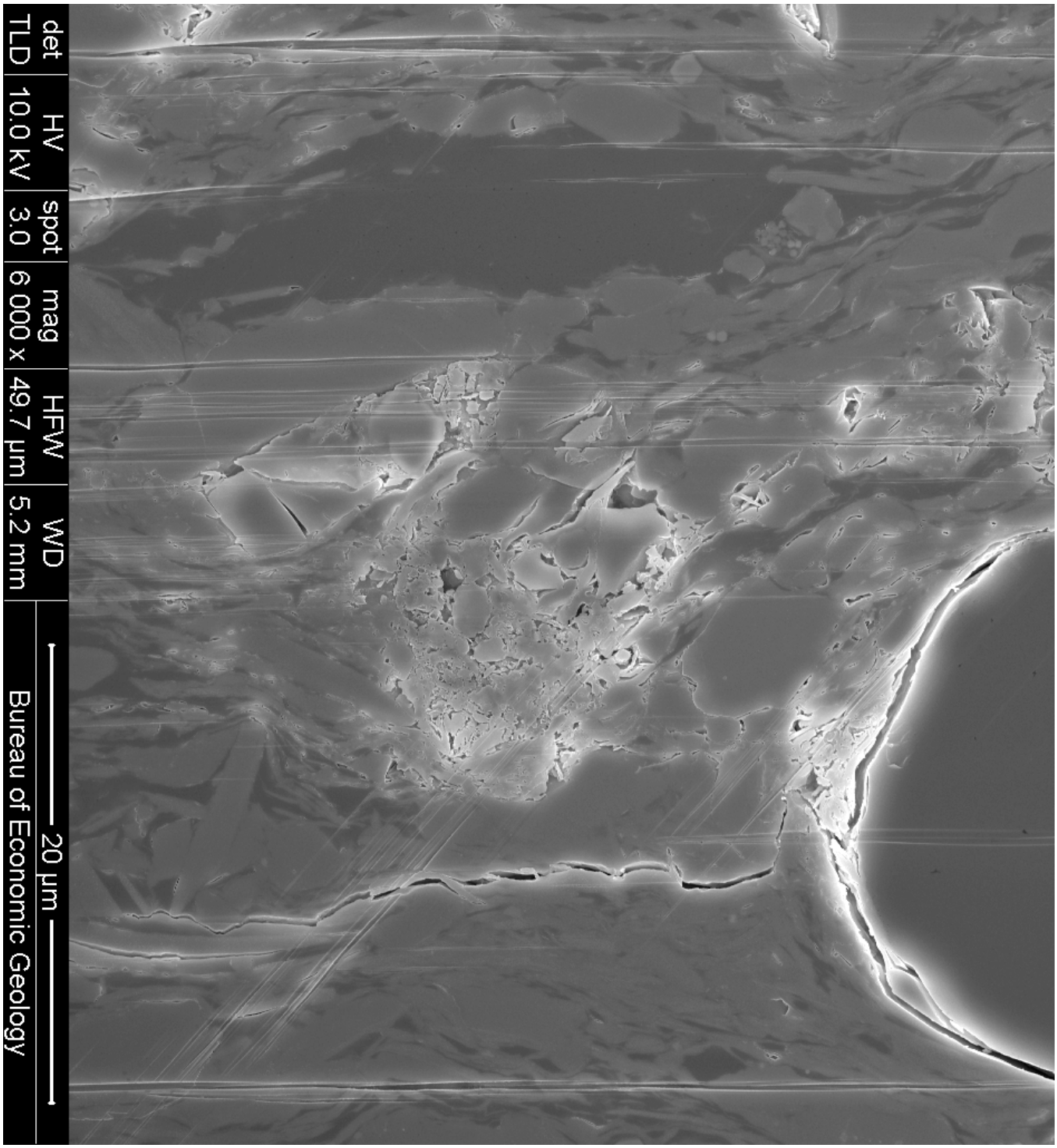

Figure 16. Interparticulate micro- and nanoporosity, argon-ion beam-milled sample at a depth of 1,887 ft; 6,000X magnification. Fracturing along grain boundary and striations are artifacts of sample preparation. Through the lens secondary electron image emphasizes porosity as bright areas. Photo by Robert Reed, Texas Bureau of Economic Geology.

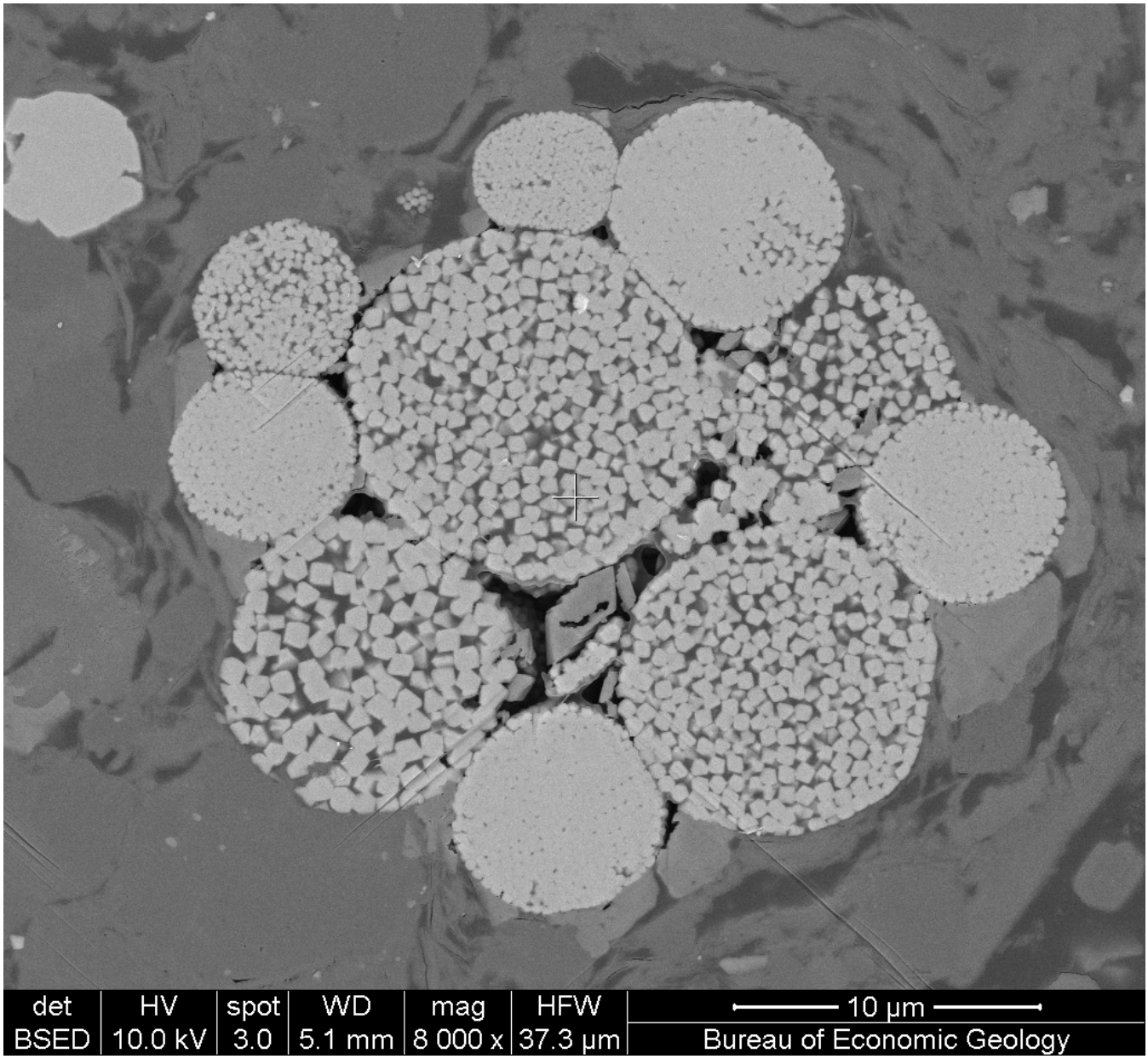

Figure 17. Intraparticle micro- and nanoporosity in a pyrite framboid. Argon-ion beam-milled sample, 1,879 ft depth, 8,000X magnification. Backscatter electron images emphasize compositional differences; thus, pyrite is bright. See also false-color version on cover. Photo by Robert Reed, Texas Bureau of Economic Geology.

Key Findings

1. With an average permeability of 9.48×10^{-5} md, pore throats averaging 0.047 µ, and having adequate mechanical integrity, the New Albany Shale is expected to be an effective secondary seal for carbon sequestered in deeper formations. Natural fracturing may limit seal efficiency in some areas, especially where heavily faulted.
2. Total organic carbon and Rock-Eval porosity data indicate that the New Albany Shale is a good to excellent potential source rock with abundant marine Type II oil-prone kerogen, but thermal alteration index, T_{max}, and percent Ro indicate low thermal maturity. Considering the good gas show encountered during drilling and low gas saturations, the New Albany Shale in the area of the Blan well may be a marginal producer. Horizontal drilling and fracture

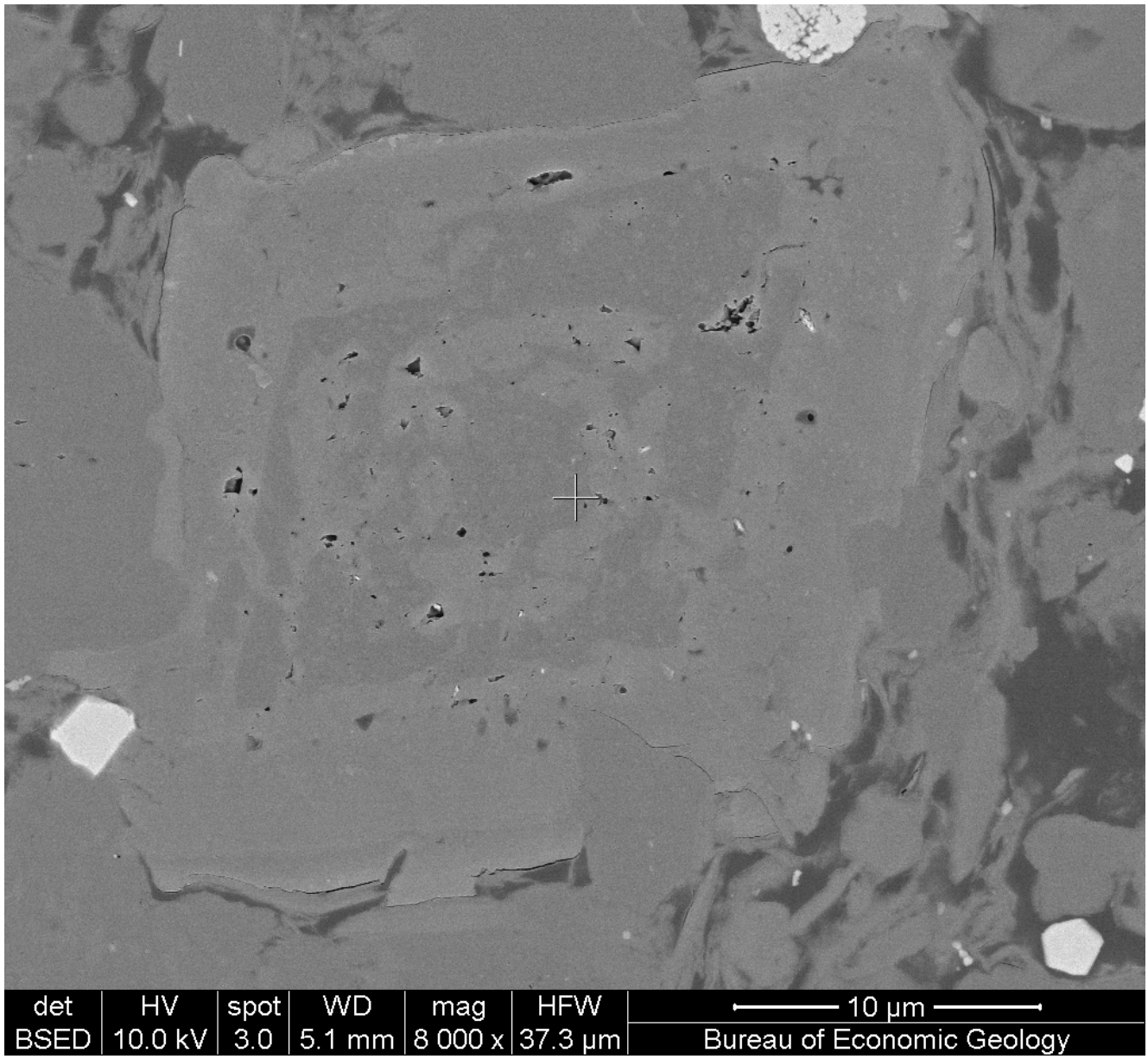

Figure 18. Intraparticle nanoporosity in accessory, diagenetic mineral (zoned dolomite rhombohedron), argon-ion beam-milled sample, 1,879 ft depth, 8,000X magnification. Backscatter electron images emphasize compositional differences. Photo by Robert Reed, Texas Bureau of Economic Geology.

stimulation will likely be required to recover economic quantities of natural gas.

3. Adsorption isotherms indicate preferential adsorption of CO_2. This property can enhance the sealing efficiency of the New Albany Shale by adsorbing and immobilizing any CO_2 that might migrate from deeper zones and suggests a mechanism to enhance natural gas production. The ability to inject CO_2 into shale remains to be demonstrated.

Acknowledgments

I would like to thank Rep. Rocky Adkins, Kentucky House District 99, for his leadership and persistence in promoting energy in Kentucky, which led to the passage of House Bill 1. The Kentucky General Assembly, Peabody Energy, Conoco Phillips, E.On US (LG&E), TVA, the Illinois Office of Coal Development and the Illinois State Geological Survey, the National Energy Technology Laboratory, GEO Consultants LLC, Schlumberger Carbon Services, Smith Management Co., and Wyatt, Tar-

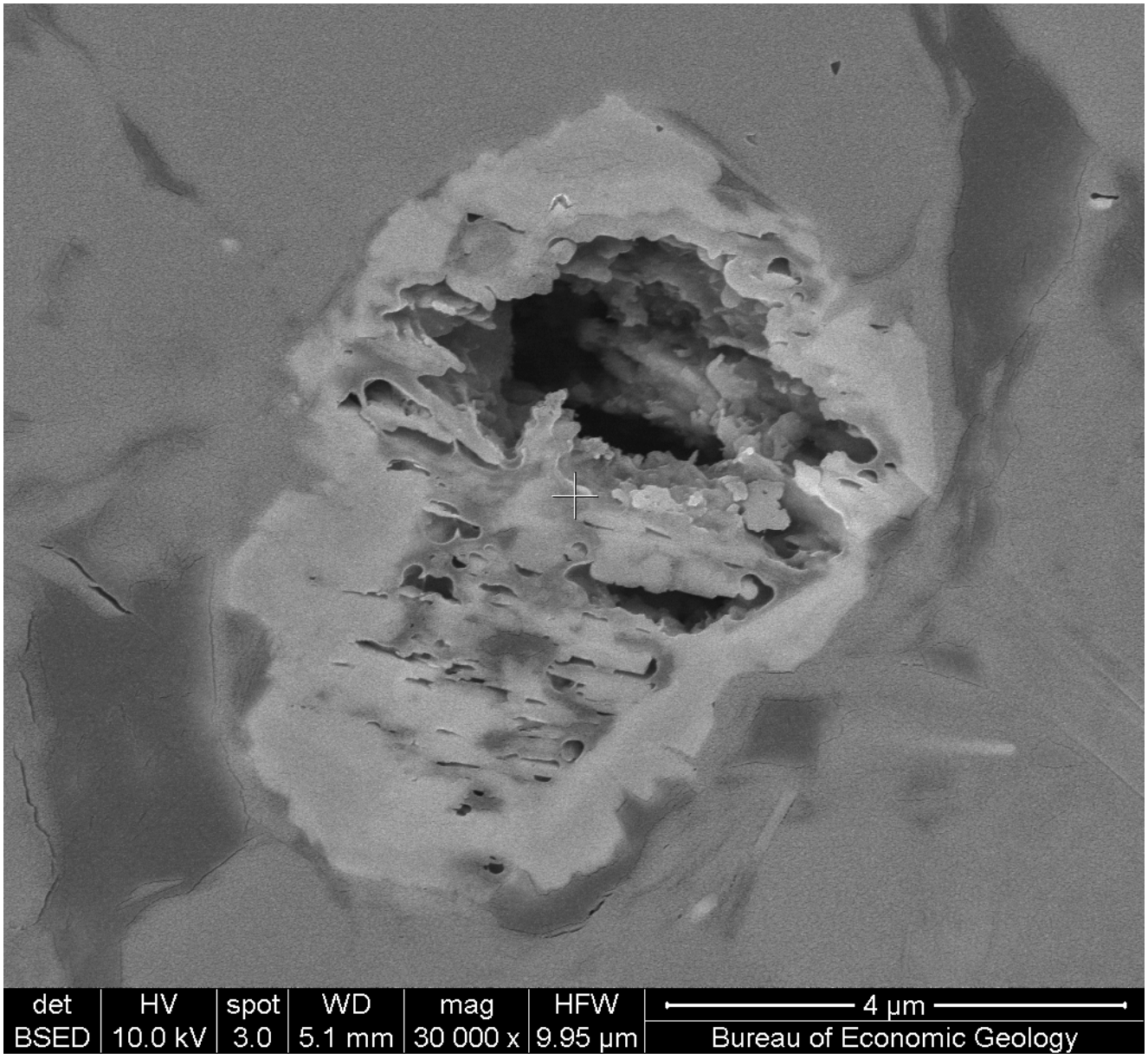

Figure 19. Intraparticle micro- and nanoporosity in degraded organic particle, argon-ion beam-milled sample, 1,879 ft depth, 30,000X magnification. Backscatter electron images emphasize compositional differences. Photo by Robert Reed, Texas Bureau of Economic Geology.

rant and Combs, LLP provided funds and in-kind services that made this project possible. The drill site was provided by Marvin and Brenda Blan. All laboratory analyses, the thin-section descriptions, and the standard SEM images and descriptions were performed by Weatherford Laboratories. Argon-ion beam-milled samples were prepared and photographed by Stephen Ruppel and Robert Reed, Bureau of Economic Geology at the University of Texas–Austin, who provided insight into the interpretation of those images.

References Cited

Ambrose, R.J., Hartman, R.C., Diaz-Campos, M., Akkutlu, I.Y., and Sondergeld, C.H., 2010, New pore-scale considerations for shale gas in place calculations: Society of Petroleum Engineers Unconventional Gas Conference, 23–25 February 2010, Pittsburgh, Pa., Society of Petroleum Engineers, 131772-MS, p. 17.

Boswell, R., 1996, Play UDs: Upper Devonian black shales, *in* Roen, J.B., and Walker, B.J., eds.,

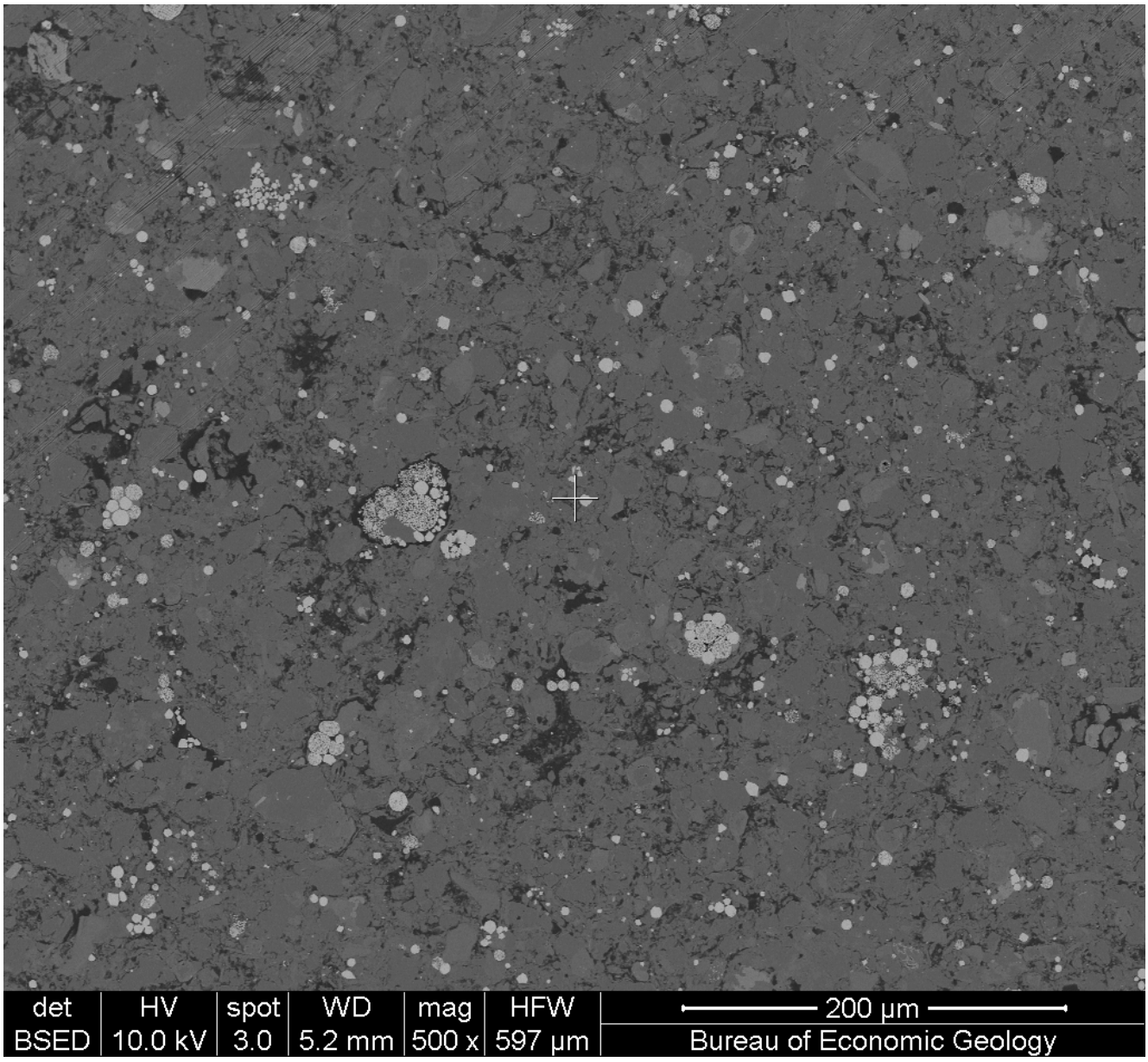

Figure 20. Ubiquitous pyrite framboids suggest intraparticulate porosity may be a significant component of total porosity in the New Albany Shale. Argon-ion beam-milled sample, 1,879 ft depth, 500X magnification. Backscatter electron images emphasize compositional differences; thus, pyrite is bright. Photo by Robert Reed, Texas Bureau of Economic Geology.

The atlas of major Appalachian gas plays: West Virginia Geological and Economic Survey, Publication V-25, p. 93–99.

Bowersox, J.R., and Williams, D.A., in press, The western Kentucky deep saline reservoir CO_2 storage test: Results of the Kentucky Geological Survey Marvin Blan No. 1 well, east-central Hancock County, Kentucky: Kentucky Geological Survey, ser. 12, Report of Investigations.

Busch, A., Alles, S., Gensterblum, Y., Prinz, D., Dewhurst, D.N., Raven, M.D., Stanjek, H., and Krooss, B.M., 2008, Carbon dioxide storage potential of shales: International Journal of Greenhouse Gas Control, v. 2, no. 3, p. 297–308.

Bustin, R.M., Bustin, A.M.M., Cui, X., Ross, D.J.K., and Pathi, V.S.M., 2008, Impact of shale properties on pore structure and storage characteristics: Society of Petroleum Engineers Shale Gas Production Conference,

16–18 November 2008, Fort Worth, Texas, 119892-MS, 28 p.

Carr, T., Frailey, S., Reeves, S.R., Rupp, J., and Smith, S., 2008, Methodology for development of geologic storage estimates for carbon dioxide: Capacity and Fairways Subgroup, Geologic Working Group, U.S. Department of Energy Regional Carbon Sequestration Partnerships, U.S. Department of Energy, National Energy Technology Laboratories Carbon Sequestration Program, 36 p.

Choquette, P.W., and Pray, L.C., 1970, Geologic nomenclature and classification of porosity in sedimentary carbonates: American Association of Petroleum Geologists Bulletin, v. 54, no. 2, p. 207–250.

Cole, G.A., Abu-Ali, M.A., Aoudeh, S.M., Carrigan, W.J., Chen, H.H., Colling, E.L., Gwathney, W.J., Al-Hajji, A.A., Halpern, H.I., Jones, P.J., Al-Sharidi, S.H., and Tobey, M.H., 1994, Organic geochemistry of the Paleozoic petroleum system of Saudi Arabia: Energy and Fuels, v. 8, no. 6, p. 1425–1442.

Eyl, W.C., 1922, Special oil and gas edition, map of Kentucky: An original compilation: Kentucky Geological Survey, ser. 6, scale approximately 1:250,000.

Gentzis, T., de Freitas, T., Goodarzi, F., Melchin, M., and Lenz, A., 1996, Thermal maturity of lower Paleozoic sedimentary successions in Arctic Canada: American Association of Petroleum Geologists Bulletin, v. 80, no. 7, p. 1065–1084.

Hamilton-Smith, T., 1993, Gas exploration in the Devonian shales of Kentucky: Kentucky Geological Survey, ser. 11, Bulletin 4, 31 p.

Hasenmueller, N.R., 1993, New Albany Shale (Devonian and Mississippian) of the Illinois Basin, *in* Roen, J.B., and Kepferle, R.C., eds., Petroleum geology of the Devonian and Mississippian black shale of eastern North America: U.S. Geological Survey Bulletin 1909, p. C1–C19.

Hasenmueller, N.R., Comer, J.B., Morse, D.G., Nuttall, B.C., DeChurch, D., Hill, B.T., Hill, R.T., Irwin, P.N., Like, K.K., Sowder, K., Thompson, T.A., and Zoltin, A., 2000, GIS compilation of gas potential of the New Albany Shale in the Illinois Basin: Illinois Basin Consortium, Gas Research Institute CD-ROM GRI-00/0068.

Jarvie, D.M., 1991, Total organic carbon (TOC) analysis, *in* Merrill, R.K., ed., Source and migration processes and evaluation techniques: American Association of Petroleum Geologists, p. 113–118.

Jillson, W.R., 1922, The conservation of natural gas in Kentucky [1st ed.]: Louisville, Ky., J.P. Morton & Co., 152 p.

Lash, G.G., and Lash, E., 2011, Kicking down the well: AAPG Explorer, www.aapg.org/explorer/2011/09sep/natgashist0911.cfm [accessed 26-Mar-2012].

Loucks, R.G., Reed, R.M., Ruppel, S.C., and Hammes, U., 2012, Spectrum of pore types and networks in mudrocks and a descriptive classification for matrix-related mudrock pores: American Association of Petroleum Geologists Bulletin, v. 96, no. 6, p. 1071–1098.

Loucks, R.G., Reed, R.M., Ruppel, S.C., and Jarvie, D.M., 2009, Morphology, genesis, and distribution of nanometer-scale pores in siliceous mudstones of the Mississippian Barnett Shale: Journal of Sedimentary Research, v. 79, no. 12, p. 848–861.

Loucks, R.G., Ruppel, S.C., Reed, R.M., and Hammes, U., 2011, Origin and classification of pores in mudstones from shale-gas systems: American Association of Petroleum Geologists International Conference and Exhibition, Milan, Italy, AAPG Search and Discovery Article 40855, www.searchanddiscovery.com/documents/2011/40855loucks/ndx_loucks.pdf [accessed 06-Jan-2013].

Merrill, R.K., ed., 1991, Source and migration processes and evaluation techniques: American Association of Petroleum Geologists, Handbook of Petroleum Geology, 213 p.

Miller, A.M., 1919, The geology of Kentucky: A classified compendium of state reports and other publications with critical comment based on original investigations: Kentucky Geological Survey, ser. 5, Bulletin 2, 392 p.

Natural Gas, 2003, History: Natural Gas Supply Association, www.naturalgas.org/overview/history.asp [accessed 28-Jul-2009].

Nuccio, V.F., and Hatch, J.R., 1996, Vitrinite reflectance suppression in the New Albany Shale, Illinois Basin—Vitrinite reflectance and Rock-Eval data: U.S. Geological Survey Open-File Report 96-665, 37 p.

Nuttall, B.C., Drahovzal, J.A., Eble, C.F., and Bustin, R.M., 2009, Regional assessment of suitability of organic-rich gas shales for carbon sequestration: An example from the Devonian shales of the Illinois and Appalachian Basins, Kentucky, *in* Grobe, M., Pashin, J., and Dodge, R.L., eds., Carbon dioxide sequestration in geological media—State of the science: American Association of Petroleum Geologists Studies in Geology 59, p. 173–190.

Orton, E., 1891, Report on the occurrence of petroleum, natural gas and asphalt rock in western Kentucky, based on examinations made in 1888 and 1889: Frankfort, Kentucky Geological Survey, ser. 2, v. E, 233 p.

Philip, R.P., and Galvez-Sinibaldi, A., 1991, Characterization of organic matter by various pyrolysis techniques, *in* Merrill, R.K., ed., Source and migration processes and evaluation techniques: American Association of Petroleum Geologists, Handbook of Petroleum Geology, p. 107–112.

Roen, J.B., and Kepferle, R.C., eds., 1993, Petroleum geology of the Devonian and Mississippian black shale of eastern North America: U.S. Geological Survey Bulletin 1909, various pagination.

Ross, D.J., and Bustin, R.M., 2008, The importance of pore structural heterogeneities for shale gas reservoir evaluation: American Association of Petroleum Geologists, AAPG Search and Discovery Article 110071: www.searchanddiscovery.com/documents/2008/08109ross/ndx_ross.pdf [accessed 06-Jan-2013].

Rouquerol, J., Avnir, D., Fairbridge, C.W., Everett, D.H., Haynes, J.H., Pernicone, N., Ramsay, J.D.F., Sing, K.S.W., and Unger, K.K., 1994, Recommendations for the characterization of porous solids: Pure and Applied Chemistry, v. 66, no. 8, p. 1739–1758.

Scherer, G.W., 2004, Measuring permeability of rigid materials by a beam-bending method: IV, transversely isotropic plate: Journal of the American Ceramic Society, v. 87, no. 8, p. 1517–1524.

Scherer, G.W., Valenza, J.J., II, and Simmons, G., 2007, New methods to measure liquid permeability in porous materials: Cement and Concrete Research, v. 37, p. 386–397.

Schlegel, M.E., McIntosh, J.C., Bates, B.L., Kirk, M.F., and Martini, A.M., 2011, Comparison of fluid geochemistry and microbiology of multiple organic-rich reservoirs in the Illinois Basin, USA: Evidence for controls on methanogenesis and microbial transport: Geochimica et Cosmochimica Acta, v. 75, p. 1903–1919.

Schmoker, J.W., 1993, Use of formation-density logs to determine organic-carbon content in Devonian shales of the western Appalachian Basin and an additional example based on the Bakken Formation of the Williston Basin, *in* Roen, J.B., and Kepferle, R.C., eds., Petroleum geology of the Devonian and Mississippian black shale of eastern North America: U.S. Geological Survey Bulletin 1909, p. J1–J14.

Sondergeld, C.H., Newsham, K.E., Comisky, J.T., Rice, M.C., and Rai, C.S., 2010, Petrophysical considerations in evaluating and producing shale gas resources: Society of Petroleum Engineers Unconventional Gas Conference, 23–25 February 2010: Pittsburgh, Pa., Society of Petroleum Engineers, 131768-MS, 34 p.

Sutton, A.H., and Wagner, O.E. Jr., 1930, Geologic map of Meade County, Kentucky: Kentucky Geological Survey, ser. 6, scale 1:62,500.

Tissot, B.P., and Welte, D.H., 1984, Petroleum formation and occurrence [2d ed.]: New York, Springer-Verlag, 699 p.

U.S. Department of Energy, Office of Fossil Energy, 2001, History of natural gas: U.S. Department of Energy, Office of Fossil Energy, www.fe.doe.gov/education/gas_history.html [accessed 14-Jun-2001].

Weatherford Laboratories, 2009, Wireline services log interpretation chart book: Houston, Texas, Weatherford Laboratories, 206 p.

White, S.P., Allis, R.G., Moore, J., Chidsey, T., Morgan, C., Gwynn, W., and Adams, M., 2003,

Natural CO_2 reservoirs on the Colorado Plateau and southern Rocky Mountains, USA: A numerical model, *in* Gale, J., and Kaya, Y., eds., Greenhouse Gas Control Technologies—6th International Conference: Oxford, Pergamon, p. 423–428.

Zdravkov, B.D., Cermak, J.J., Sefara, M., and Janku, J., 2007, Pore classification in the characterization of porous materials: A perspective: Central European Journal of Chemistry, v. 5, no. 2, p. 385–395.

Appendix A: Primary Bedding Styles

Bioturbation

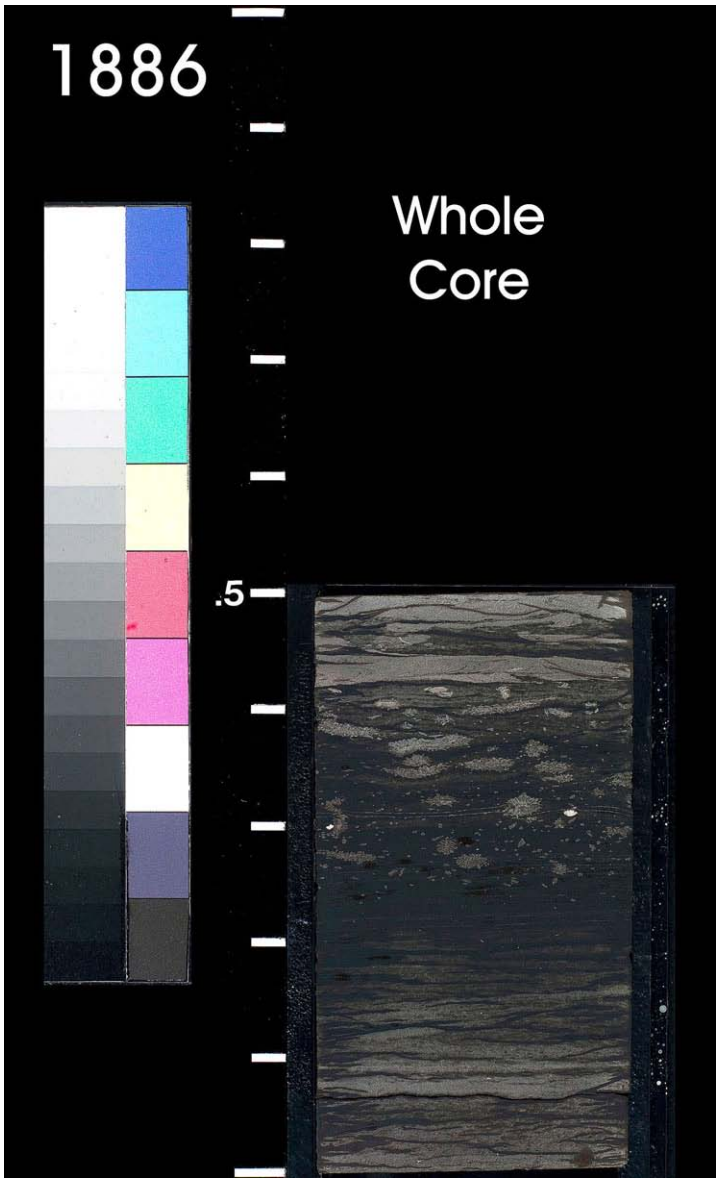

Irregular and wavy-bedded, silt-rich laminae (lighter colored) above bioturbated bedding with dispersed pyrite framboids filling burrow traces.

Figure A-1. Example of bioturbation in the New Albany Shale from 1,886.57–1,886.75 ft.

Low-Permeability Laminae

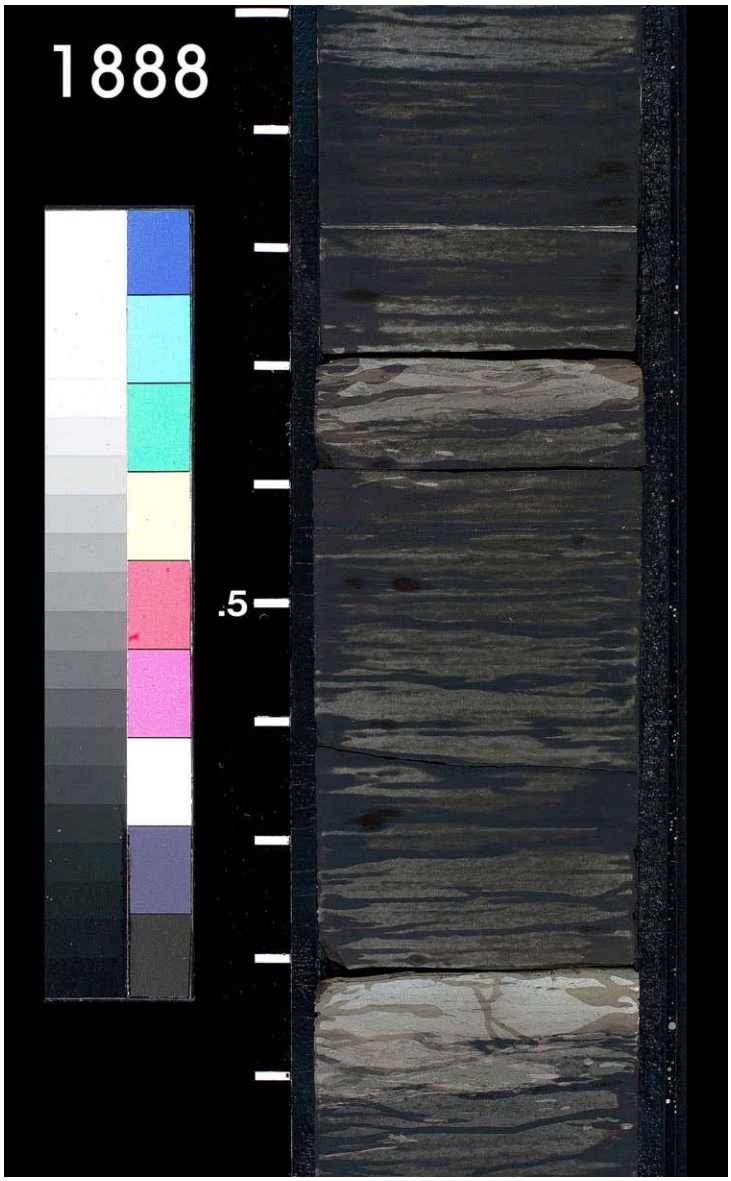

Irregular, ruddy brown laminae of finely dispersed, silty particles are often associated with zones that appear lighter gray and dry when the surface is sprayed, on available core slabs (left: 1,888.30–1,888.40 ft and 1,888.80–1,888.95 ft). A mild hydrochloric acid solution applied across these zones typically reacts, indicating the presence of ferroan-carbonate cement and lower permeability due to cementation (below).

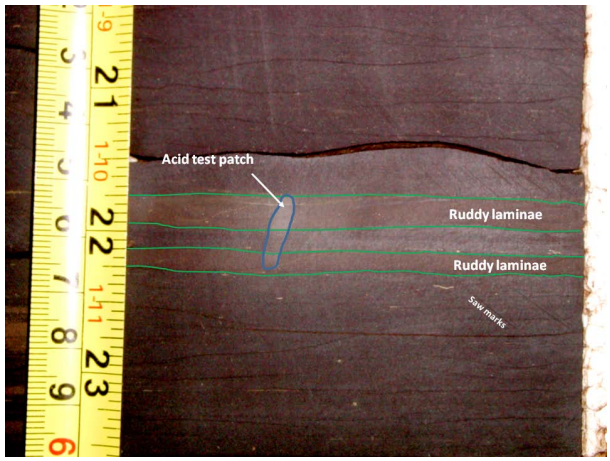

Figure A-2. Typical irregular to wavy and ripple-laminated lithology, showing alternating organic-rich and often carbonate-cemented, silt-rich laminae. Left: Core slab showing interval from 1,888.80–1,888.95 ft. Right: Core macrophoto illustrating dry appearance.

Appendix B: Macrophotography, Thin Sections, and SEM Microscopy

This appendix presents compiled analytical data, imagery, and descriptions for three selected intervals of the New Albany Shale core from the Kentucky Geological Survey Marvin Blan No. 1 well, Hancock County, Ky. The compilations consist of:

- X-ray CT images of the core in sealed aluminum core barrels, as received by Weatherford Laboratories
- Macro core photographs of a cut slab
- Thin-section descriptions keyed to gridded guide images, with matching page-size images
- Discussions of SEM photographs, with keyed guide images and matching page-size images
- SEM images of focused ion-beam prepared scenes (if available)

Thin-section and SEM images refer to specific areas indicated by grid coordinate designations consisting of a letter (row) and number (column); for example, "C12" refers to the coordinate of a specific feature in an image. A reference designation may also refer to a range of coordinates describing the location of the feature in the image; for example, "B–C1–B15" refers to a feature extending from coordinates B1 and C1 across the image to coordinate B15.

The SEM images in this report were acquired with different detectors to emphasize selected petrophysical attributes:

- BSE: Backscatter electron image, documenting compositional variations; also BSED
- SE: Secondary electron image, documenting topographic variation of sample surface
- TLSE: Through the lens secondary electron image, emphasizing porosity; also TLD

Sample 1-7P, 1,881 ft

Shale rock properties: 1,881.00–1,881.15 ft
Pressure decay permeability (dry): 1.22E-04 md
Porosity (dry, helium): 6.0 percent
Grain density (dry): 2.51 g/cm^3
Leco TOC: 8.05 weight-percent hydrocarbon

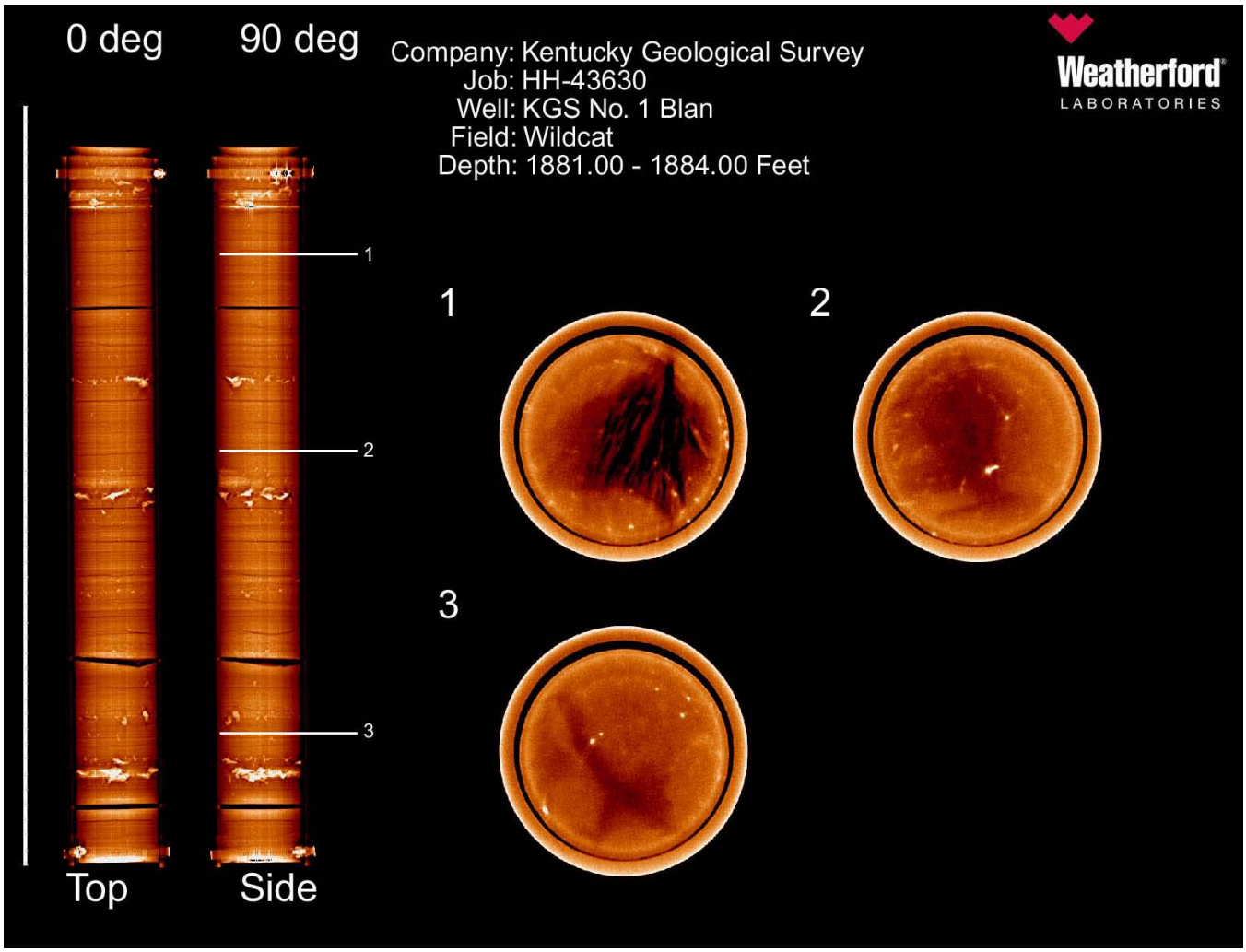

Figure B-1. CT scan of New Albany Shale interval, 1,881–1,884 ft, showing thin-bedded character of shale. Bright spots and laminae indicate carbonate- and pyrite-rich zones.

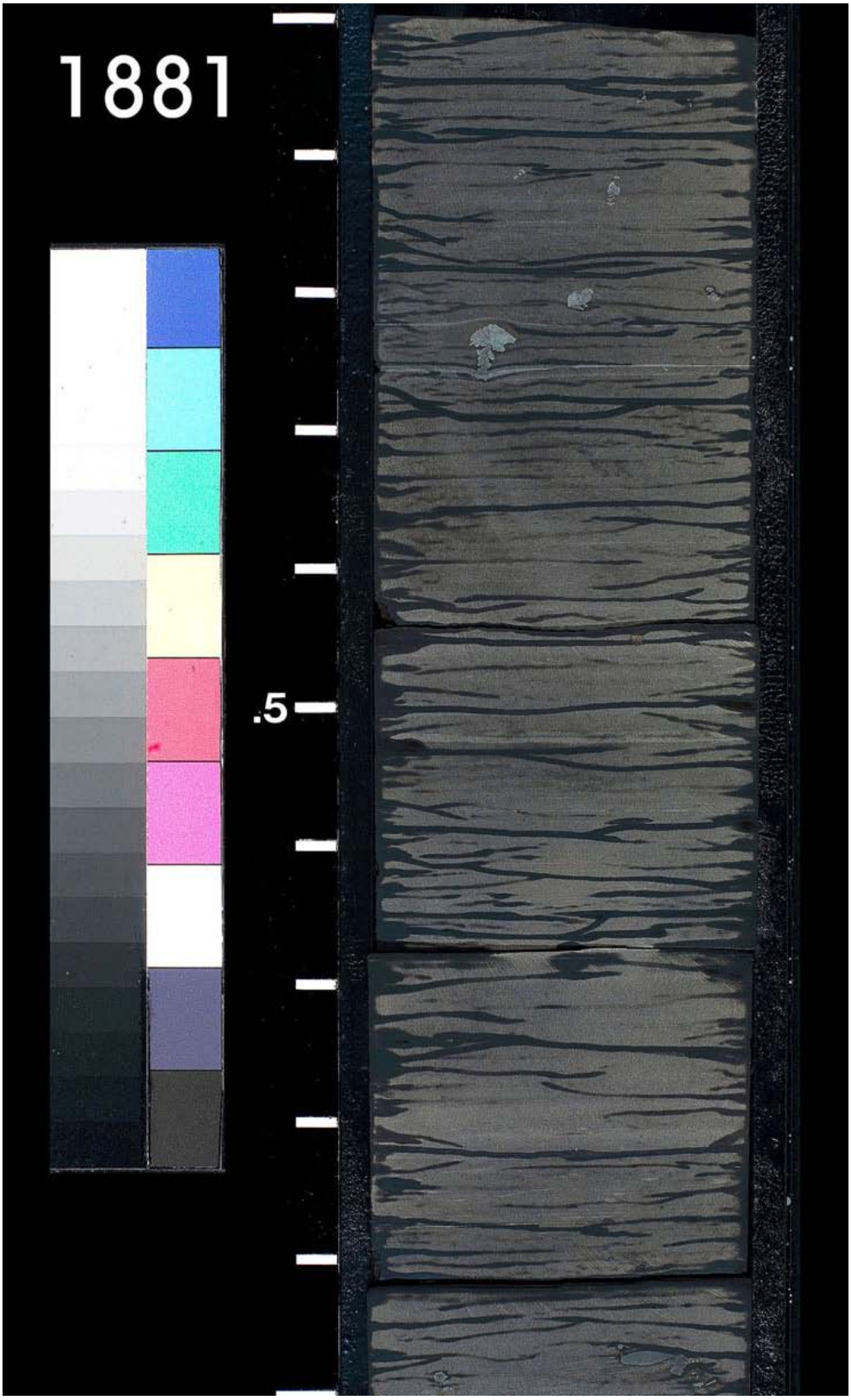

Figure B-2. Cut slab of New Albany Shale core interval, 1,881–1,882 ft, showing mostly parallel to wavy laminations and compaction features. Distortion and draping of bedding around pyrite nodule at 1,881.25 ft is related to compaction and dewatering.

Thin-Section Description

Lithology. Slightly ferroan-dolomitic, silty shale.

Texture. Silt-rich, parallel laminations (B–C1–B15, Fig. B-3A) interlayered with matrix and organic-rich laminations (C–H1–15, Fig. B-3A). Common horizontal burrows. Numerous spores (J–K3, C12, H-J10, Fig. B-3A) are flattened (H–J10, Fig. B-3A) or filled by authigenic minerals, including apatite (E11, Fig. B-3B). Common agglutinated foraminifera tests have been crushed by mechanical compaction. Sparse phosphatic bone fragments. Silt grains display angular to subrounded outlines.

Detrital Grains. In order of abundance: quartz (most abundant, J9, B1, Fig. B-3B), plagioclase, spores *(Tasmanites,* H–J9–10, Fig. B-3A; E13, Fig. B-3B), agglutinated foraminifera tests (F5, Fig. B-3A), muscovite (G–H14, Fig. B-3B), phosphatic bone fragments (K11, Fig. B-3B), biotite.

Matrix. Pervasive argillaceous matrix is intermixed with clay-size quartz and feldspar particles, as well as partially pyritized organic material (C–D9, Fig. B-3B) that occurs as stringers or minute particles. X-ray diffraction analysis reveals the presence of 47 weight-percent clay minerals, primarily illite (46 weight-percent), mixed-layer illite/smectite (1 weight-percent), kaolinite (trace), and chlorite (trace).

Cements and Replacement Minerals. Common pyrite, including framboids (D–E15, G11, J4, Fig. B-3B), replaces organic material (G–H4, Fig. B-3B) and has developed within the clay-rich matrix (J1.5, Fig. B-3B). Minor ferroan dolomite (B13.5, Fig. B-3B) partially replaces spore walls and partially replaces grains (B–C11, Fig. B-3B) or cement (B7–8, Fig. B-3B) silt grains within silt-rich laminations. Minor titanium dioxide crystal aggregates occur throughout the matrix as a replacement of titanium-bearing minerals. Rare apatite crystals fill spores (E10, Fig. B-3B).

Pore System. Partings along parallel laminations are artifacts of the sampling process; no visible pores were identified.

Magnification. Figure B-3A: 50X. Figure B-3B: 200X.

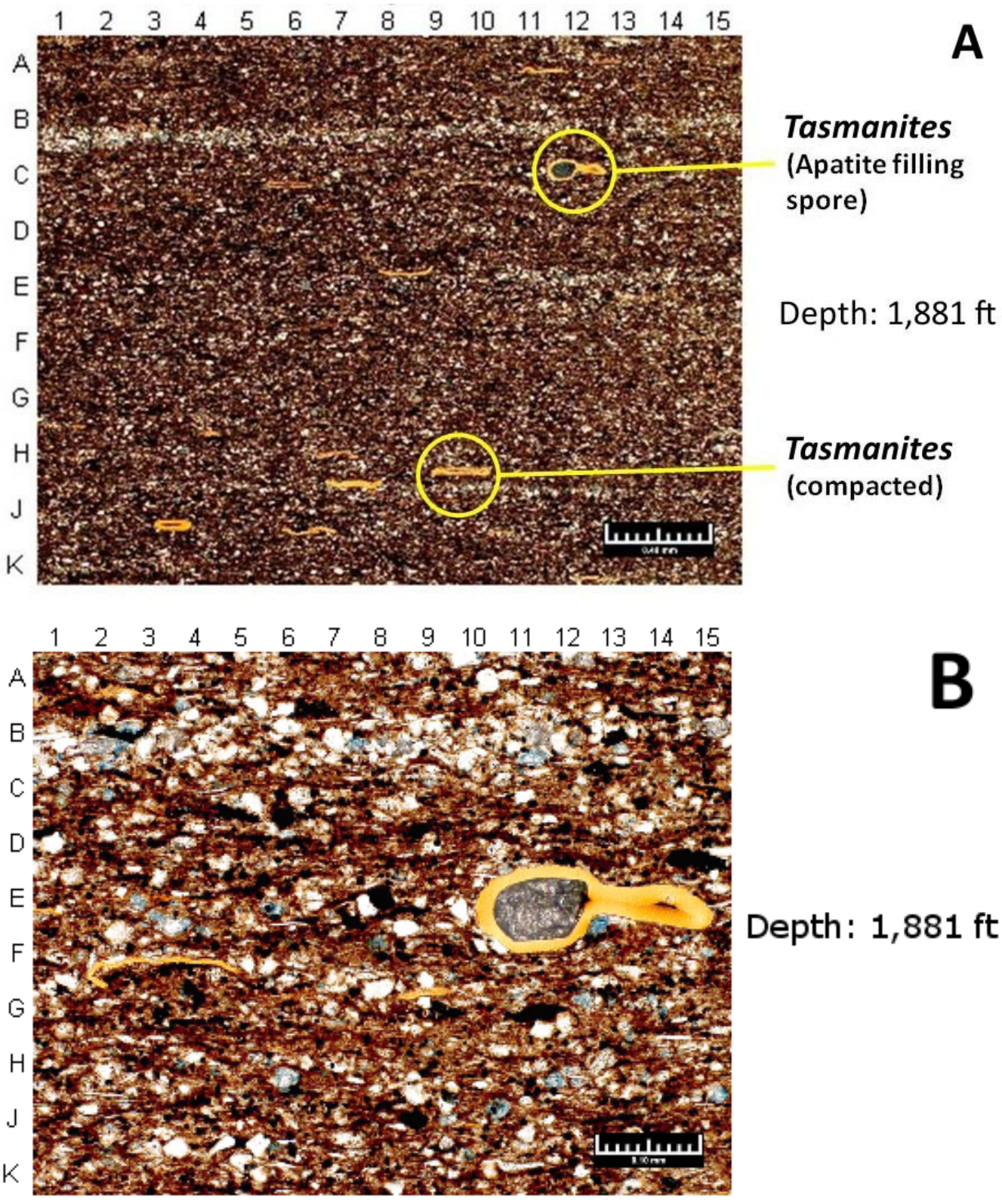

Figure B-3. Weatherford Laboratories grid coordinate reference images for New Albany Shale sample 1-7P, 1,881 ft.

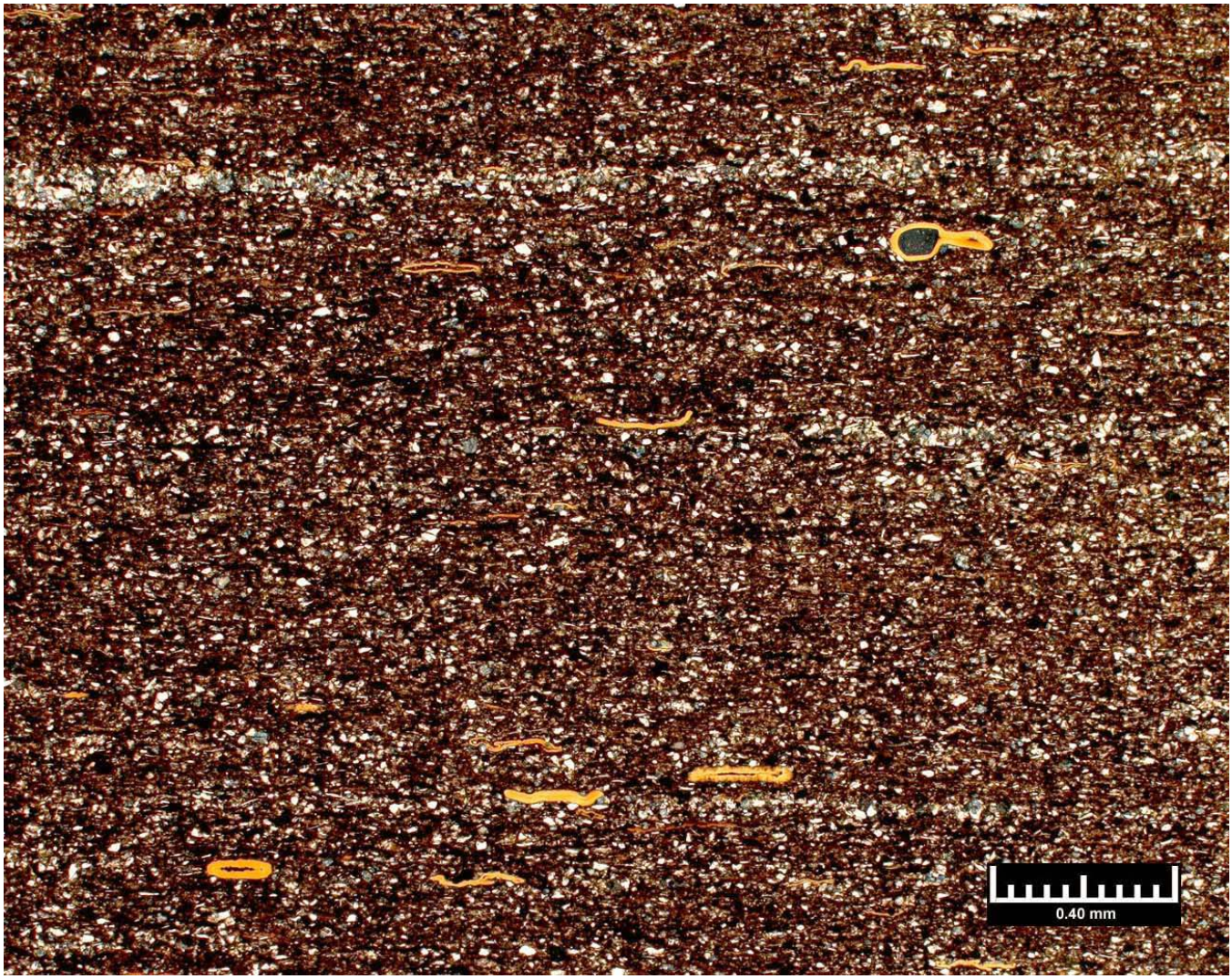

Figure B-4. New Albany Shale, sample 1-7P, 1,881 ft, full-size thin-section image corresponding to Figure B-3A, magnification 50X.

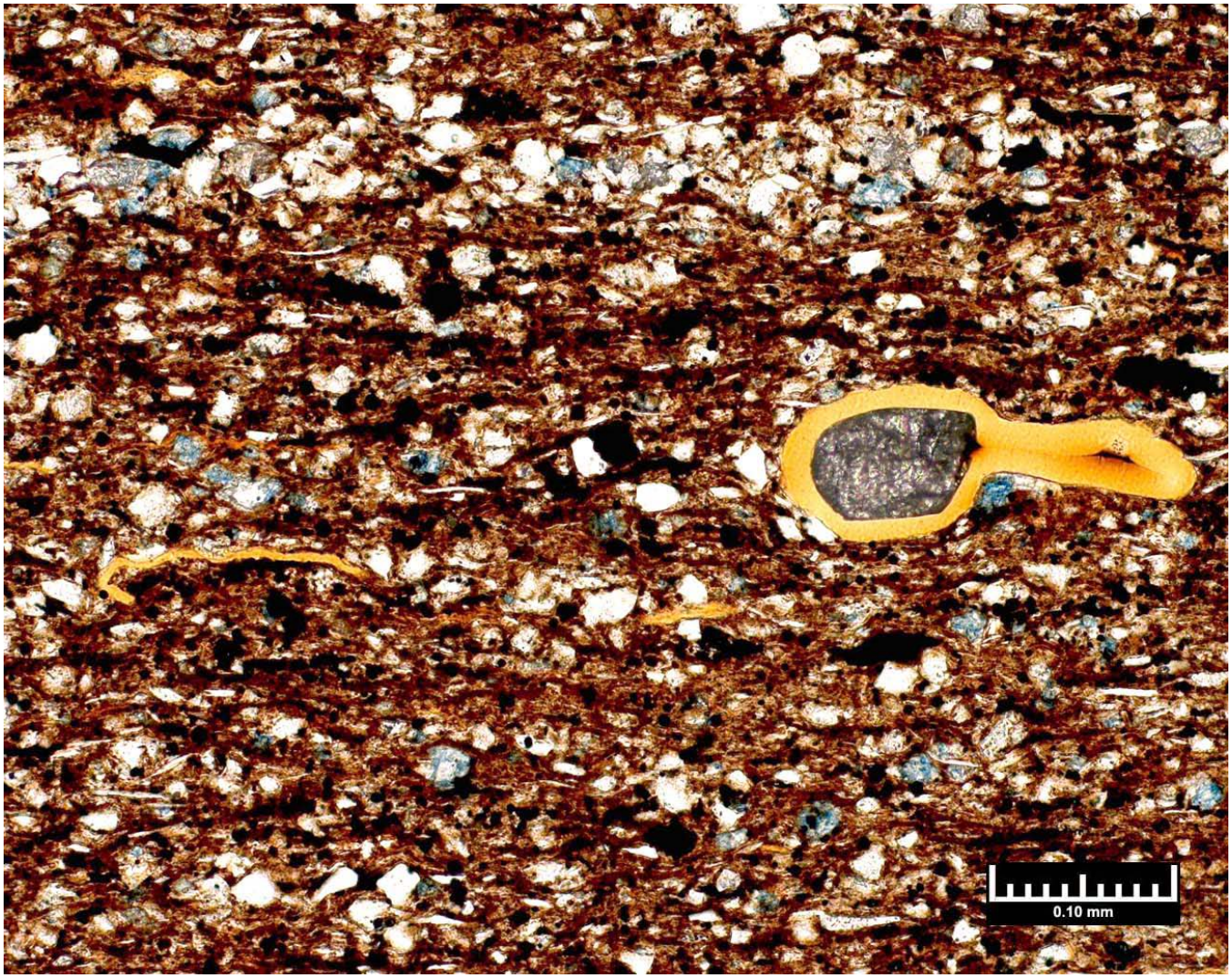

Figure B-5. New Albany Shale, sample 1-7P, 1,881 ft, full-size thin-section image corresponding to Figure B-3B, magnification 200X.

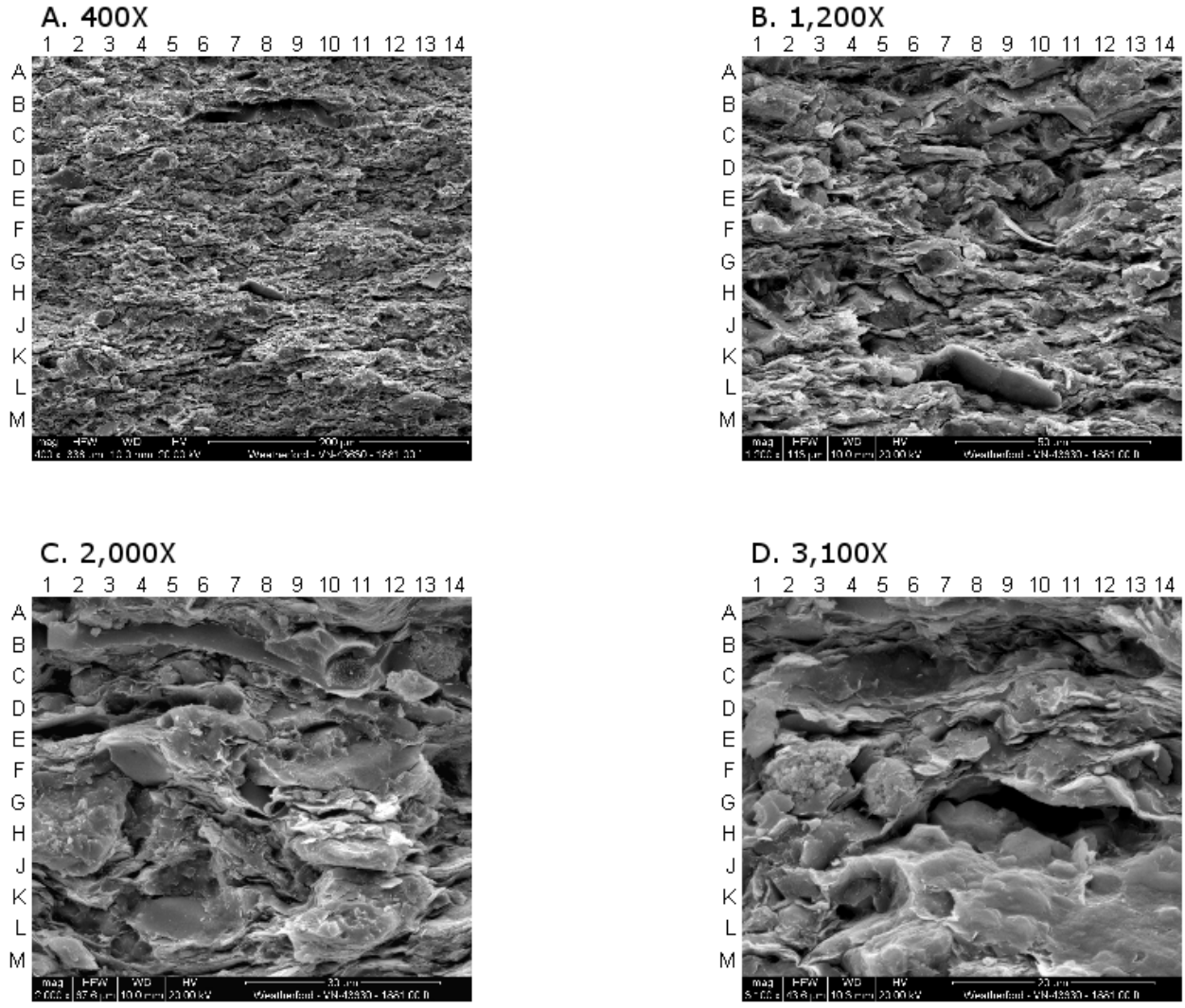

Figure B-6. Scanning electron photomicrographs of the New Albany Shale with coordinate references. Sample 1-7P, 1,881 ft.

Discussion

Well-developed, elongate grain alignment is revealed in the following images of a slightly ferroan, dolomitic, silty shale (Fig. B-6A–D). Numerous heterogeneously distributed silt grains composed primarily of quartz (E–F1, Fig. B-6B; L5, Fig. B-6C) and enveloped by clay-rich matrix. Ferroan dolomite (L2, Fig. B-6C) also occurs between clay or organic material particles. Common *Tasmanites* spores (B9, Fig. B-6C; F–G2, Fig. B-6D) are partially replaced by framboidal pyrite (C11, Fig. B-6C) and filled by apatite crystals (G2, Fig. B-6C), pyrite, or quartz. Flattened, aligned clay particles (G–J8–14, Fig. B-6B), organic matter, and spores (B8, Fig. B-6A) display orientation parallel to the bedding plane and comprise most of the matrix. Illite, the dominant clay mineral, commonly displays crenulated outlines (L–M6–9, Fig. B-6C). Numerous micropores (F8, Fig. B-6C; G11, Fig. B-6D) occur within the clay- and organic-rich matrix and range from approximately 7 µ to slightly greater than 20 µ. X-ray diffraction analysis revealed 47 weight-percent clay minerals, consisting of illite (46 weight-percent), mixed-layer illite/smectite (1 weight-percent), chlorite (trace), and kaolinite (trace).

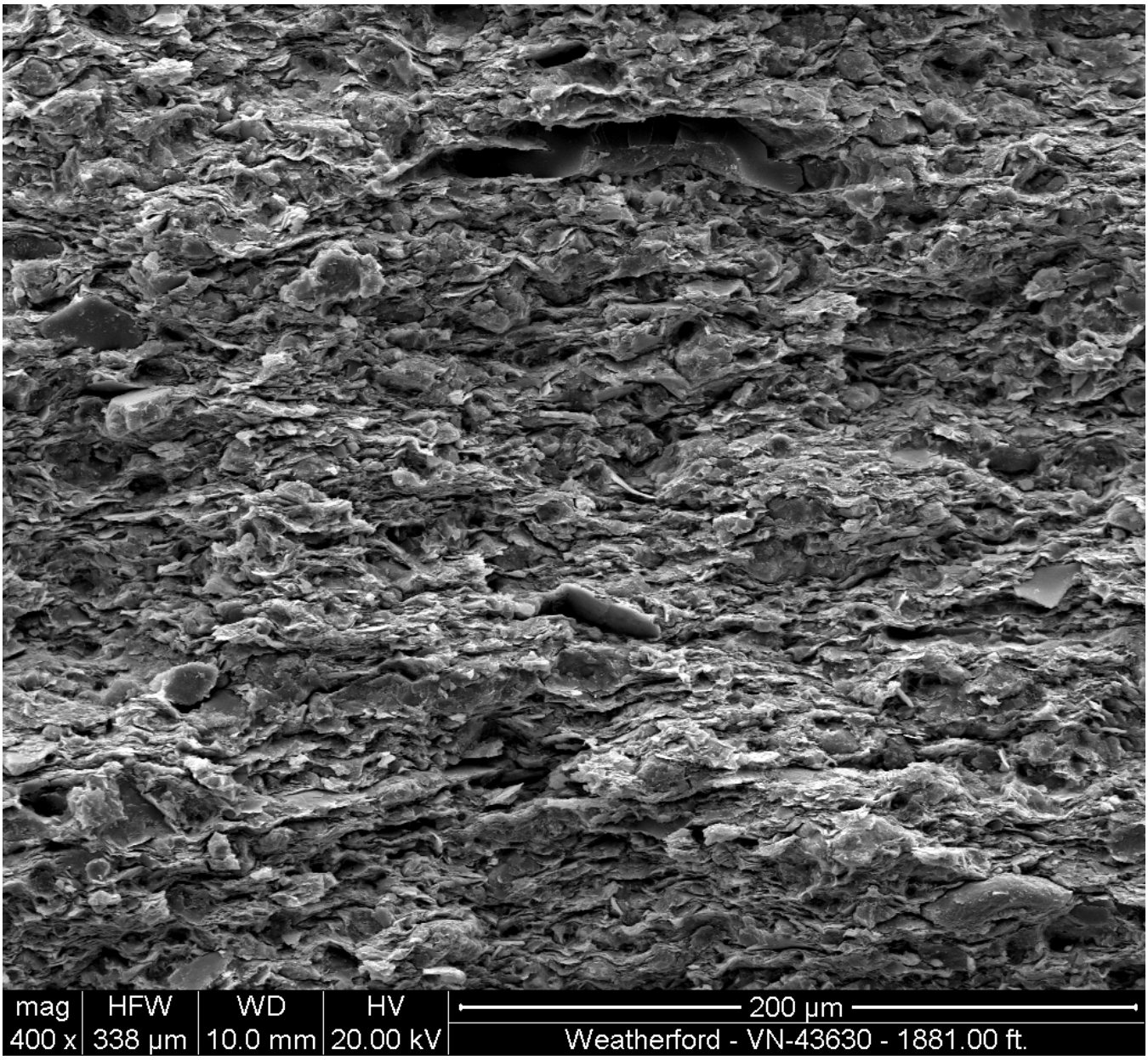

Figure B-7. New Albany Shale, sample 1-7P, 1,881 ft, full-size scanning electron photomicrograph corresponding to Figure B-6A, magnification 400X.

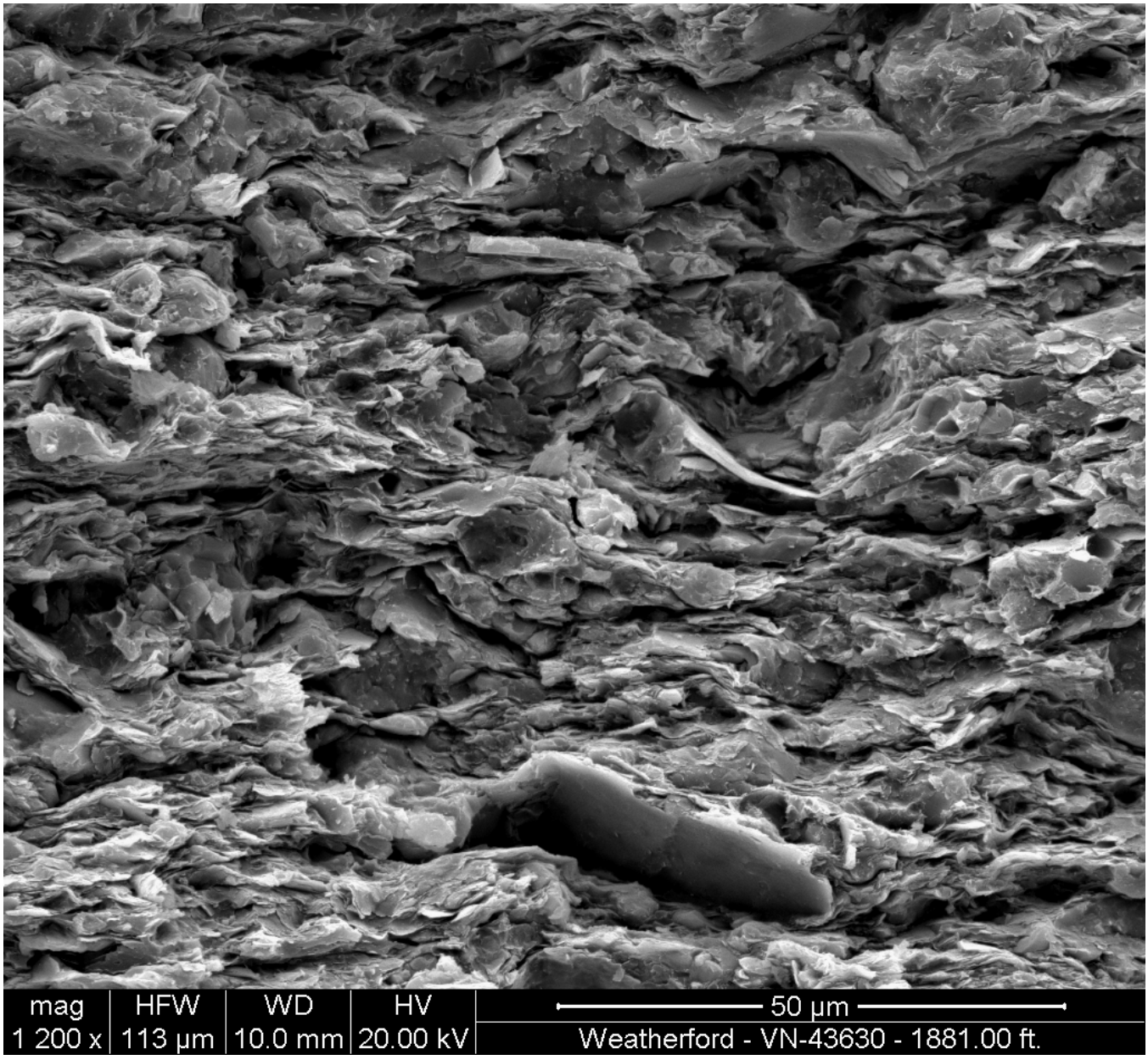

Figure B-8. New Albany Shale, sample 1-7P, 1,881 ft, full-size scanning electron photomicrograph corresponding to Figure B-6B, magnification 1,200X.

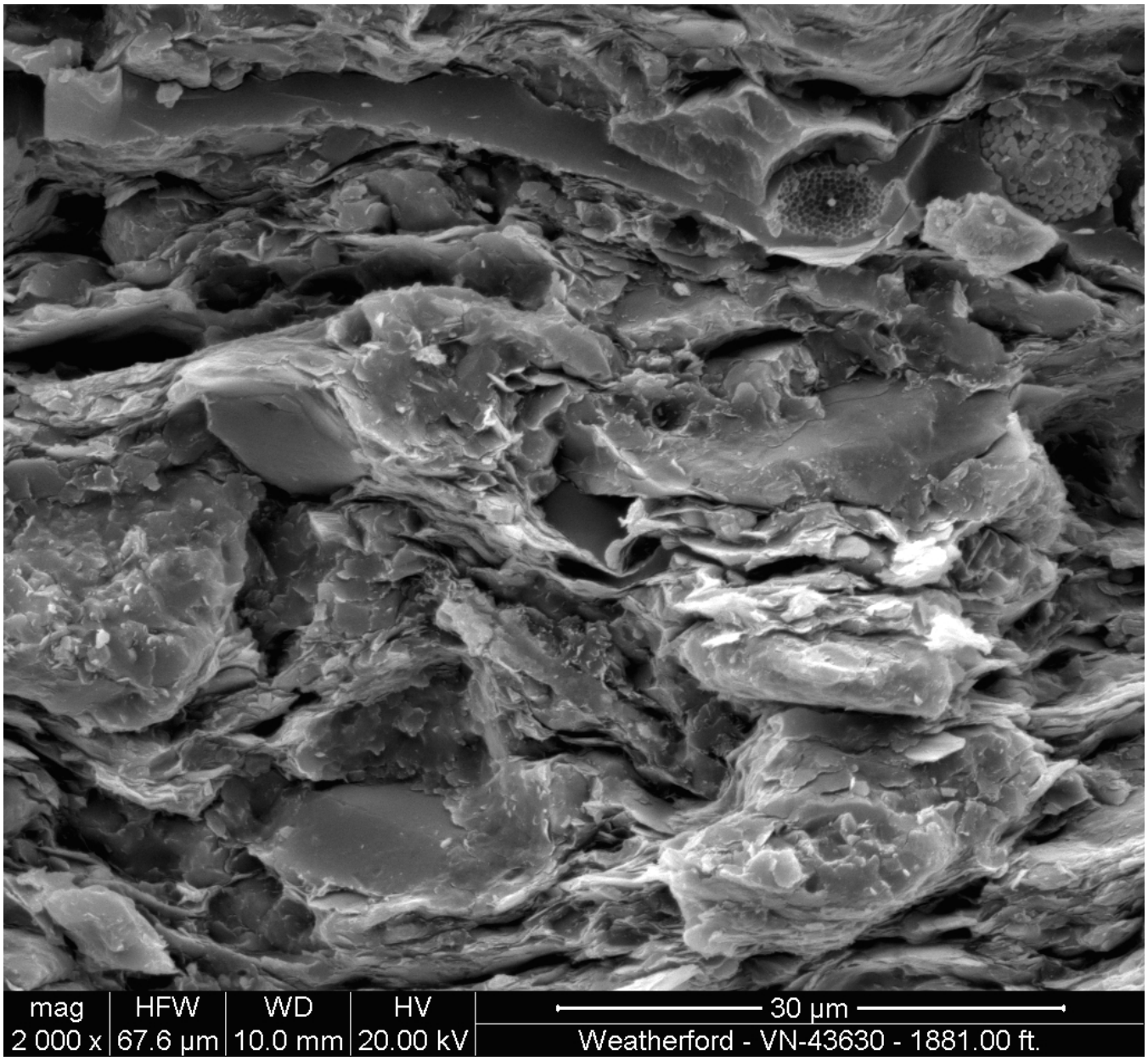

Figure B-9. New Albany Shale, sample 1-7P, 1,881 ft, full-size scanning electron photomicrograph corresponding to Figure B-6C, magnification 2,000X.

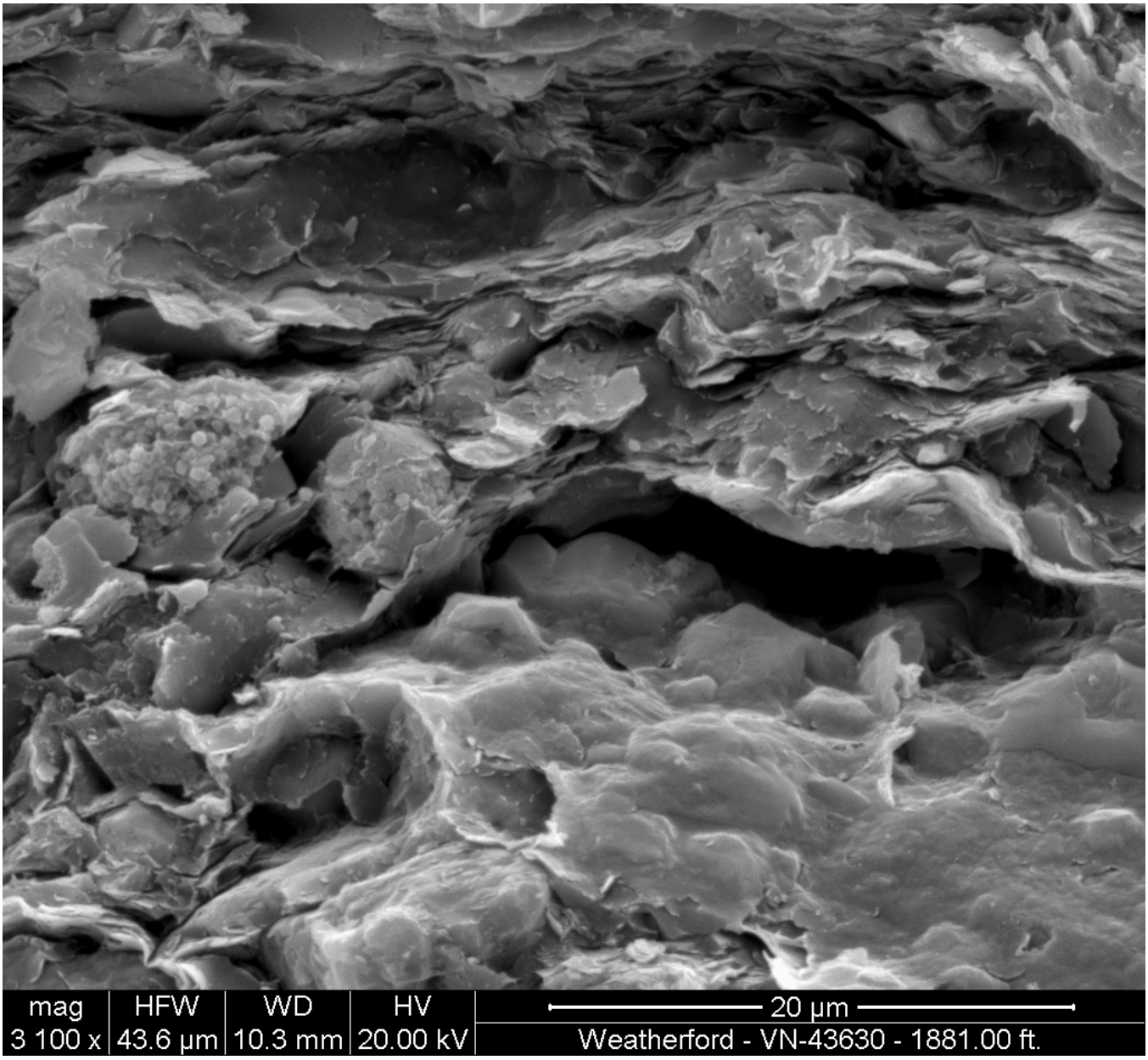

Figure B-10. New Albany Shale, sample 1-7P, 1,881 ft, full-size scanning electron photomicrograph corresponding to Figure B-6D, magnification 3,100X.

Sample 1-21P, 1,895 ft

Shale rock properties: 1,895.00–1,895.10 ft
Pressure decay permeability (dry): 7.77E-06 md
Porosity (dry, helium): 6.1 percent
Grain density (dry): 2.57 g/cm^3
Leco TOC: 4.75 weight-percent hydrocarbon

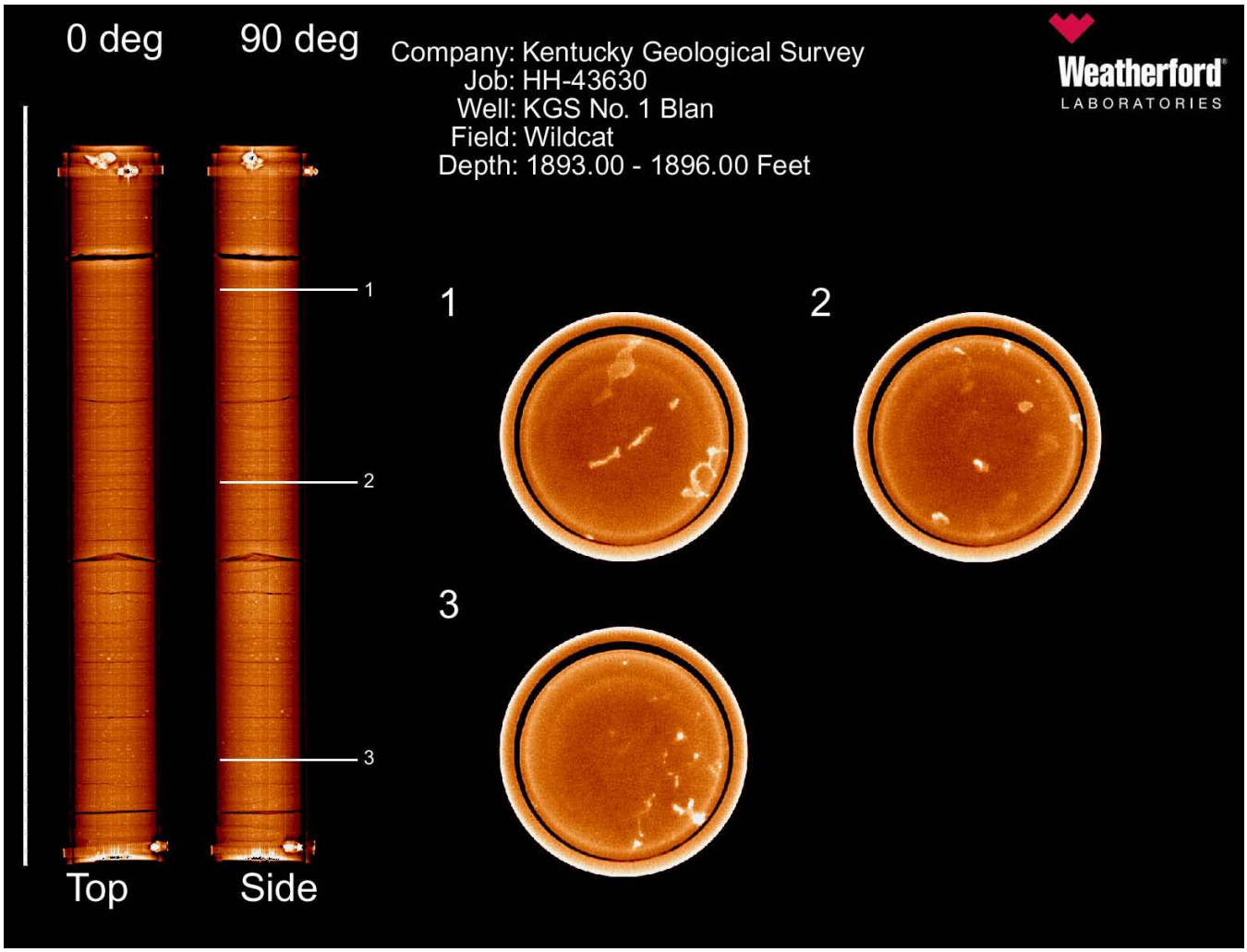

Figure B-11. CT scan of New Albany Shale interval, 1,893–1,866 ft.

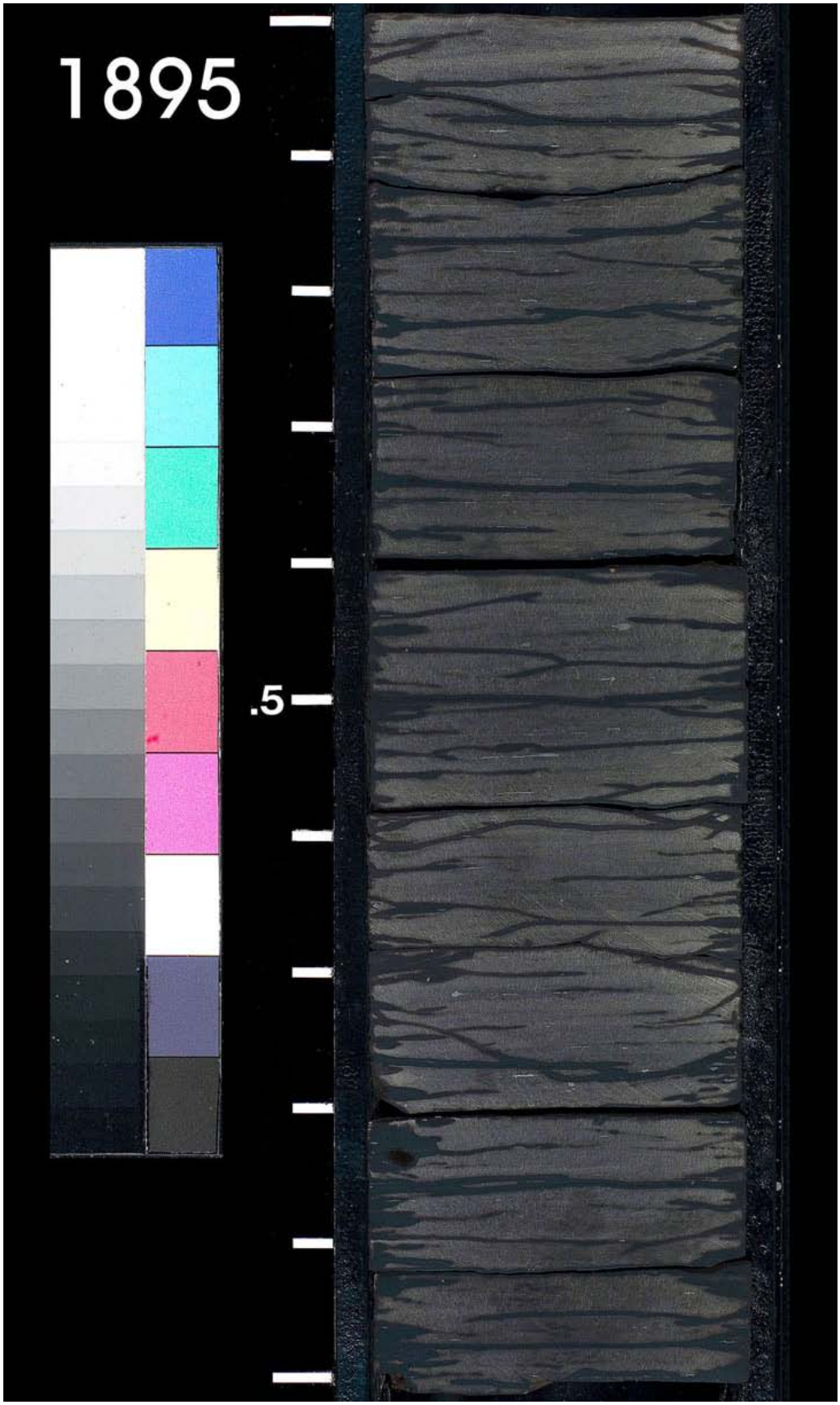

Figure B-12. Cut slab of New Albany Shale core interval, 1,895–1,896 ft.

Thin-Section Description

Lithology. Slightly ferroan-dolomitic, silty shale.

Texture. Discontinuous, parallel laminations disturbed by horizontal burrows that contain locally abundant pyrite. Numerous heterogeneously distributed orange *Tasminites* spores (A5, C12, Fig. B-13B) are locally abundant. Minor agglutinated foraminifera tests (H–J9, Fig. B-13A). Common organic material stringers (G6, Fig. B-13B) are distributed throughout the sample. Rare phosphatic bone fragments (F5, Fig. B-13A). Silt grains display angular to subrounded outlines.

Detrital Grains. In order of abundance: quartz (E11, Fig. B-13B), plagioclase, spores (C12, H2, Fig. B-13B), agglutinated foraminifera tests, muscovite (A11, Fig. B-13B), phosphatic bone fragments (F5, Fig. B-13A), biotite.

Matrix. Abundant matrix material is dominantly composed of clay minerals with subordinate amounts of clay-size quartz and feldspar particles and partially pyritized organic material (B–C4, Fig. B-13B) occurring as stringers or minute particles. Results of X-ray diffraction analysis revealed 53 weight-percent total clay minerals, composed of illite (52 weight-percent), mixed-layer illite/smectite (1 weight-percent), kaolinite (trace), and chlorite (trace).

Cements and Replacement Minerals. Minor ferroan dolomite occurs as a partial replacement of spore walls (H1, Fig. B-13B), matrix (F–G14, Fig. B-13B), and as partial cement fill within spores (C14, Fig. B-13B). Minor pyrite fills horizontal burrows, highlighting shape and location, replaces organic material (A–B11, Fig. B-13B), partially fills spores (D–E2, Fig. B-13B), and has developed within the clay-rich matrix (E1, Fig. B-13B). Minor titanium dioxide crystal aggregates occur throughout the matrix as replacement of titanium-bearing minerals. Rare apatite crystals fill spores.

Pore System. Partings along parallel laminations are artifacts of the sampling process; no visible pores were identified.

Magnification. Figure B-13A: 50X. Figure B-13B: 200X.

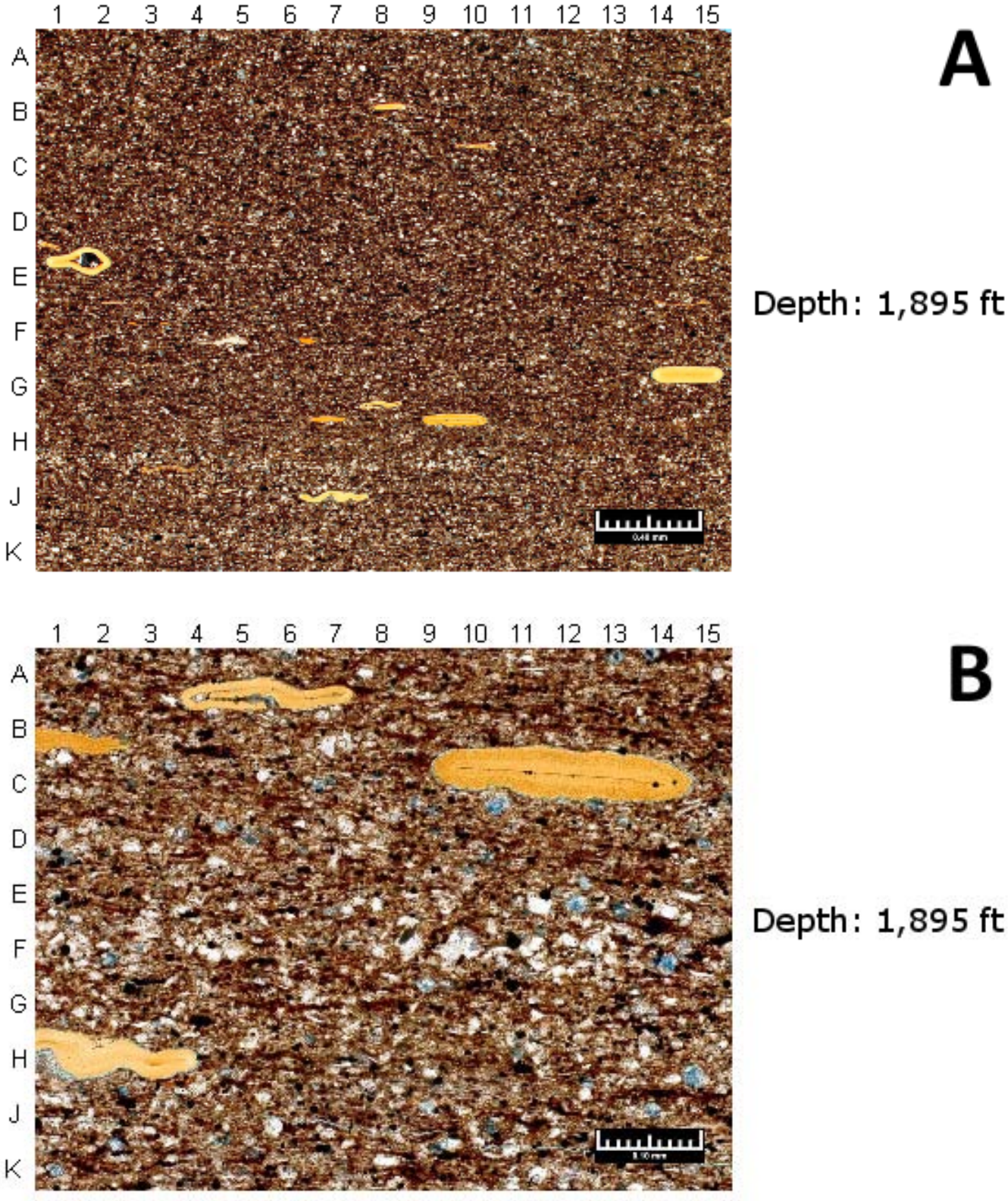

Figure B-13. Weatherford Laboratories grid reference images for New Albany Shale sample 1-21P, 1,895 ft.

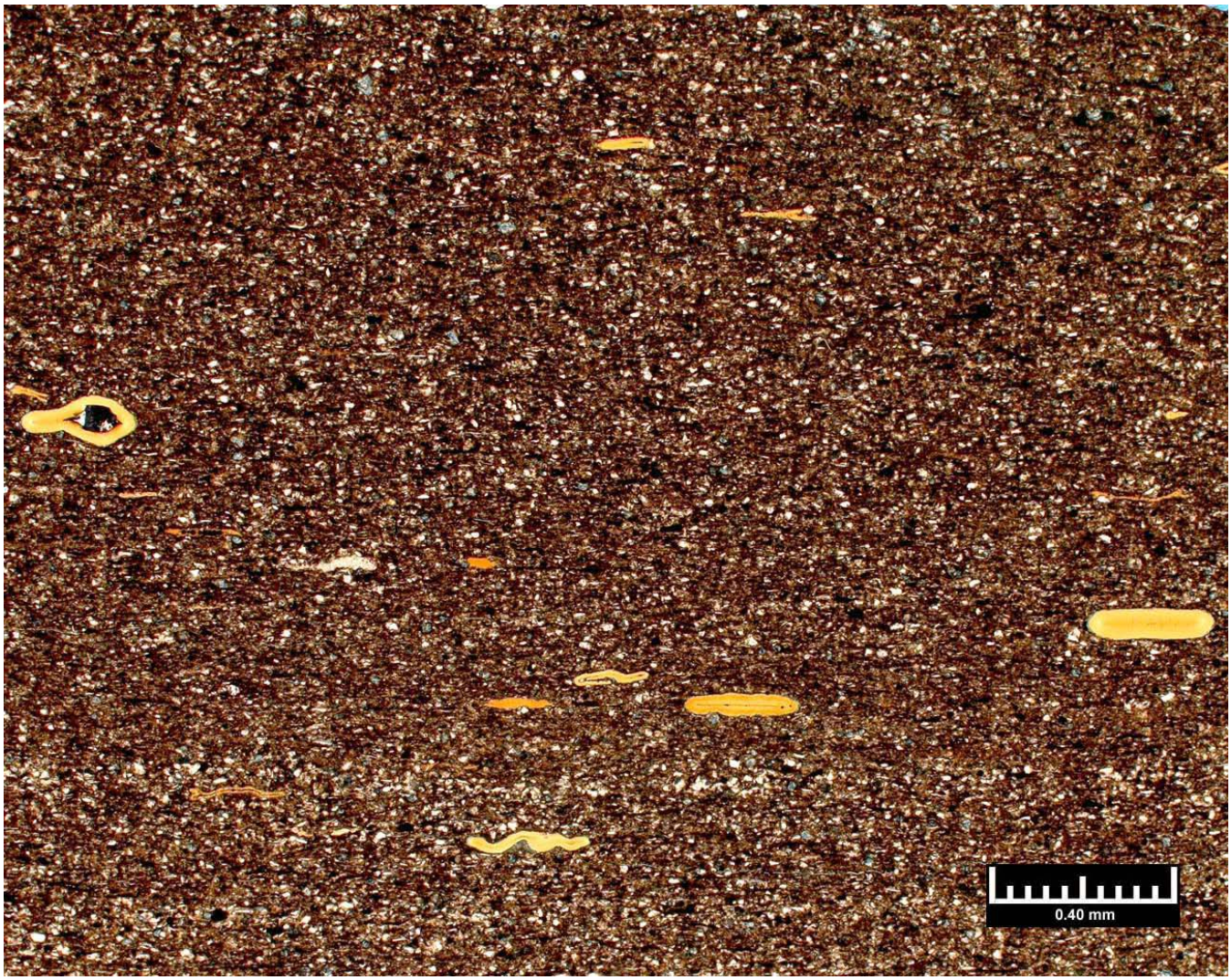

Figure B-14. New Albany Shale, sample 1-21P, 1,895 ft, full-size thin-section image corresponding to Figure B-13A, magnification 50X.

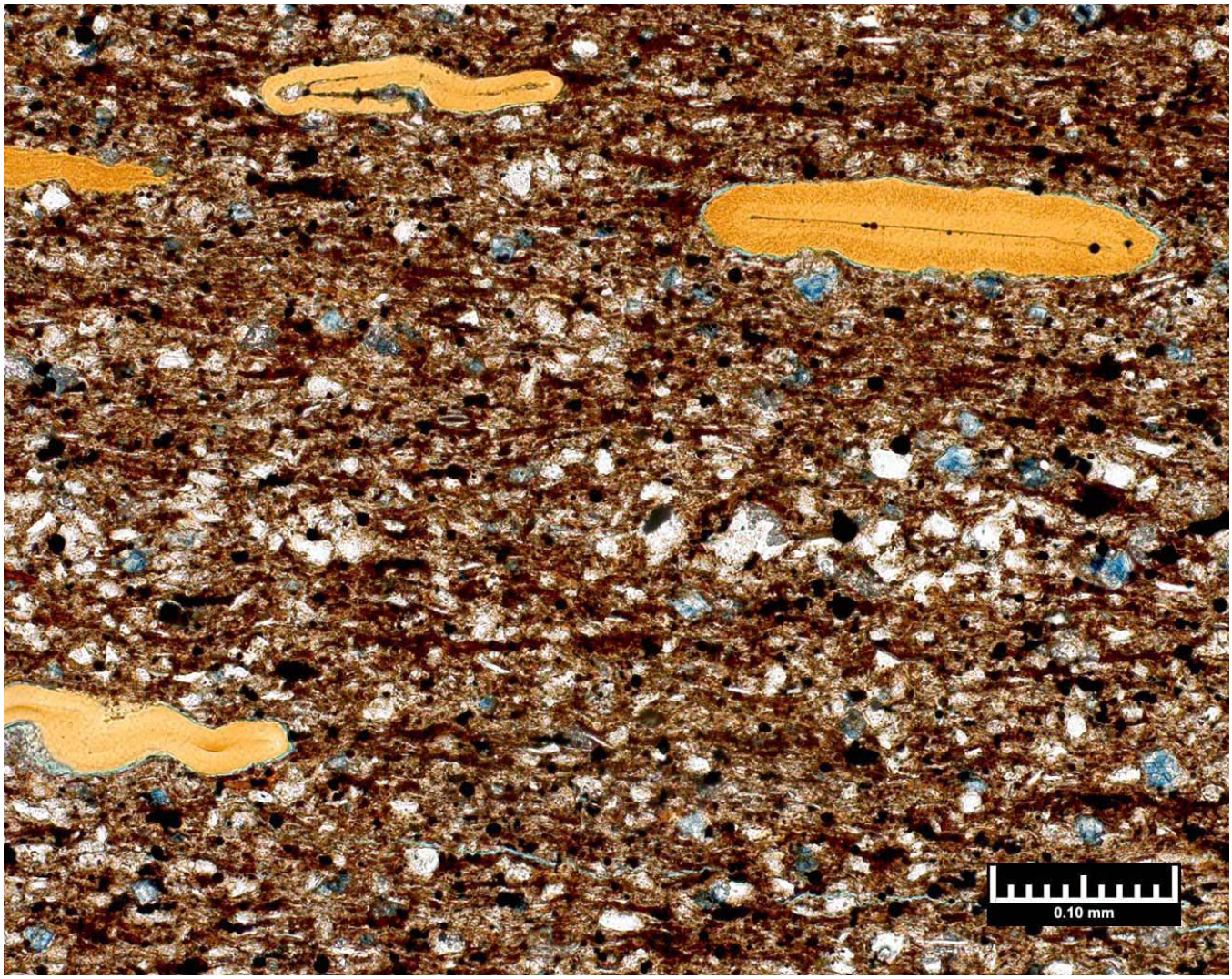

Figure B-15. New Albany Shale, sample 1-21P, 1,895 ft, full-size thin-section image corresponding to Figure B-13B, magnification 200X.

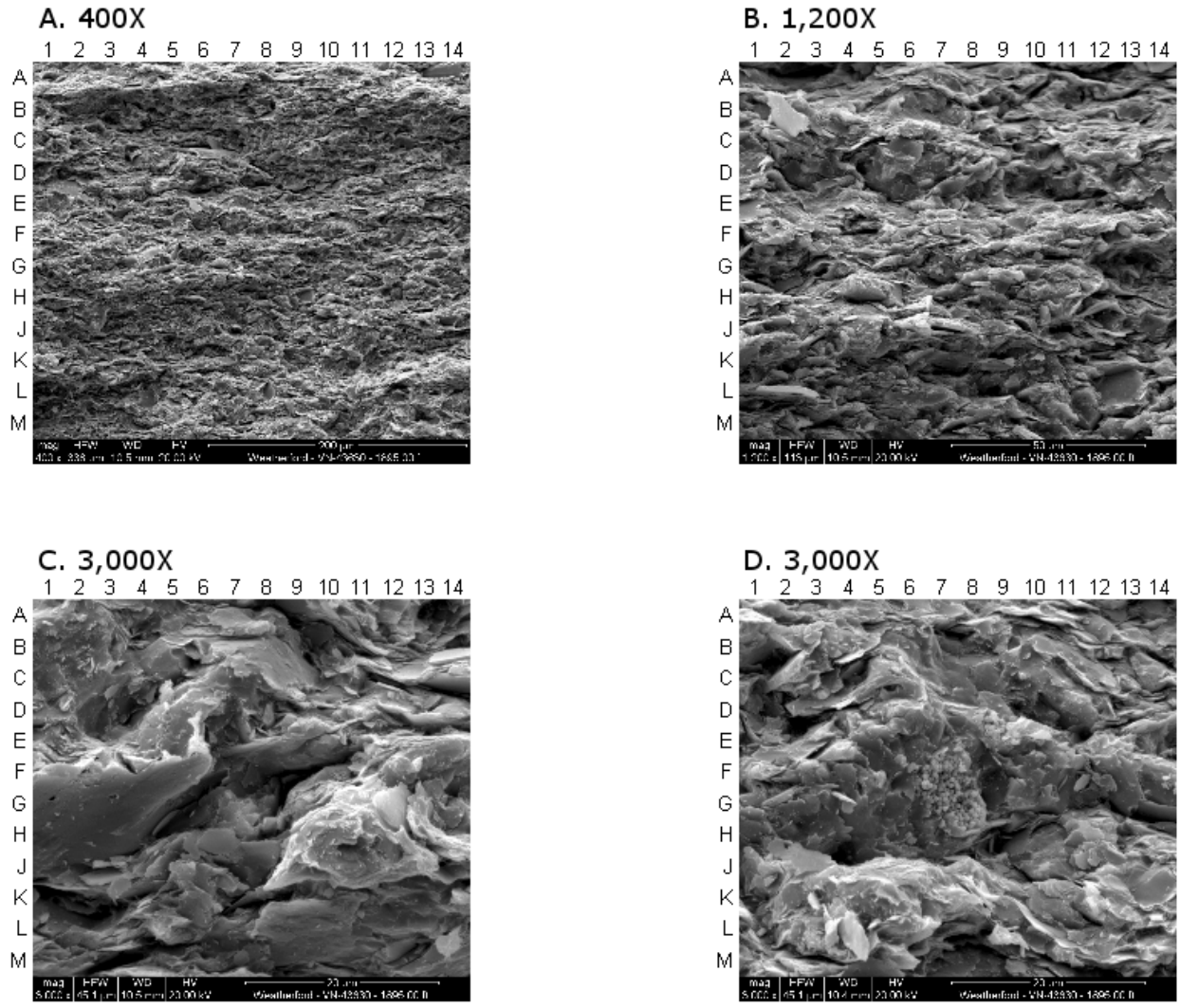

Figure B-16. Scanning electron photomicrographs of the New Albany Shale with coordinate references, sample 1-21P, 1,895 ft.

Discussion

Well-developed elongate grain alignment is revealed in the images of a slightly ferroan, dolomitic, silty shale (Fig. B-16A–D). Numerous heterogeneously distributed silt grains are composed primarily of quartz (E–F1, Fig. B-16B; L5, Big. B-16C) and enveloped by clay-rich matrix. Ferroan dolomite (L2, Fig. B-16C) also occurs between clay or organic-material particles. Common *Tasmanites* spores (B9, Fig. B-16C; F–G2, Fig. B-16D) are partially replaced by framboidal pyrite (C11, Fig. B-16C) and filled by apatite crystals (G2, Fig. B-16C), pyrite, or quartz. Flattened, aligned clay particles (G–J8-14, Fig. B-16B), organic matter, and spores (B8, Fig. B-16A) display parallel orientation to the bedding plane and comprise most of the matrix. Illite, the dominant clay mineral, commonly displays crenulated outlines (L–M6–9, Fig. B-16C). Numerous micropores (F8, Fig. B-16C; G11, Fig. B-16D) occur within the clay- and organic-rich matrix and range from approximately 7 µ to slightly greater than 20 µ. X-ray diffraction analysis results reveal 47 weight-percent clay minerals, consisting of illite (46 weight-percent), mixed-layer illite/smectite (1 weight-percent), chlorite (trace), and kaolinite (trace).

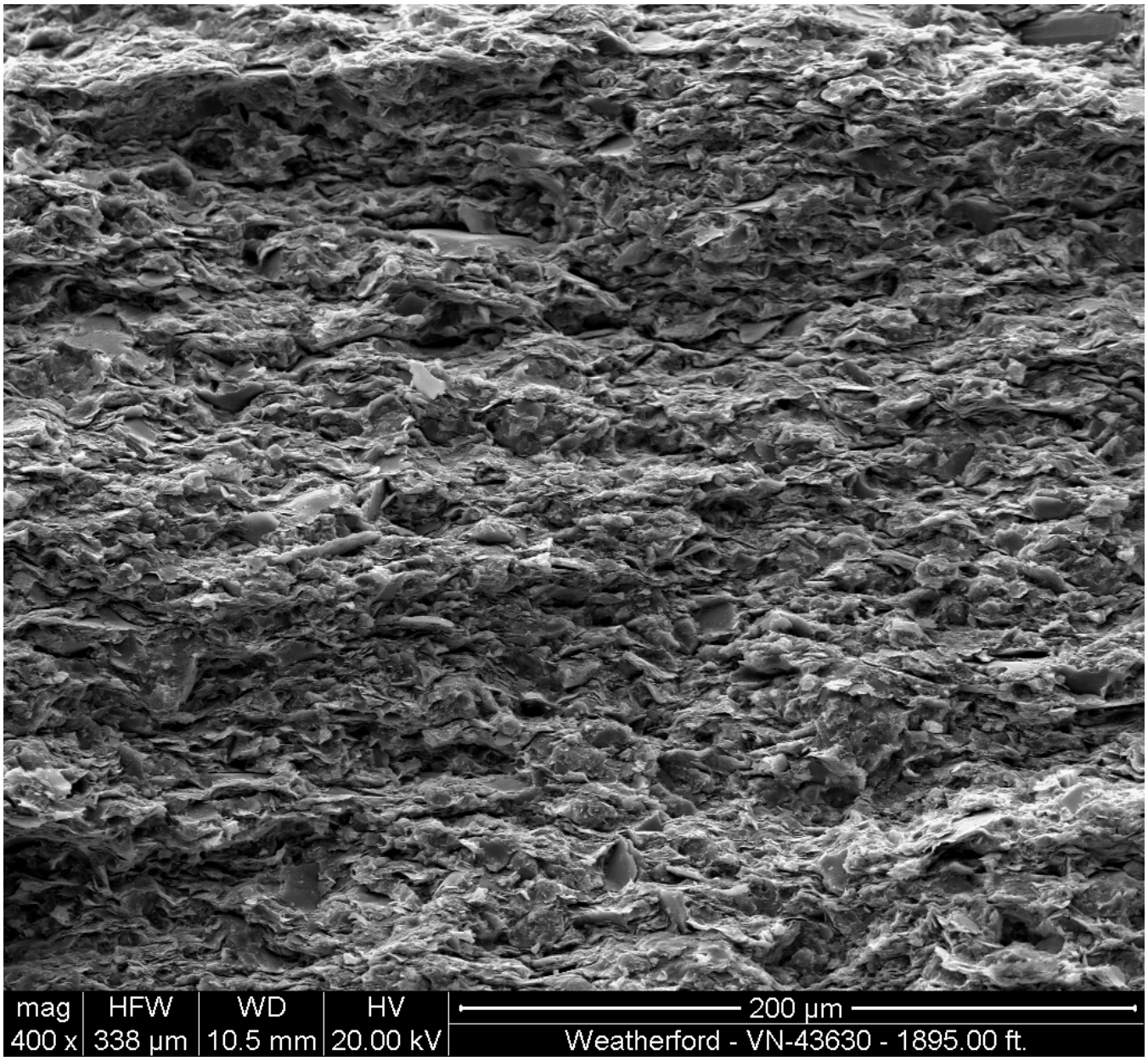

Figure B-17. New Albany Shale, sample 1-21P, 1,895 ft, full-size scanning electron photomicrograph corresponding to Figure B-16A, magnification 400X.

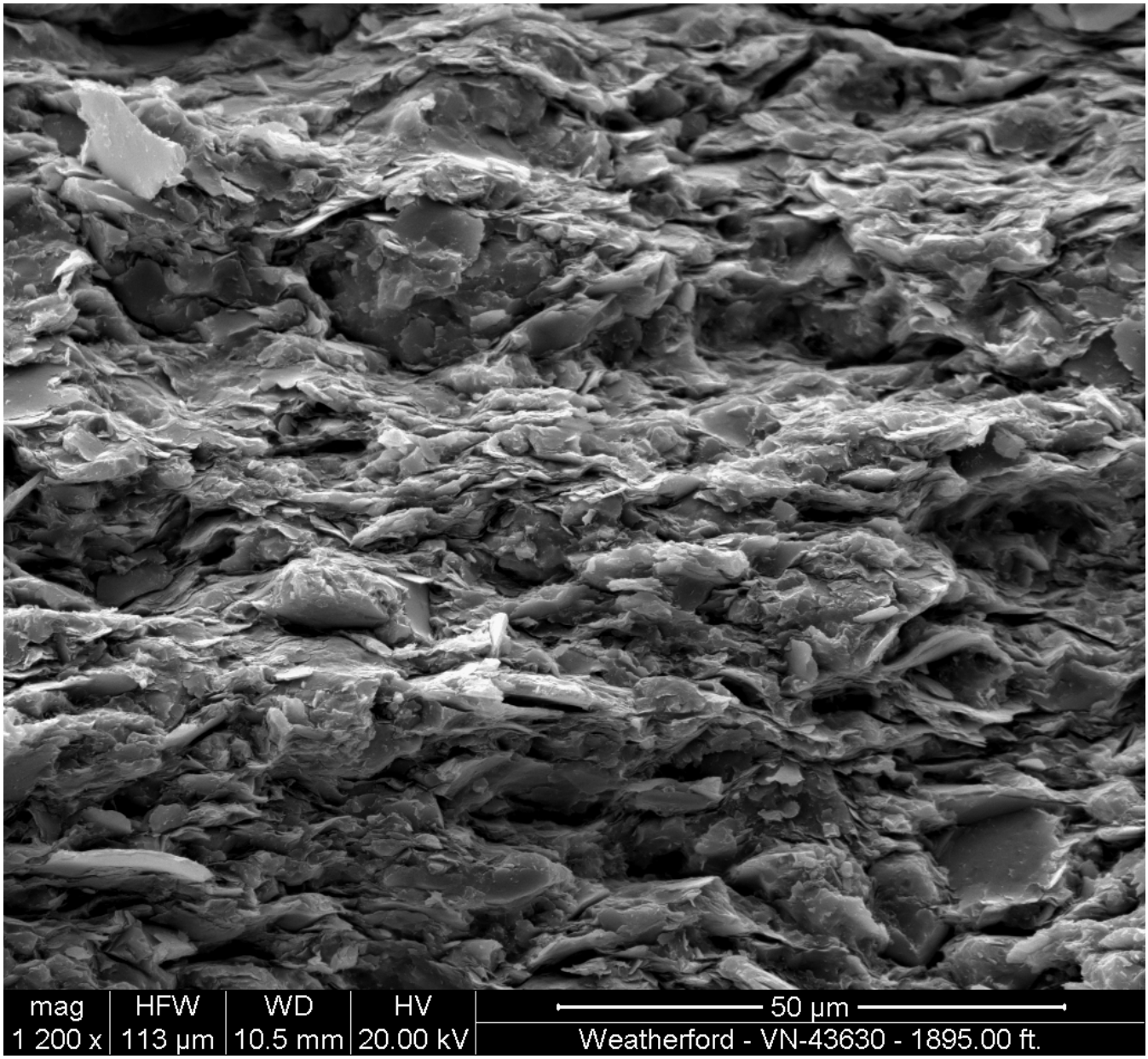

Figure B-18. New Albany Shale, sample 1-21P, 1,895 ft, full-size scanning electron photomicrograph corresponding to Figure B-16B, magnification 1,200X.

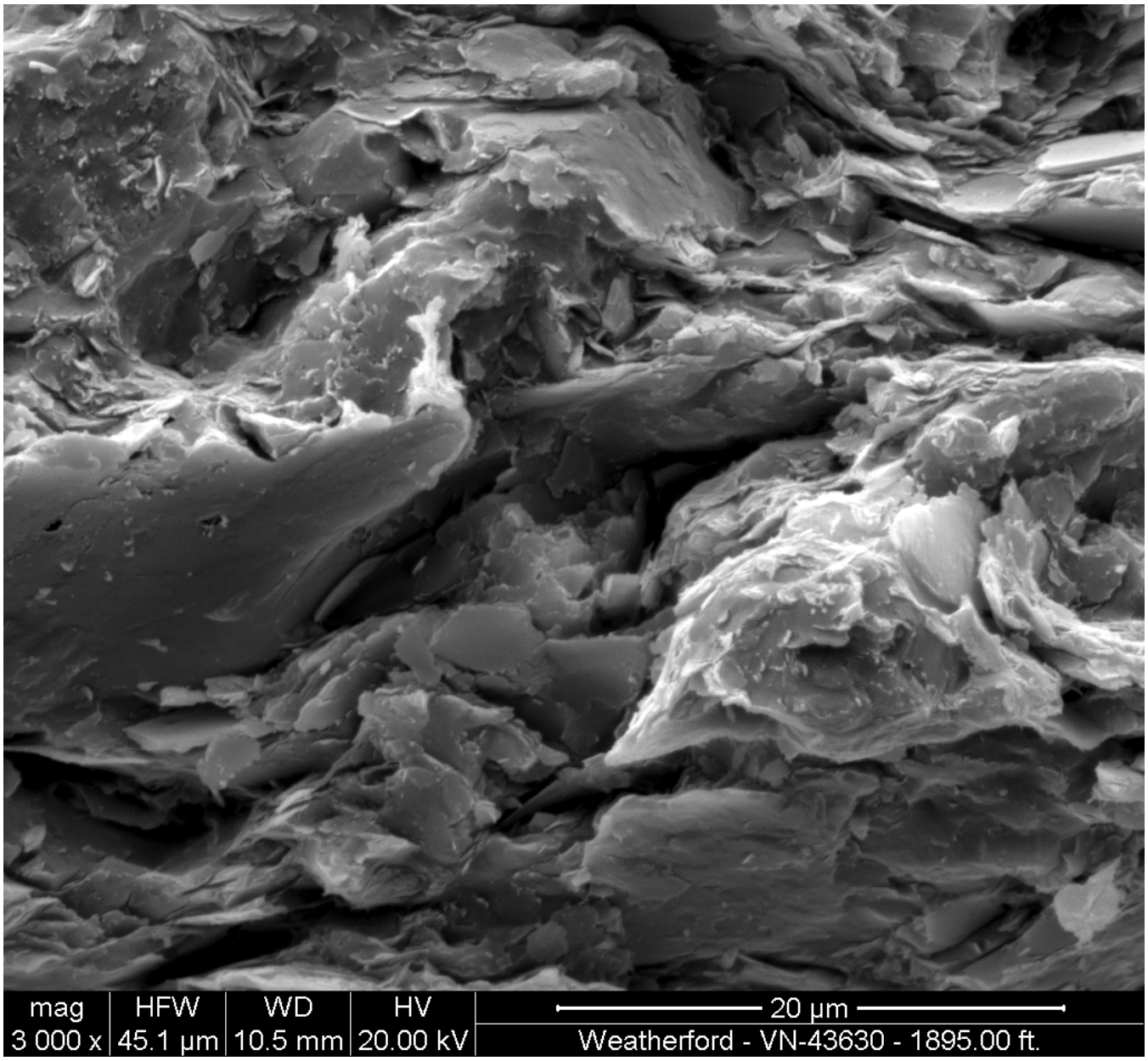

Figure B-19. New Albany Shale, sample 1-21P, 1,895 ft, full-size scanning electron photomicrograph corresponding to Figure B-16C, magnification 3,000X.

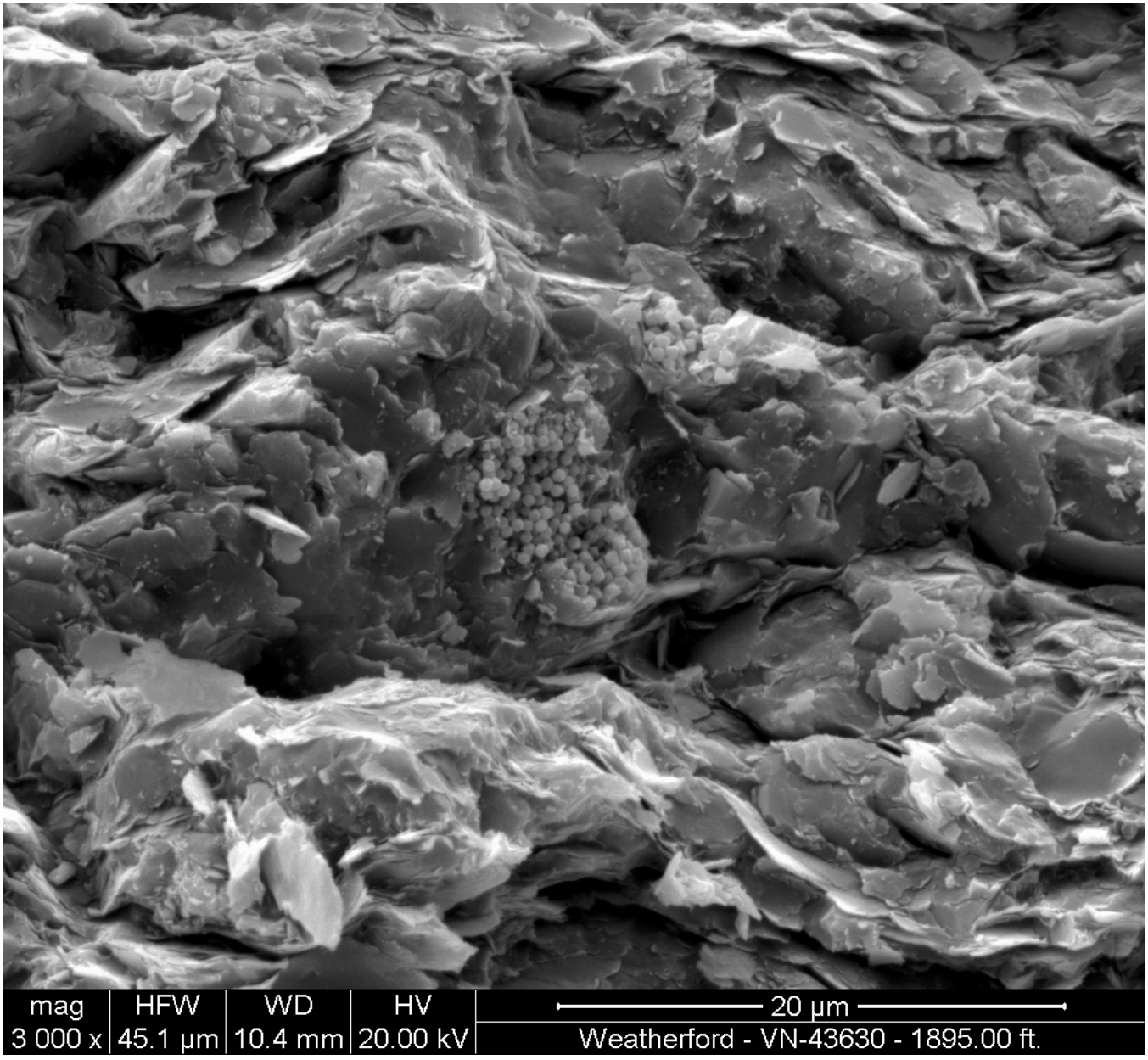

Figure B-20. New Albany Shale, sample 1-21P, 1,895 ft, full-size scanning electron photomicrograph corresponding to Figure B-16D, magnification 3,000X.

Sample 1-25P, 1,899.9 ft

Shale rock properties: 1,899.90–1,900.00 ft
Pressure decay permeability (dry): 6.96E-05 md
Porosity (dry, helium): 5.7 percent
Grain density (dry): 2.45 g/cm^3
Leco TOC: 8.32 weight-percent hydrocarbon

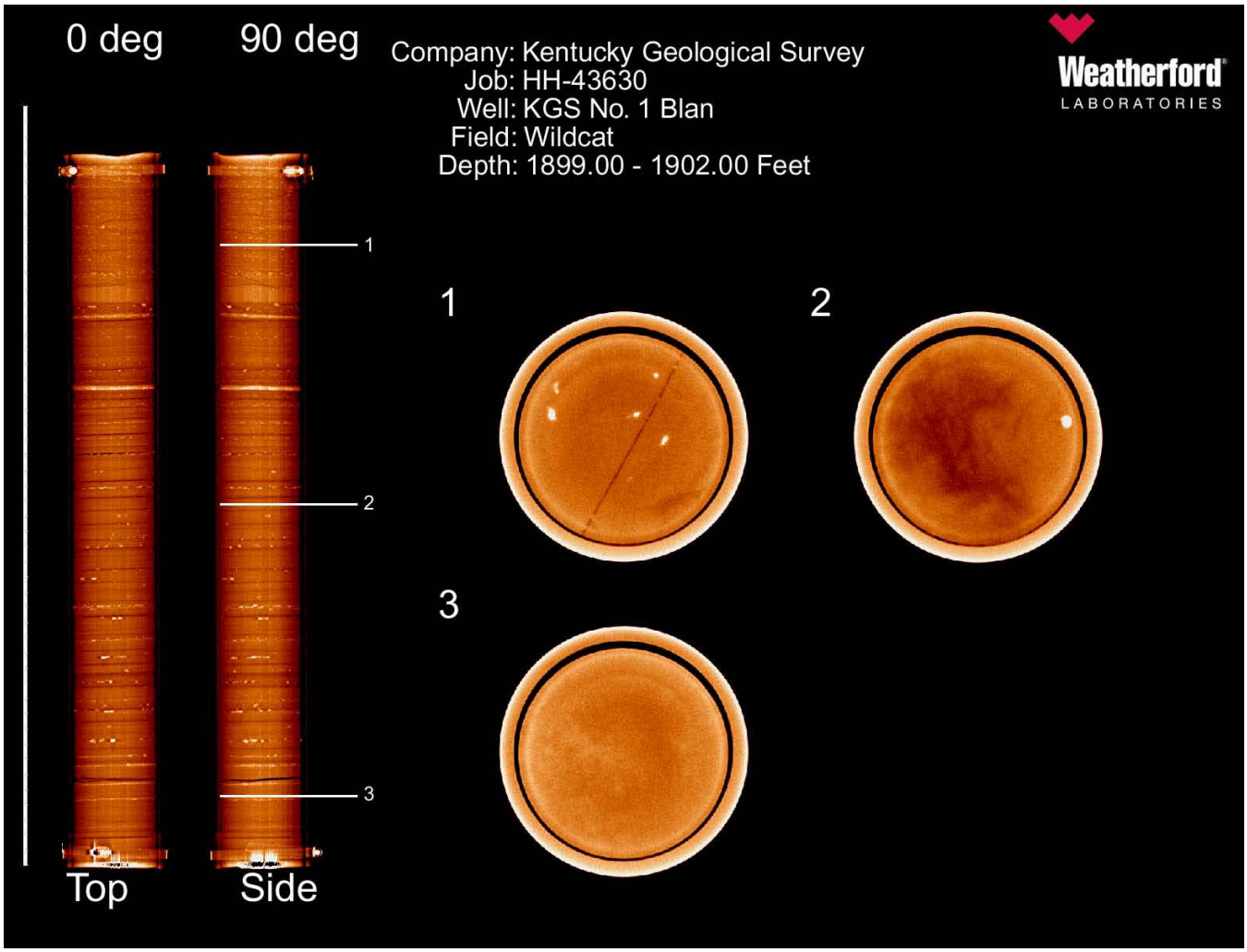

Figure B-21. CT scan of New Albany Shale interval, 1,899–1,902 ft.

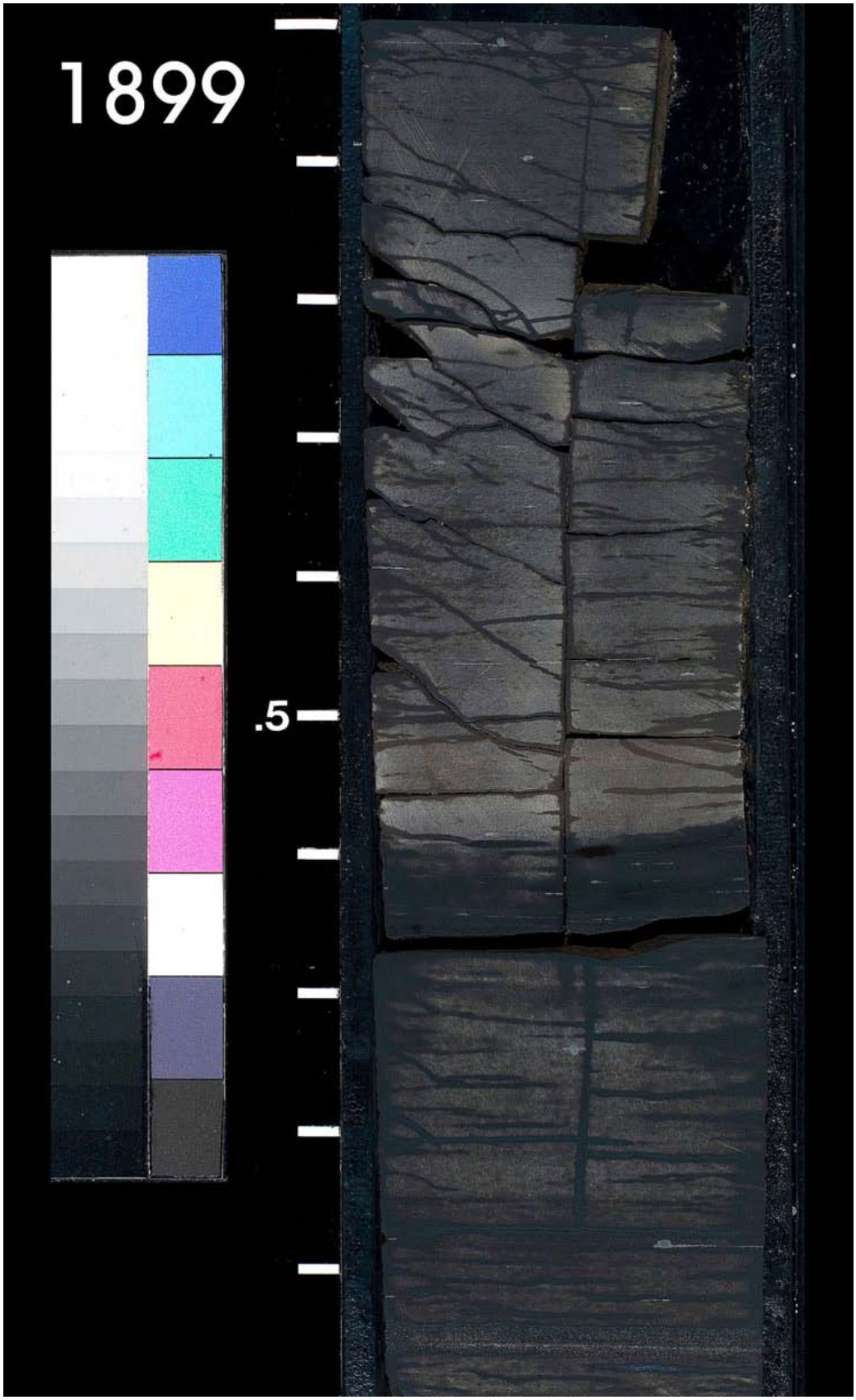

Figure B-22. Cut slab of New Albany Shale core interval, 1,899–1,900 ft.

Thin-Section Description

Lithology. Slightly ferroan-dolomitic, fossiliferous, sandy and silty shale.

Texture. Sand-rich laminations (G–H4, Fig. B-23A) contain numerous *Tasmanites* spores that are flattened (H–J10, Fig. B-23A) or filled by authigenic chalcedony (G14, Fig. B-23B) or pyrite (D6, Fig. B-23B). Sparse, thin laminations contain concentrations of subangular to rounded silt grains and sparse, crushed, agglutinated foraminifera tests. An extensively pyrite-replaced lamination is observed.

Detrital Grains. In order of abundance: quartz (H–J7, Fig. B-23B), spores (G–H7.5, Fig. B-23A; J11, Fig. B-23B), agglutinated foraminifera tests, plagioclase, muscovite (E–F13, Fig. B-23B), phosphatic bone fragments, biotite.

Matrix. Matrix material consists of a mixture of clay minerals, as well as lesser clay-size quartz and feldspar particles and partially pyritized organic material (G2, Fig. B-23B) as stringers or minute particles. No X-ray diffraction analysis was performed on this sample.

Cements and Replacement Minerals. Common chalcedony has crystallized as a spore-filling authigenic mineral (G14, Fig. B-23B), as well as crystalline aggregates, which replace spore walls (C–D9, Fig. B-23B). Minor ferroan dolomite occurs as a spore-filling mineral (D–E6.5, Fig. B-23A), dark blue mineral (D9, Fig. B-23B), and as partial replacements of spore walls and as partial replacement of matrix (A–B11, Fig. B-23B). Common, irregularly distributed pyrite, including framboids, replaces organic material (A–B11, Fig. B-23B), partially fills spores (E–F10, Fig. B-23B) and has developed within the clay-rich matrix (D–E13.5, Fig. B-23B). Minor calcite fills spore cavities (A2, Fig. B-23A). Rare nonferroan dolomite partially replaces spore walls. Rare titanium dioxide crystal aggregates replace titanium-bearing minerals.

Pore System. Partings along parallel laminations are artifacts of the coring or sampling process. Rare moldic pores are identified within spores. Other apparent pores (B8, D–E5, Fig. B-23A) are likely the result of plucking during thin-section preparation.

Magnification. Figure B-23A: 50X. Figure B-23B: 200X.

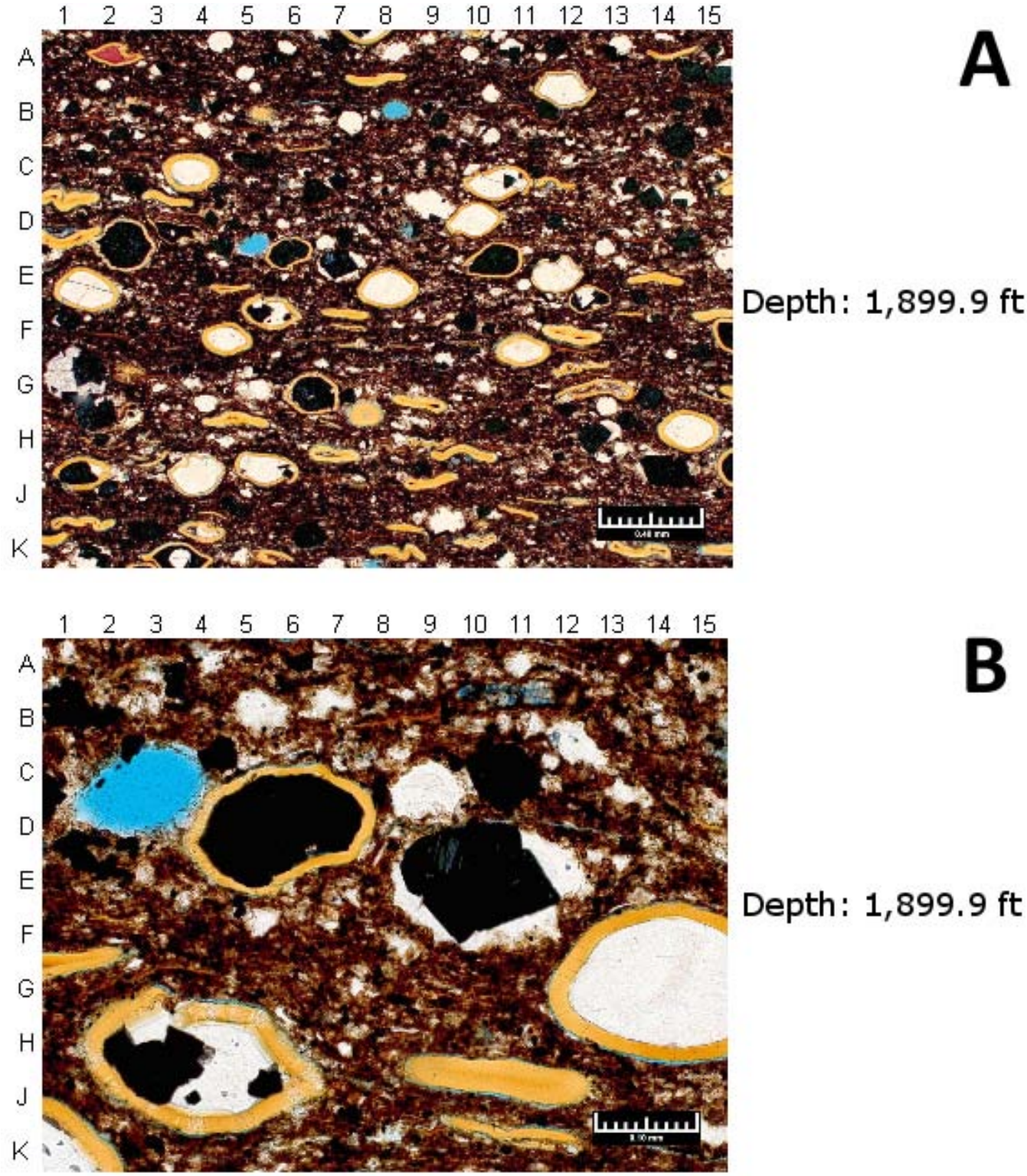

Figure B-23. Weatherford Laboratories grid coordinate reference plates for New Albany Shale sample 1-25P, 1,899.9 ft.

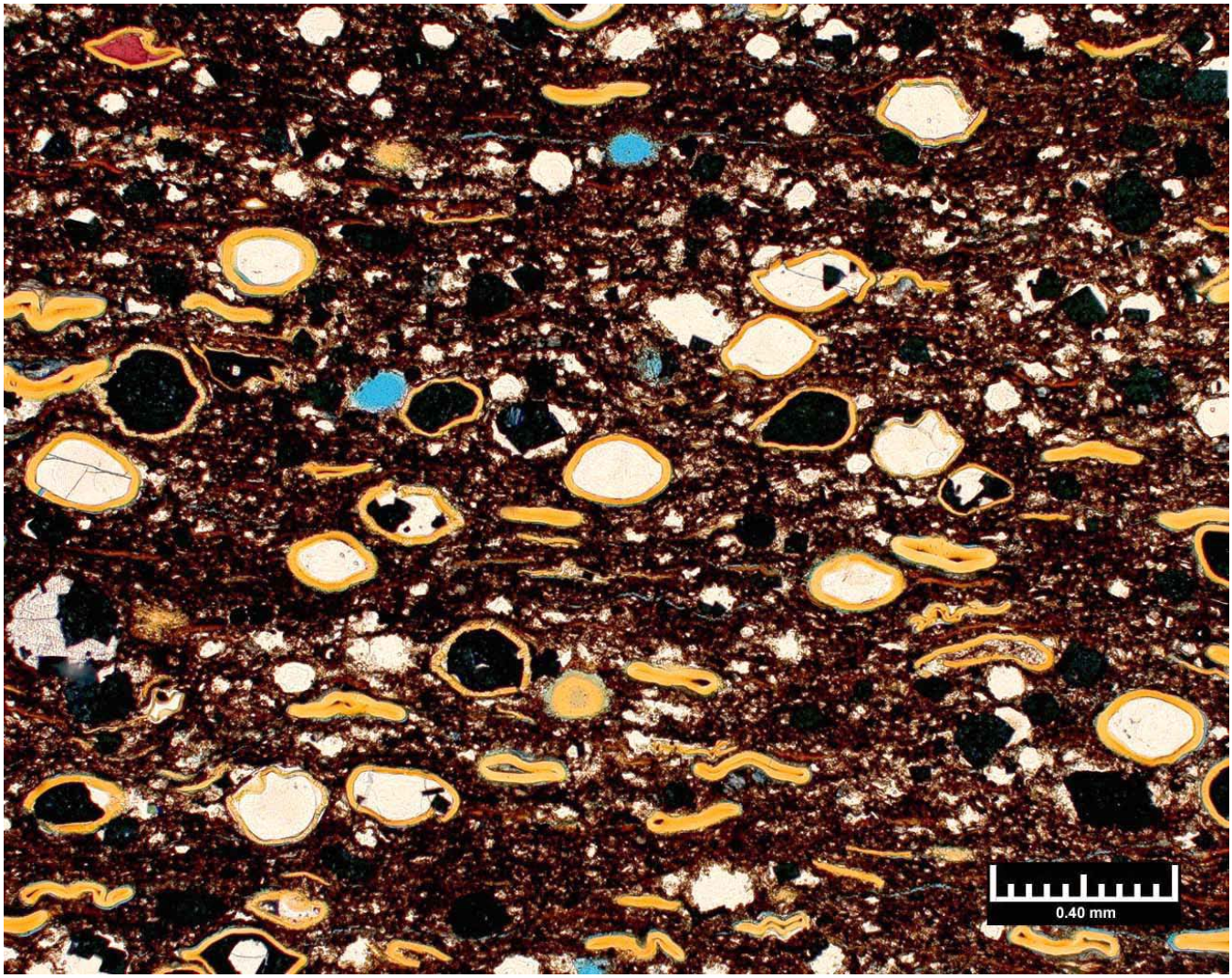

Figure B-24. New Albany Shale, sample 1-25P, 1,899.9 ft, full-size thin-section image corresponding to Figure B-23A, magnification 50X.

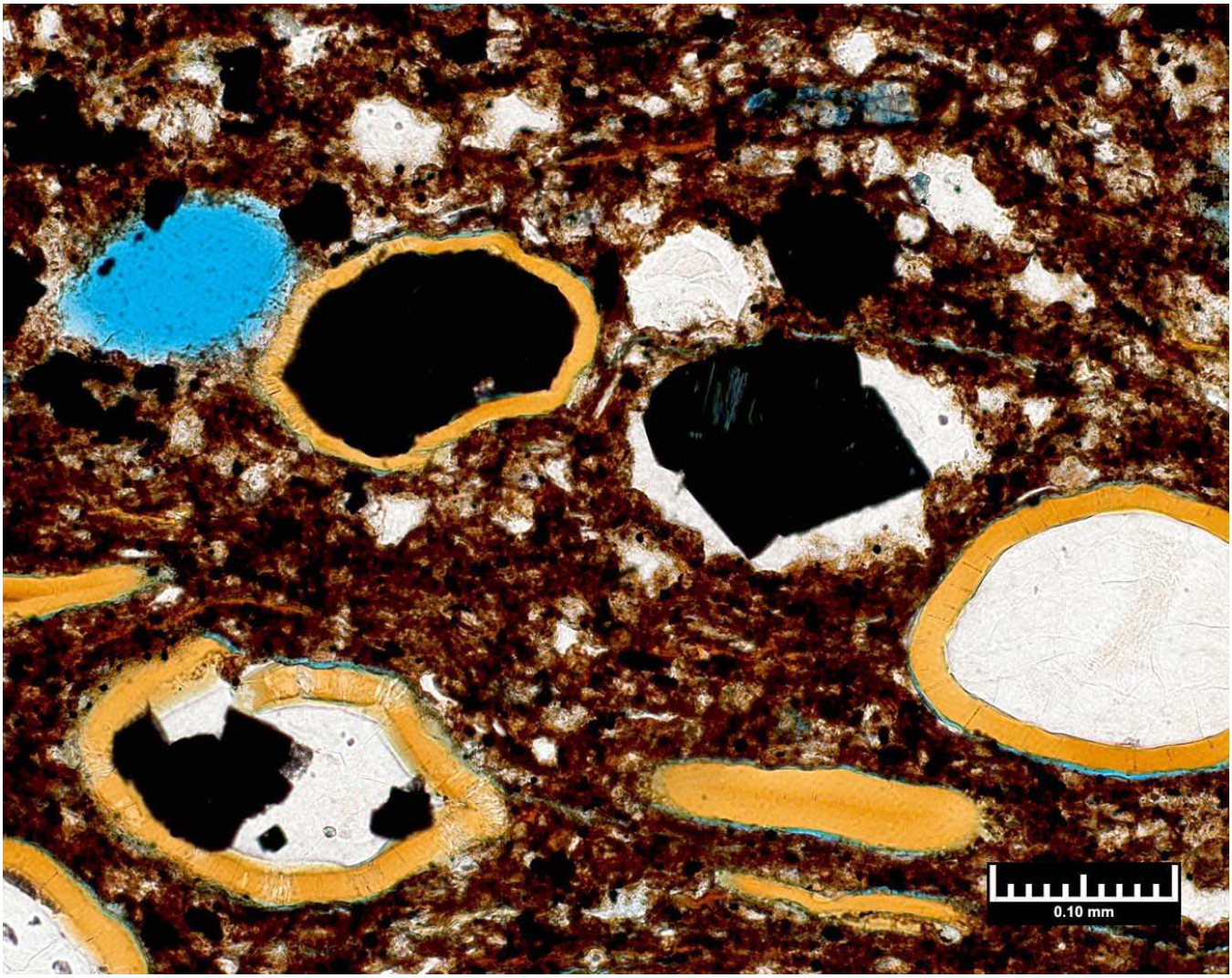

Figure B-25. New Albany Shale, sample 1-25P, 1,899.9 ft, full-size thin-section image corresponding to Figure B-23B, magnification 200X.

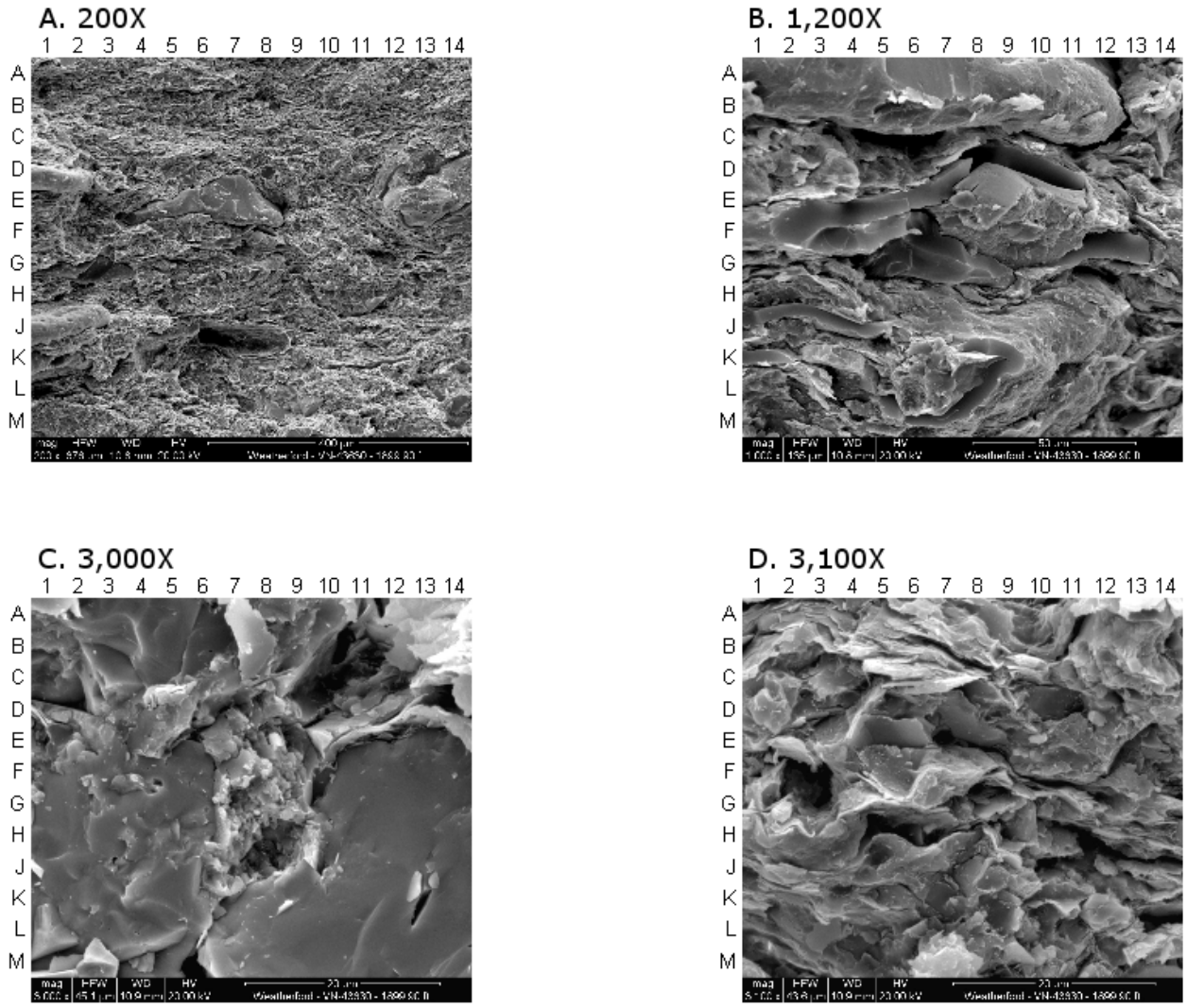

Figure B-26. Scanning electron photomicrographs of the New Albany Shale with coordinate references, sample 1-25P, 1,899.9 ft.

Discussion

Well-defined fissility (Fig. B-26A) is highlighted in the images of silty, slightly ferroan-dolomitic shale. Common silt-size quartz grains (H4, Fig. B-26B; B–C13.5, Fig. B-26D) are enveloped by abundant illitic matrix (A–B11–14, Fig. B-26C). Scattered ferroan dolomite crystals (H–J14, L13, Fig. B-26B) have crystallized between illite platelets or partially envelop adjacent clay flakes (L13.5, Fig. B-26B). The matrix occasionally displays illite fibrils (E10.5, Fig. B-26B), indicating the illite is partially recrystallized. Heterogeneously distributed spores (F9, Fig. B-26D) are filled by framboidal pyrite (F7, Fig. B-26D), quartz, or apatite. Many of the spores have been flattened and do not contain authigenic minerals. X-ray diffraction analysis reveals 53 weight-percent clay minerals, consisting of illite (52 weight-percent), mixed-layer illite/smectite (1 weight-percent), chlorite (trace), and kaolinite (trace). Figure B-31 presents a pseudo-color analysis of some of the porosity types observed in the New Albany Shale. The dark, uniform blue at the bottom of the image is an unidentified organic matter particle, possibly *Tasmanites*. The red to bright yellow color highlights intragranular micro- and nanoscale porosity in the matrix material. The parallel, northeast–southwest-trending linear features are artifacts of the focused-ion-beam processing of the sample.

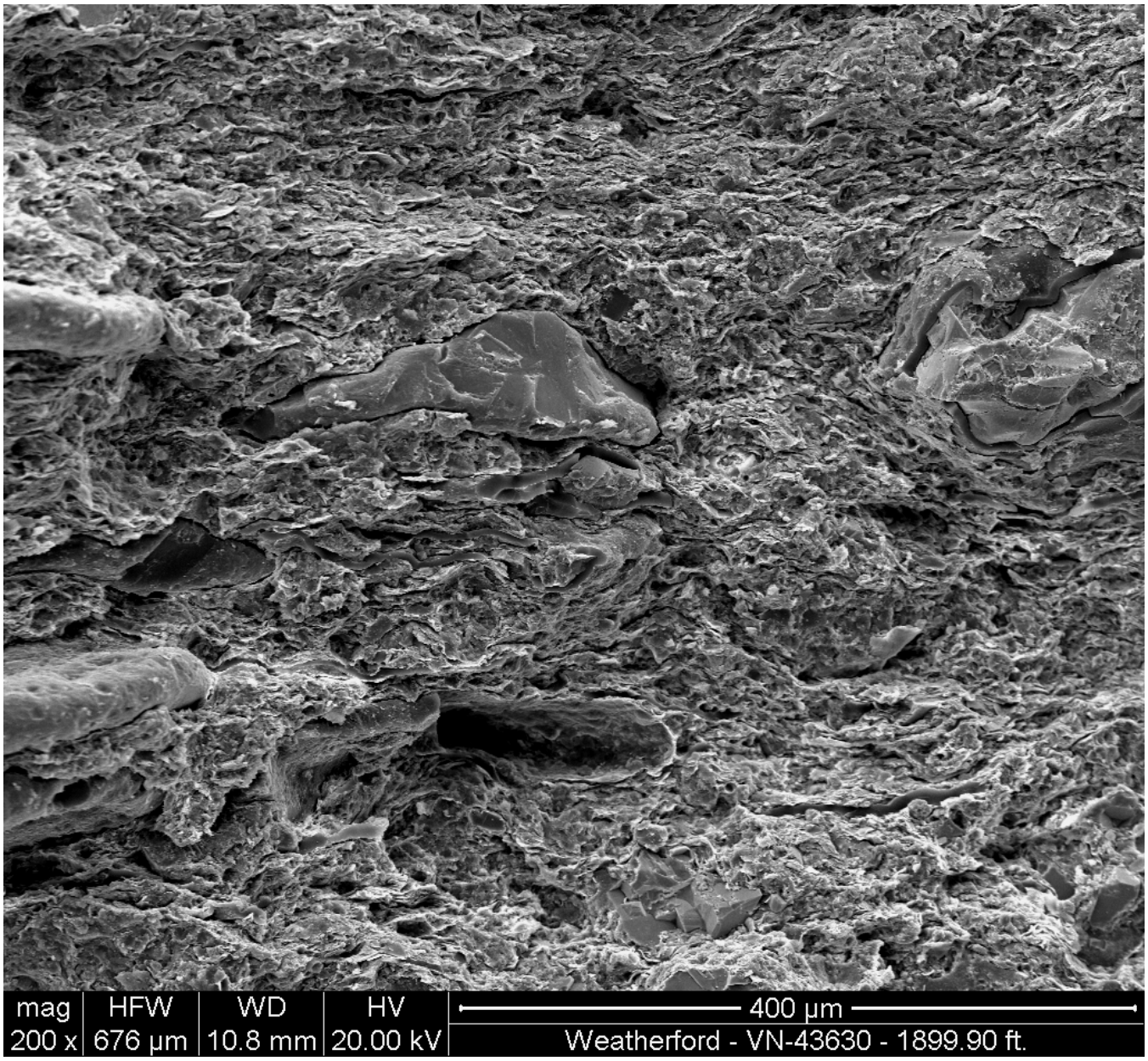

Figure B-27. New Albany Shale, sample 1-25P, 1,899.9 ft, full-size scanning electron photomicrograph corresponding to Figure B-26A, magnification 200X.

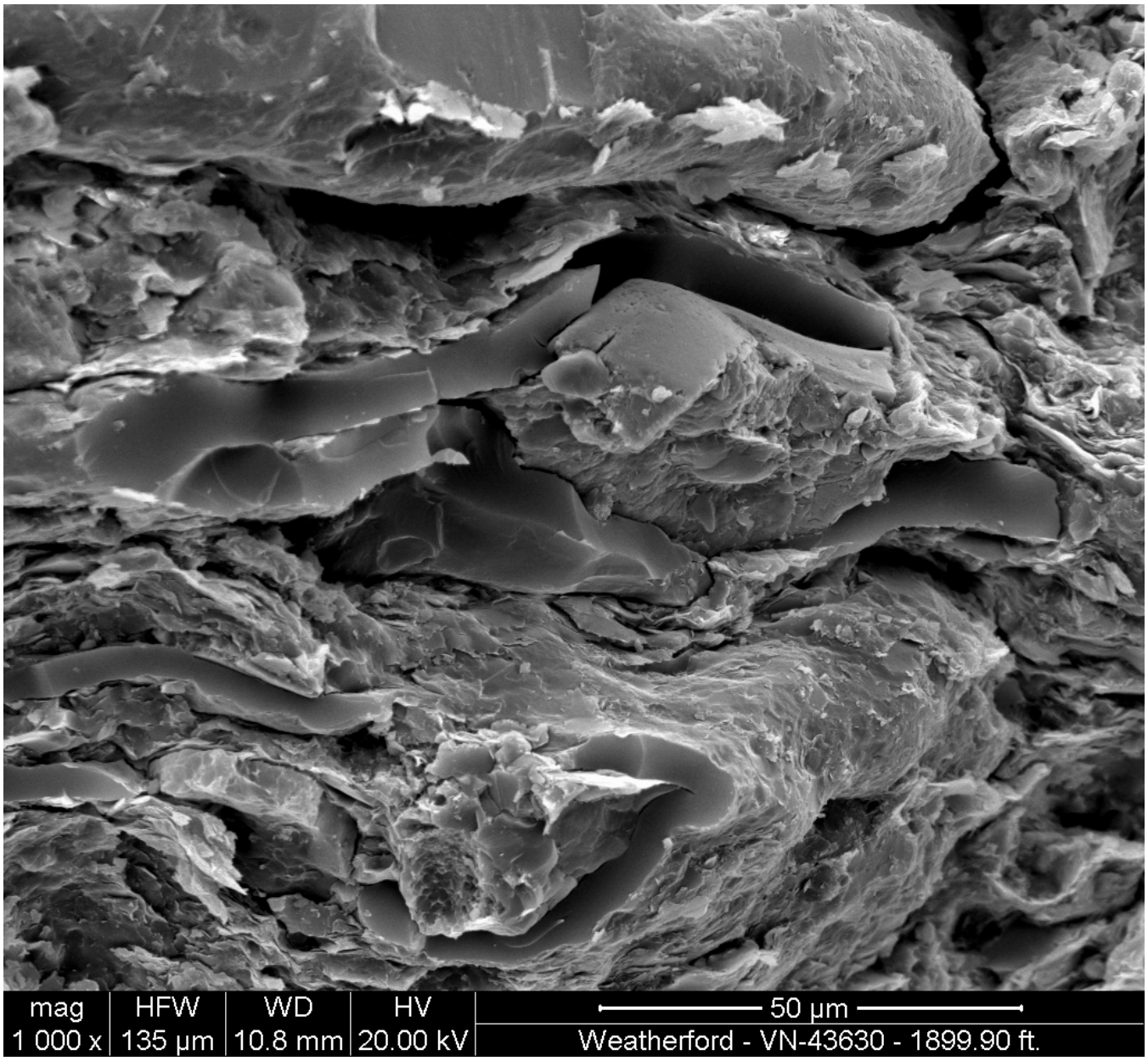

Figure B-28. New Albany Shale, sample 1-25P, 1,899.9 ft, full-size scanning electron photomicrograph corresponding to Figure B-26B, magnification 1,000X.

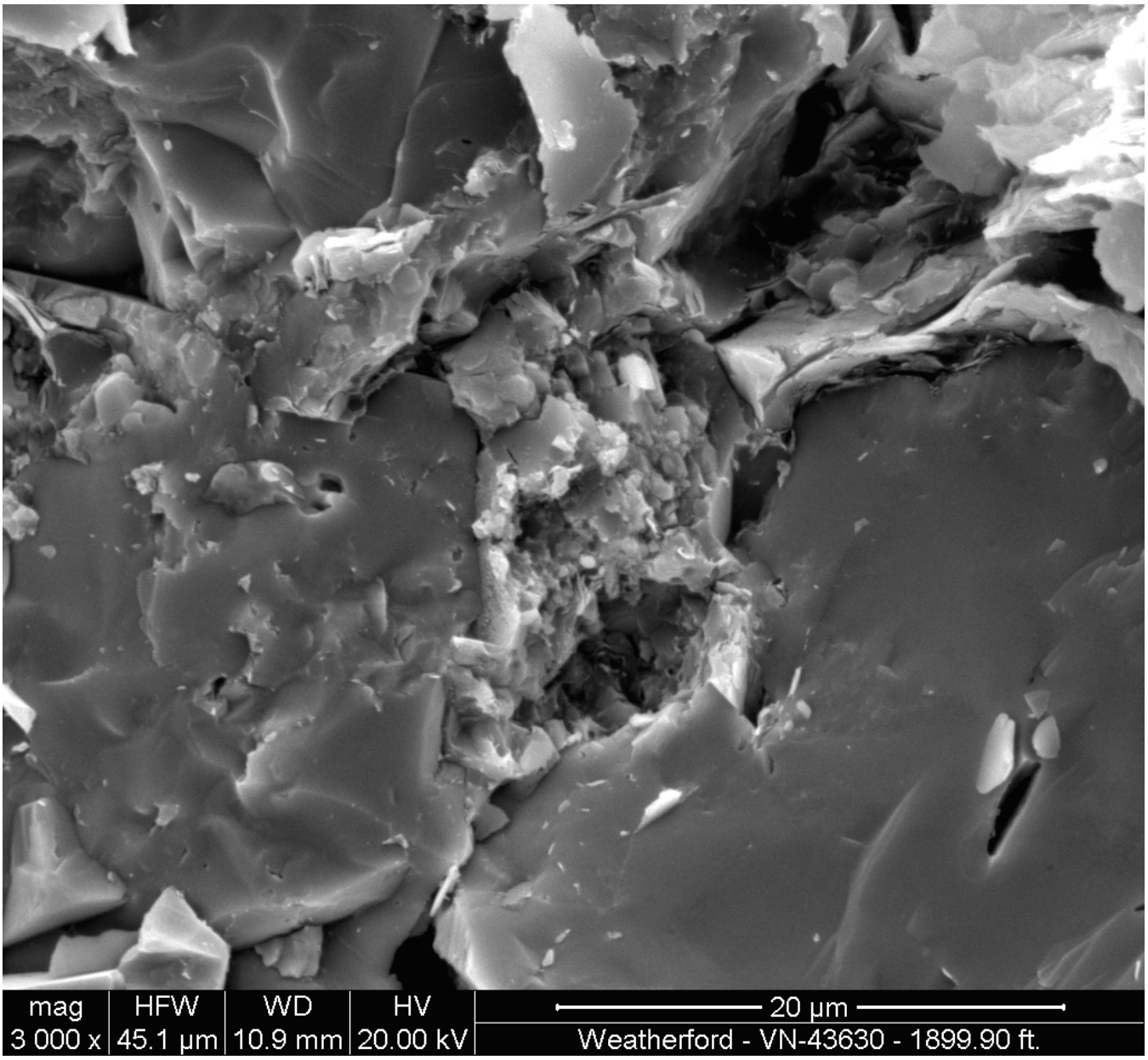

Figure B-29. New Albany Shale, sample 1-25P, 1,899.9 ft, full-size scanning electron photomicrograph corresponding to Figure B-26C, magnification 3,000X.

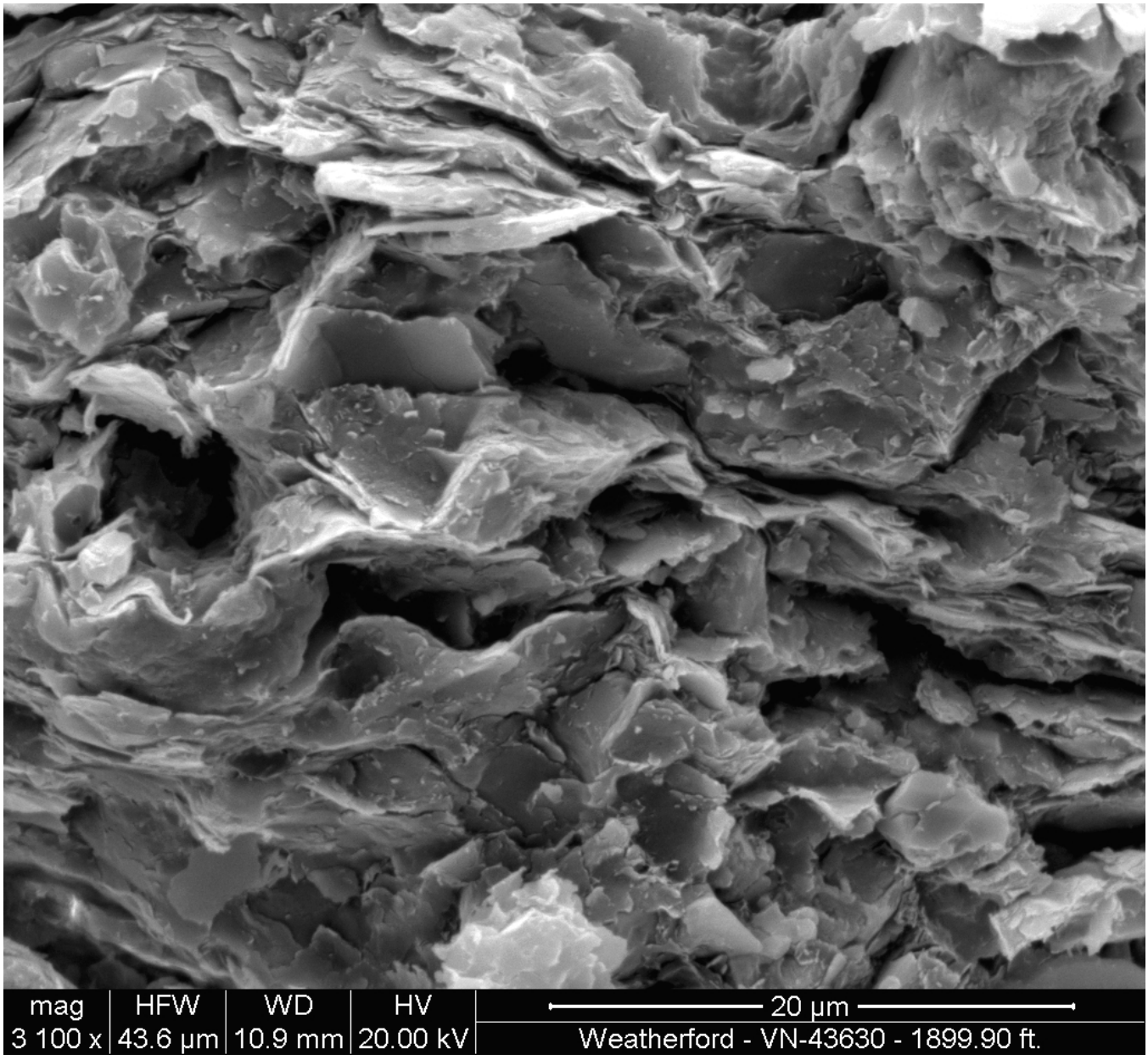

Figure B-30. New Albany Shale, sample 1-25P, 1,899.9 ft, full-size scanning electron photomicrograph corresponding to Figure B-26D, magnification 3,100X.

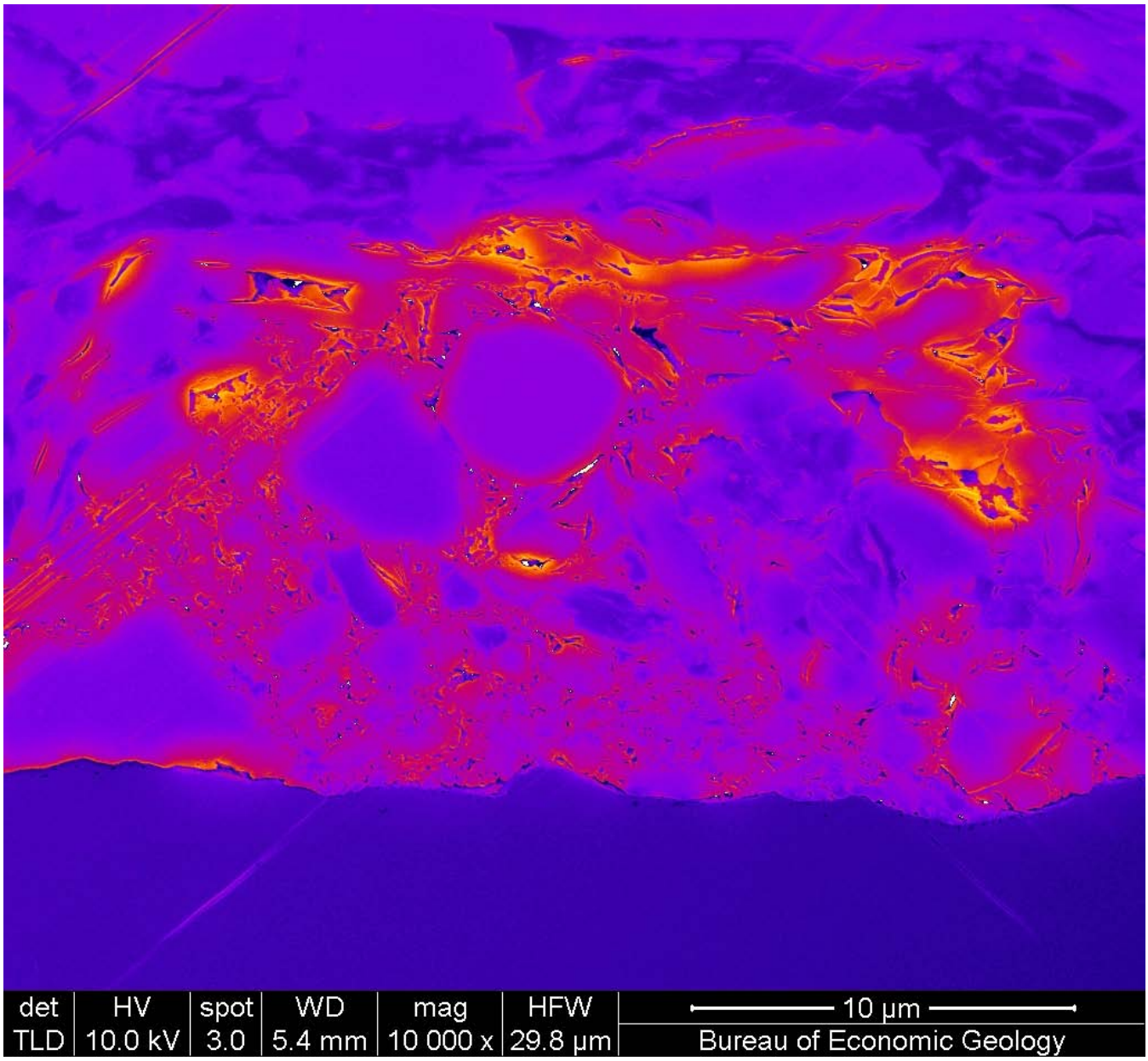

Figure B-31. New Albany Shale false-color argon-ion beam-milled scanning electron photomicrograph showing porosity types. Depth: 1,899 ft. Magnification: 10,000X. Photo by Robert Reed, Texas Bureau of Economic Geology; post-processing by Brandon C. Nuttall.